



UNIVERSIDADE DA BEIRA INTERIOR
Engenharia

Numerical Modeling of Cooling Water Droplets using a Two-Way Coupling Approach

(Versão Corrigida Após Defesa)

André Filipe Romão Franco

Dissertação para obtenção do Grau de Mestre em
Engenharia Aeronáutica
(ciclo de estudos integrado)

Orientador: Prof. Doutor André Resende Rodrigues da Silva

Covilhã, Maio de 2019

Dedication

To my uncle and grandparents.

One thing I have learned in a long life: that all our science, measured against reality, is primitive and childlike - and yet it is the most precious thing we have.

Albert Einstein

Acknowledgments

First of all, I would like to thank my supervisor, Professor André Silva for all the help, patience and guidance throughout this dissertation.

I would like to acknowledge the opportunity to work at AEROG - Aeronautics and Astronautics Research Center, and would like to thank Professor Jorge Barata for this opportunity.

I would like to thank all my lab partners, especially Daniela Ribeiro, Gabriel Carrolo, Daniel Rodrigues, Gonçalo Pacheco, Inês Ferrão, Cátia Moura, Rodolfo Lopes and Leandro Magalhães for their companionship along this work.

I would like to thank all my friends, especially Cátia Miguel, João Rocha, Luís Romeiro, Nídia Ribau, Luís Oliveira and Francisco Figueira, for being present in all the good and bad moments throughout these years.

To my girlfriend and best friend Flávia Morais, thank you for everything. For supporting me always with a smile and especially for all the patience.

Finally, I would like to thank all my family but in particular my parents and sister for trusting me and for all the support and dedication.

To all, thank you!

Resumo

A presente dissertação centra-se no estudo do processo de arrefecimento e congelamento de gotas de água em queda livre. O fenómeno de congelamento é de extrema relevância na área de Engenharia Aeronáutica, uma vez que devido ao impacto de gotas nas superfícies sustentadoras de uma aeronave e conseqüente acumulação de gelo poderão ocorrer incidentes e acidentes com as aeronaves.

Como forma de impedir a formação e acumulação de gelo, existem diversos sistemas para combater este perigo. As áreas críticas de uma aeronave estão normalmente protegidas por sistemas anti gelo. No entanto, embora estes métodos consigam evaporar gotas de água ou derreter o gelo acumulado, existe ainda a possibilidade de formação de gelo a jusante devido a um novo congelamento da mistura gelo-água em áreas desprotegidas.

Desta forma, surge uma necessidade de estudar e adaptar os modelos físicos e matemáticos existentes para uma melhor aproximação a situações reais, por forma a contribuir para uma melhor compreensão deste fenómeno e conseqüentemente levar a uma redução do número de incidentes e acidentes, melhorando as condições de segurança.

O objetivo deste trabalho passa pela realização de um estudo numérico com o intuito de estudar o arrefecimento de gotas de água em queda livre para diferentes diâmetros e razões de humidade do ar. As correlações de Ranz-Marshall são utilizadas, com e sem a adição de um fator de correção, para além da abordagem de Abramzon e Sirignano, como forma de considerar os efeitos de convecção. O modelo utilizado é de *Two-Way Coupling* e as previsões são comparadas com dados experimentais e previsões numéricas cuja abordagem foi *One-Way Coupling*.

Palavras-chave

Transmissão de calor e massa, Razão de humidade, Arrefecimento, Congelamento, *Two-Way Coupling*

Resumo Alargado

A presente dissertação centra-se no estudo do processo de arrefecimento e congelamento de gotas de água em queda livre. O fenómeno de congelamento é de extrema relevância na área de Engenharia Aeronáutica, uma vez que devido ao impacto de gotas nas superfícies sustentadores de uma aeronave e conseqüente acumulação de gelo, poderão ocorrer incidentes e acidentes com as aeronaves. Uma acumulação de apenas 0.4 mm poderá levar a uma perda de sustentação de até 25 %. Como forma de impedir a formação e acumulação de gelo, existem diversos sistemas para combater este perigo. Métodos tais como libertar fluidos anti gelo ou forçar ar quente por forma a derreter o gelo são formas empregues no combate a este perigo. As áreas críticas de uma aeronave estão normalmente protegidas por estes sistemas anti gelo. No entanto, embora estes métodos consigam evaporar gotas de água ou derreter o gelo acumulado, existe ainda a possibilidade de formação de gelo a jusante devido a um novo congelamento da mistura gelo-água em áreas desprotegidas.

De forma a compreendermos o fenómeno de congelamento e o efeito de acumulação de gelo e podermos simulá-los com a maior eficiência possível, surge uma necessidade de estudar e adaptar os modelos físicos e matemáticos existentes para uma melhor aproximação a situações reais, por forma a contribuir para uma redução do número de incidentes e acidentes, melhorando as condições de segurança.

O objetivo deste trabalho passa pela realização de um estudo numérico com o intuito de estudar o arrefecimento de gotas de água em queda livre para diferentes diâmetros e razões de humidade. O processo de arrefecimento trata-se de uma fase fundamental do fenómeno de congelamento e poderá estar presente em diversas fases deste.

Um modelo *Two-Way Coupling* é utilizado como ferramenta para realizar previsões que são comparadas com dados experimentais e previsões realizadas com um modelo *One-Way Coupling*. São consideradas as correlações de Ranz-Marshall, com e sem um fator de correção, para além da abordagem de Abramzon e Sirignano, como forma de ter em conta os efeitos de convecção. Comprova-se que para razões de humidade elevadas, verifica-se regime transiente, enquanto para razões de humidade reduzidas regime permanente. Verifica-se que as diferentes correlações utilizadas têm bastantes semelhanças nas previsões, aproximando-se cada vez mais à medida que a razão de humidade é aumentada.

Conclui-se que foi possível modelar numericamente o arrefecimento de gotas de água em queda livre através de um modelo *Two-Way Coupling* e prever com rigor as condições de regime transiente.

Abstract

The present dissertation focuses on the study of the process of cooling and freezing of free falling water droplets. The freezing phenomenon is of extreme relevance in aviation since the impact of drops on lifting surfaces of an aircraft and consequent accretion can lead to the occurrence of incidents and accidents.

In order to prevent the formation and accretion of ice, there are several systems to combat this hazard. Critical areas of an aircraft are usually protected by these de-icing systems. However, although these methods can evaporate drops of water or melt the accreted ice, there is still the possibility of downstream ice formation due to new freezing of the ice-water mixture in unprotected areas.

Thus, there is a need to study and adapt the existing physical and mathematical models for a better approximation to real-life situations, in order to contribute to a better understanding of this phenomenon and consequently lead to a reduction in the number of incidents and accidents, safety conditions.

The objective of this work is to perform a numerical study with the purpose of studying the cooling of free falling water droplets for different diameters and humidity ratios. Ranz-Marshall relations are used, with and without a correction factor, in addition to the Abramzon and Sirignano approach to take into account the effects of convection. A Two-Way Coupling approach is used being the predictions compared with experimental data and numerical predictions in a One-Way Coupling approach.

Keywords

Heat and mass transfer, Humidity ratio, Cooling, Freezing, Two-Way Coupling

Index

Chapter I:

1. Introduction	3
1.1 Motivation	8
1.2 Objectives	8
1.3 Overview	8

Chapter II:

2. Physical Models	13
2.1 Introduction	13
2.2 Two-Phase Flow	15
2.3 Phase Change Phenomena	16
2.3.1 The Stefan Problem	18
2.4 Physical Phenomena	19
2.4.1 Heat Transfer	20
2.4.2 Freezing Phenomena	20
2.5 Freezing models	22
2.5.1 Four Stage Freezing Model	22
2.5.2 Three Stage Freezing Model	26
2.5.3 Moving boundary models	28

Chapter III:

3. Mathematical Models	33
3.1 One-Way Coupling Model	33
3.2 Two-Way Coupling Model	35
3.2.1 Continuous phase	36
3.2.2 Dispersed phase	39
3.2.3 Interaction between the continuous and the dispersed phase	41
3.2.4 Solution procedure	41
3.3 Computational domain configuration	42
3.3.1 Boundary Conditions	44
3.4 Cooling Model	44
3.4.1 Convection effects correlations	46
3.5 Initial conditions	49
3.6 Grid Independence	49

Chapter IV:

4. Results and Discussion	53
---------------------------	----

4.1 Influence of humidity ratio and drop diameter on the cooling process of a single drop free falling	53
4.1.1 Ranz-Marshall classical formulation	53
4.1.2 Ranz-Marshall classical formulation, Ranz-Marshall correction factor and Abramzon and Sirignano correlations	57
4.2 Influence of humidity ratio and drop diameter on the cooling process of drop free falling considering a flow mass ratio of $0.1 \text{ kg}_{\text{water}}/\text{kg}_{\text{air}}$	62
4.2.1 Ranz-Marshall classical formulation, Ranz-Marshall correction factor and Abramzon and Sirignano correlations	62
4.3. Summary	66
<u>Chapter V:</u>	
5. Conclusions and Future Work	71
<u>Chapter VI:</u>	
6. Bibliographic References	75
<u>Attachments:</u>	
Attachment A. List of publications	83

List of Figures

Chapter II:

- Figure 2.1** - Cooling curves for a) normal freezing and b) with supercooling, adapted from Alexiades and Solomon (1993). 17
- Figure 2.2** - Schematic of a freezing droplet, adapted from Hindmarsh et al. (2003). 21
- Figure 2.3** - Temperature transition of the four stages of freezing of a droplet: 1- pre-cooling or supercooling; 2-recalescence; 3-freezing; 4-cooling or tempering, adapted from Tanner (2010). 22

Chapter III:

- Figure 3.1** - Heat and mass balance of a column of air in a differential element, adapted from Magalhães (2016). 34
- Figure 3.2** - Flowchart for the calculation of the rate of cooling of a system of drops in free fall, adapted from Magalhães (2016). 35
- Figure 3.3** - Flowchart of the iterative process, adapted from Rodrigues (2016). 42
- Figure 3.4** - Computational Domain. 43
- Figure 3.5** - Computational Domain in a 2D schematic. 43
- Figure 3.6** - Grid independence for positions of a) $x/l=0.25$, b) $x/l=0.50$, c) $x/l=0.75$, d) $x/l=1.00$, e) $x/l=1.50$ and f) $x/l=2.00$. 50

Chapter IV:

- Figure 4.1** - Variation on a single drop temperature falling through the air for a humidity ratio of 0.29 and a diameter of a) 3 mm and b) 5 mm. 54
- Figure 4.2** - Variation on a single drop temperature falling through the air for a humidity ratio of 0.36 and a diameter of a) 3 mm, b) 4 mm, c) 5 mm and d) 6 mm. 55
- Figure 4.3** - Variation on a single drop temperature falling through the air for a humidity ratio of 0.52 and a diameter of a) 4 mm and b) 6 mm. 56
- Figure 4.4** - Variation on a single drop temperature falling through the air for a humidity ratio of 1.00 and a diameter of a) 3 mm, b) 4 mm, c) 5 mm and d) 6 mm. 57
- Figure 4.5** - Variation on a single drop temperature falling through the air for a humidity ratio of 0.29 and a diameter of a) 3 mm and b) 5 mm for different correlations. 59
- Figure 4.6** - Variation on a single drop temperature falling through the air for a humidity ratio of 0.36 and a diameter of a) 3 mm, b) 4 mm, c) 5 mm and d) 6 mm for different correlations. 60

Figure 4.7 - Variation on a single drop temperature falling through the air for a humidity ratio of 0.52 and a diameter of a) 4 mm and b) 6 mm for different correlations.	61
Figure 4.8 - Variation on a single drop temperature falling through the air for a humidity ratio of 1.00 and a diameter of a) 3 mm, b) 4 mm, c) 5 mm and d) 6 mm for different correlations.	62
Figure 4.9 - Variation on drop temperature falling through the air for a humidity ratio of 0.29 and a diameter of a) 3 mm and b) 5 mm for a flow mass ratio of 0.1 and different correlations.	63
Figure 4.10 - Variation on drop temperature falling through the air for a humidity ratio of 0.36 and a diameter of a) 3 mm, b) 4 mm, c) 5 mm and d) 6 mm for a flow mass ratio of 0.1 and different correlations.	64
Figure 4.11 - Variation on drop temperature falling through the air for a humidity ratio of 0.52 and a diameter of a) 4 mm and b) 6 mm for a flow mass ratio of 0.1 and different correlations.	65
Figure 4.12 - Variation on drop temperature falling through the air for a humidity ratio of 1.00 and a diameter of a) 3 mm, b) 4 mm, c) 5 mm and d) 6 mm for a flow mass ratio of 0.1 and different correlations.	66

List of Tables

Chapter I:

Table 1.1 - ASRS Icing related Incidents by Flight-Stage, adapted from Jones et al. (2008).	4
Table 1.2 - ASRS Icing related Incidents by Engine Type, adapted from Jones et al. (2008).	4
Table 1.3 - Types of ice, adapted from Cao et al. (2018).	5
Table 1.4 - Characteristics of glaze ice and rime ice, adapted from Cao et al. (2018).	6
Table 1.5 - Icing codes.	6

Chapter II:

Table 2.1 - Physical factors involved in a phase change, adapted from Alexiades and Solomon (1993).	19
--	----

Chapter III:

Table 3.1 - Terms in the general form of the differential equation.	38
Table 3.2 - Coefficients of the “k-ε” turbulence model, adapted from Launder and Spalding (1974).	38
Table 3.3 - Source terms of the dispersed phase, adapted from Sommerfeld (1998).	41
Table 3.4 - Initial conditions for the simulations.	49

Chapter IV:

Table 4.1 - Initial conditions for the simulation of a humidity ratio of 0.29.	54
Table 4.2 - Initial conditions for the simulation of a humidity ratio of 0.36.	55
Table 4.3 - Initial conditions for the simulation of a humidity ratio of 0.52.	56
Table 4.4 - Initial conditions for the simulation of a humidity ratio of 1.00.	56
Table 4.5 - Convection effects correlations.	58

Nomenclature

B	Transfer number	-
B_M	Mass transfer number	-
B_T	Thermal transfer number	-
C.F.	Correction factor	-
C_D	Drag coefficient	-
C_p	Specific heat at constant pressure	$\text{m}^2/\text{s}^2/\text{K}$
D	Droplet diameter	M
D_g	Diffusion coefficient	-
E_v	Activation energy	J/kg
F	Correction factor	-
F_M	Correction factor	-
F_T	Correction factor	-
g	Gravitational acceleration	m/s^2
G	Turbulence energy production term	$\text{kg}/\text{m}/\text{s}^3$
hr	Humidity ratio	-
h_0	Convective heat transfer coefficient	-
h_m	Convective mass transfer coefficient	-
k	Turbulent kinetic energy	m^2/s^2
k_d	Heat conduction coefficient inside the droplet	-
k_g	Thermal conductivity of the ambient gas	$\text{kg m}/\text{s}^3/\text{K}$
k_m	Kinetic coefficient	-
L	Latent heat	m^2/s^2
m_g	Air mass flow	kg/s
m_w	Water mass flow	kg/s
\dot{m}	Rate of cooling	kg/s
P	Pressure	$\text{kg}/\text{m}/\text{s}^2$
q_h	Heat flux due to convective heat transfer	W/m^2
q_m	Heat flux due to convective mass transfer	W/m^2
q_r	Heat flux due to thermal radiation	W/m^2
Q_L	Heat penetrating inside the droplet	$\text{kg m}^2/\text{s}^3$
S	Source term	-
T	Temperature	K
T_f	Equilibrium freezing temperature	K
T_m	Melting temperature	K
T_n	Nucleation temperature	K

T_s	Solidification temperature	K
U	Velocity	m/s
V	Vertical component of velocity	m/s
V_f	Portion of droplet volume that is solidified	m ³
V_g	Velocity of the gas	m/s
Vol	Volume	m ³
W	Humidity	-
W_s	Saturation humidity	-
x	Horizontal coordinate	m
Y	Mass fraction	-
z	Vertical coordinate	m

Greek Symbols

Γ	Effective diffusion coefficient	-
ε	Rate of dissipation of turbulence energy	m ² /s ³
μ	Viscosity	kg/m/s
ρ	Density	kg/m ³
σ	Surface tension	kg/s ²
τ	Dimensionless temperature variation	-
τ_d	Droplet relaxation time	s
Φ	Dependent variable	-

Subscripts

d	Related to the droplet	-
g	Related to the gas	-
h	Related to heat transfer	-
m	Related to mass transfer	-
r	Related to radiation	-
sd	Related to the droplet surface	-
v	Related to the vapor	-
w	Related to water	-

Non-dimensional numbers

Bi	Biot number	-
Nu	Nusselt number	-
Pr	Prandtl number	-
Re	Reynolds number	-
Sc	Schmidt number	-
Sh	Sherwood number	-

List of Acronyms

AOPA	Aircraft Owners and Pilots Association
ASRS	Aviation Safety Reporting System
CFD	Computational Fluid Dynamics
FAA	Federal Aviation Administration
ICAO	International Civil Aviation Organization
LWC	Liquid Water Content
NASA	National Aeronautics and Space Administration
PCM	Phase Change Material
QUICK	Quadratic Upstream Interpolation for Convective Kinetics
SIMPLE	Semi-Implicit Method for Pressure-Linked Equations
SLD	Supercooled Large Droplet
TDMA	Tri-Diagonal Matrix Algorithm

Chapter I

Introduction

1. Introduction

1.1 Motivation

The present work aims to study the cooling of free falling water droplets, as part of the process of freezing. This study consequently leads to the research of ice formation on the surfaces of an aircraft, which presents itself as a topic of extreme interest in aeronautical engineering. Due to the various applications of an aircraft, they are required to operate in all types of weather conditions in order to accomplish their proposed mission.

The necessity of studying the process of freezing in aircraft surfaces arises from the several accidents and incidents that occurred due to this atmospheric phenomena. An accretion of ice of merely 0.4 mm on a wing upper surface may cause a loss of 25% of lift and decrease the stall angle of attack by 6° , as Myers et al. (2002) point it out and aircraft often fly under subfreezing temperatures, as Zhou et al. (2015) refer.

As Ruberto et al. (2016) stated, although suffering sub-zero temperatures, the droplets can still be liquid, being called supercooled. Whenever an aircraft flies through clouds at an ambient temperature below freezing, SLD (Supercooled Water Droplets) suspended in the clouds can impact and accrete ice mainly on the leading edge of the wing, on the tail and around engines intakes, according to Elliot and Smith (2015).

Cao et al. (2015) made reference to statistic data given from the American Safety Advisor, from AOPA (Aircraft Owners and Pilots Association) respecting to iced aircraft flight accidents from 1999 to 2000 and concluded that 12% of all accidents which took place in adverse weather conditions occurred due to icing and 92% of the accidents induced by icing took place in in-flight icing. Caliskan and Hajiyev (2013), regarding the icing related accidents in large and small commercial aircraft between 1998 and 2007, resorted to a NASA (National Aeronautics and Space Administration) database to conclude that 730 accidents occurred due to the icing phenomena.

As Cao et al. (2018) stated, between 1986 and 1996, the passenger mortality rate reached 39% among 42 aircraft icing accidents, accordingly to ICAO (International Civil Aviation Organization).

In a report with the goal of studying the Subsonic Aircraft Safety Icing, Jones et al. (2008), gathered incident reports between January 1988 and February 2007. Table 1.1 presents the ASRS (Aviation Safety Reporting System) icing related incidents by flight stage, concluding that

the height of the incidents occurs during cruise flight with 325 incidents, followed by descent operations.

Table 1.1 - ASRS Icing related Incidents by Flight-Stage, adapted from Jones et al. (2008).

Flight stage	Number of incidents reported
Climb-out	98
Cruise	325
Descent	193
Ground	106
Landing	133

Table 1.2 shows icing related incidents grouped by engine type, being clearer that the reciprocating and turbojet aircraft are the most likely to suffer from icing.

Table 1.2 - ASRS Icing related Incidents by Engine Type, adapted from Jones et al. (2008).

Engine type	Number of incidents reported
Reciprocating	223
Turbojet	208
Turboprop	87
Unknown	46

In case of this rate of accidents stays constant and the growth in air transportation continues to climb at the current rate, accordingly to the FAA (Federal Aviation Administration) by 2025 there will be more than 4500 air travel fatalities per year due to icing related accidents, as indicated by Caliskan and Hajiyev (2013).

Accordingly to Myers et al. (2002) the growth of ice that occurs on an aircraft is mainly derived to the impact of supercooled water droplets on a cold surface. Depending on the structure of the ice and the physical changes that take place during the freezing process, there are three possibilities of ice formation: rime ice, glaze ice or mixed ice, as Zhou et al. (2015).

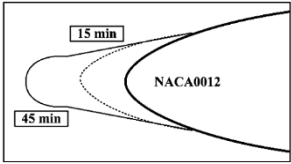
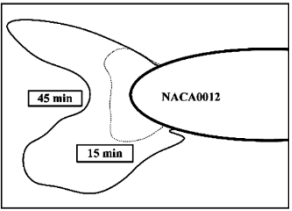

The first basic type typically occurs in very cold conditions with ambient temperature below -15°C and low airspeed and is associated with low LWC (Liquid Water Content), which implies that the droplets freeze almost instantaneously upon impact. Therefore rime ice, a regular white opaque accretion, does not involve water flow and is relatively streamlined but it has a much greater surface roughness than the wing.

The formation of glaze ice, as stated by Elliot and Smith (2015), occurs at ambient temperatures closer to freezing, at high airspeeds or when water droplets are large, which contributes to the fact that only a fraction of the droplet will freeze instantaneously. The remaining of the droplet stays liquid for some time and may flow as runback water. The ice assumes then horned shapes on both the upper and lower surfaces. It is widely distributed along the surface of the wing chord and does not have air bubbles, being transparent, dense and has an irregular shape. This type of ice is much more complex than rime ice and thus more difficult to simulate computationally.

In fact, aircraft icing has often the characteristic of a mixture of glaze and rime ice, as referred by Cao et al. (2018), with no fixed ice shape, since LWC and water droplet diameter in the atmosphere vary widely. Mixed ice is formed in the clouds with a temperature range from -20°C to -10°C. In this range of temperature the ice assumes both glaze ice characteristics with double horn shape and milky white rime ice characteristic, due to the variety of sizes of supercooled water droplets.

The different ice types are presented in Table 1.3.

Table 1.3 - Types of ice, adapted from Cao et al. (2018).

Types of ice	Rime	Glaze	Mixed
Example			

Accordingly to Zhou et al. (2015), the accretion rate and ice type depend on the airflow parameters and on the inner heat transfer characteristics. Different types of ice may influence in different ways the flight performance and even sometimes the same kind shows different effects under icing conditions.

Table 1.4 presents a summary of the characteristics of glaze ice and rime ice.

Table 1.4 - Characteristics of glaze ice and rime ice, adapted from Cao et al. (2018).

Conditions	Rime ice	Glaze ice
Temperature	Cold: less than -10°C	Warm: 0 to -10°C
LWC	Low	High
Density	Low	High
Airspeed	Low	High
Color	Milky / opaque	Glossy / clear
Texture	Rough	Smooth
Runback	No	Yes
Fragility	Fragile	Hard
Water droplet size	Small	Large
Airfoil ice shape	Streamlined / spearheaded	Single or double horn

To prevent the solidification of water droplets and consequently ice accretion on an aircraft surface, several methods to avoid and to remove the ice are implemented. Normally the critical areas of the aircraft are equipped with de-icing technology. As Elliot and Smith (2015) state, warm bleed air from engine compressors or forcing freezing point depressant fluid out of porous panels are methods to fight this hazard. However, although those measures can evaporate impinging water droplets or melt the accreted ice, there is still the potential risk of runback ice forming further downstream due to a refreezing of the ice-water mixture on unprotected areas. Accordingly to Wang et al. (2016), SLD tend to have greater inertia and are able to impinge on aircraft surfaces far beyond the limits of the ice protection systems.

In order to study ice accretion, several approaches have been developed, namely through icing tunnel testing, flight testing, natural icing testing and numerical simulation. The last method enables to investigate the entire icing envelope, becoming the major reason why it is suffering considerable progress, as Cao et al. (2016) refer. It is also an economical, efficient and accurate model to investigate this issue, as referred by Xin et al. (2014).

Several numerical models have been developed. Most of the icing codes that are used follow the Messinger method, described by Messinger (1953), in which a Stefan phase change approach is used, as stated by Kong and Liu (2012). These codes have been created by some countries or organizations and are described in Table 1.5, along with the method of calculation the droplet distribution.

Table 1.5 - Icing codes.

Icing Codes	Droplet Distribution Approach
LEWICE (NASA)	Lagrangian
TRAJICE (DRA)	Lagrangian
FENSAP-ICE	Eulerian
ONERA	Lagrangian
CIRA	Lagrangian

These icing codes are very similar in the basic simulation procedure. They can be divided into three major modules, as Cao et al. (2016) states.

The first module includes the solution of the governing equations for air flow field, which may adopt different methods in order to solve it. Earlier codes, for instance LEWICE and ONERA, may use a panel method with an appropriate compressibility correction or a Euler method to calculate the inviscid flow field.

The second module calculates droplet collection efficiency based on the airflow field solution from the previous module; the third module calculates the icing properties and generates the ice shape based on appropriate icing models.

The icing process is divided into several intervals according to certain criteria during which the airflow field and the droplet impingement characteristics are considered constant since, in practical applications, the coupling icing process is time-varying due to the ever-changing ice shape. It is regarded as quasi-steady in one simulation step.

Due to the advancement in modern CFD approaches, current icing codes like FENSAP-ICE solve the set of Navier-Stokes equations directly without any boundary layer technique involved.

Most icing codes based their icing model on the classical Messinger model, described by Messinger (1953), or its improved versions. As this kind of model was initially developed for two-dimensional cases like an airfoil, its implementation in a three-dimensional case has met with some difficulties and some special measures have been taken to get them around.

In order to calculate the droplet efficiency distribution, which is of great importance in icing simulation, two methods are possible: Lagrangian tracking method and Eulerian two-phase flow method.

The Lagrangian tracking method, as stated by Cao et al. (2016) focus on a single droplet, with its motion equation established by Newton's second law and solved by the ODE (original Differential Equation) algorithms, such as the Runge-Kutta method in order to obtain its trajectory throughout the surrounding domain. The reference frame moves with the droplets with the instantaneous position of the droplet being considered a function of the location from where the droplet originated and the time elapsed, as stated by Silva (2007). This approach requires less computational resources.

The Eulerian two-phase flow method, as Cao et al. (2016) mentions has gained more popularity over the years. It considers the droplet to be a pseudo-fluid phase, considers the reference frame stationary and solves the continuity and momentum equations regarding the droplets'

phase, for a fixed control volume, which is a similar process for the air phase. This method brings about a large amount of extra computational effort.

Accordingly to Crowe et al. (2012), coupling presents itself as an important concept in the analysis of multiphase flows. In the eventuality of one of the phases affecting the other while there is no reverse effect, the flow is One-Way Coupled. In the present dissertation, the flow will be two-way coupled, meaning that there is a mutual effect between the flows of both phases. It presupposes that not only the particle movement is affected by the flow, but the flow around the particle is also affected by the presence of particles.

It is imperative to fully comprehend the freezing process and the ice accretion effect and develop models capable of simulating it. With those, engineers could predict with maximum efficiency freezing and avoid this phenomenon or even take advantage of it and develop new technologies that ultimately will improve air travel.

1.2 Objectives

The objectives of this dissertation are the following:

- Numerically modeling the cooling of free falling water droplets, using a Two-Way Coupling approach.
- Verify if the Two-Way Coupling approach proves to be a better approximation than the One-Way Coupling approach.

The scenario analyzed in the present work consists of an injection of water droplets onto a tunnel where air is also inserted with the goal of studying the interaction between the liquid and gas phases, in order to cool water droplets.

This dissertation has the goal to contribute to the development of a model capable of simulating with accuracy the impact of water droplets onto aircraft surfaces and ice accretion.

1.3 Overview

The present dissertation is organized in 5 chapters. The current chapter provides the context and the main goals of the research undertaken. Chapter II addresses the physical models regarding cooling and freezing of water droplets. The whole process is reviewed as well as methods of numerically simulating real-life situations. Chapter III presents a description of the methodology adopted in the mathematical model implemented. A Two-Way Coupling model is

presented in which the continuous phase and the dispersed phase are distinguished and their interaction with each other is displayed. The computational domain configuration and the initial conditions are also contained in this chapter. The results of the numerical analysis are presented and examined in Chapter IV. Finally, the last chapter, Chapter V, summarizes the most important conclusions obtained throughout this research and also presents some suggestions for future work.

Chapter II

Physical Models

2. Physical Models

This chapter presents the physical models regarding the topic in study. It starts with an introduction to the topic of heat and mass transfer of cooling and freezing droplets. Section 2.2 presents the description of a two-phase flow. The following section discusses the phase change phenomena. Afterward, it is considered the freezing phenomena. Finally, Chapter II ends with the consideration of freezing models, namely a four stage, three stage and moving boundaries models.

2.1 Introduction

Heat and mass transfer of cooling and freezing droplets has always been somewhat neglected in favor of the heating and evaporation of droplets. This field in the last few years has started to being investigated in a deeper way. However, when it is necessary to approximate the investigations to the real cases, there are not enough conclusions. The aeronautics and aerospace fields are the main responsible for the development of this area of research since ice accretion presents itself as a real hazard that can contribute to a catastrophic disaster in mid-flight.

Lapple and Sheperd presented equations and drag coefficients in 1940 with the goal of calculating the trajectories of individual spherical particles in an accelerated fall in a viscous fluid. Their investigation contributed to further studies of impact and collision of droplets, such as Kóllar et al. (2015), which proved that the amount of ice accreted is determined by droplet trajectory, geometry of the icing object and air stream velocity, in the case of droplet collisions.

When Ranz and Marshall (1952) studied the evaporation from drops only a small amount of work had been done regarding the heat and mass transfer of that topic. The most relevant conclusion was the confirmation of the analogy between heat and mass transfer. They also showed that there was a correlation between the Nusselt and Sherwood numbers in terms of Reynolds, Schmidt and Prandtl numbers. Ranz and Marshall noted that when a drop of pure liquid forms a solid structure with a constant diameter, the falling rate period ensued during which the temperature of the drop rose continually, due to the heat of the crystallization and sensible heat transfer.

Yao and Shrock (1976) modified the equations elaborated by Ranz and Marshall in order to include the effects of acceleration, while experimentally studied the topic of heat and mass

transfer on freely falling drops, same as Zarlring in 1980. Nevertheless, the model developed by the researcher did not take into account changes in the air temperature and humidity as the drop falls. Analyzing the results, stated that drops that travel higher distances cool more and with smaller drops, the thermal equilibrium condition between the drops and the air is approached.

Dickinson and Marshall (1968) also considered evaporation but in this case, it was the rate of evaporation from sprays and they were able to make relations between the drops mean diameter and size distribution, initial drop velocity and air temperature, and air velocity and temperature.

Hughes and Gilliland presented in 1952 a paper with a focus on making correlations on the effect of acceleration on drag, equilibrium distortion or oscillations from prolate to oblate spherical shapes and also making emphasis on the internal circulation caused by skin friction. This study was made investigating the motion in and around drops. Magalhães et al. (2016) performed a numerical study on free falling of droplets using the Ranz-Marshall relations which enabled them to state that the drops vibrations and oscillations may play an important role in the dynamic process.

Langham and Mason presented an extensive review of nucleation temperatures of supercooled water drops in 1958. This topic was also studied for small water drops into ice in 1970, by Benson.

1969 was the year when Chao investigated and performed an analytical study on transient heat and mass transfer, including internal circulation within the drop and made an analysis on boundary layer similarity at the surface of the drop to achieve transient and steady-state Nusselt numbers.

Chen and Trezek (1977) applied to the single drop thermal performance model a wet bulb temperature weighting factor to account for local temperature and humidity variations within a field of a spray.

Nauenberg (2016) was able to take into account in his calculations the time-varying temperature at the base of a droplet on a cold surface, which had been considered a constant by several authors. His measurements showed that during the freezing process that temperature is not constant and that for small drops it varies rapidly.

Accordingly to Chen et al. (2015), the atmospheric pressure plays a significant role in the droplet growth and freezing stage. The frozen droplet diminishes with the decrease of the atmospheric pressure.

When Jin et al. (2014) performed an experimental investigation on the icing process of a water droplet on a cold surface, they concluded that after the solidification of the droplet, a layer of frost crystals appeared only on the top of the ice bead, with a shape of feathers and grew in normal direction to the surface of the ice bead, and the remaining surface of bead stayed nearly unchanged.

Recently, several authors such as Cao et al. (2016) were able to perform a numerical analysis to simulate ice accretion on aircraft wings and prove its decay on the aerodynamic performance of an aircraft.

All of this research contributed to the implementation and improvement of icing models. Without the conclusions obtained by the previous authors, it would not be possible to produce computational tools capable of simulating with accuracy the freezing phenomena.

2.2 Two-Phase Flow

Two-phase flows have gained importance in a wide variety of engineering systems in order to optimize their design and safe operation, as Ishii and Hibiki (2006) refer. It is important that the various characteristics and physics of two-phase flow be modeled and supported by experimental detailed data. The characteristic of a two-phase mixture is the presence of one or several interfaces separating the phases.

The complexity of two-phase flows regarding a single phase flow originates from the existence of multiple, deformable and moving interfaces and significant discontinuities of fluid properties and complicated flow near the interface.

Although single phase flow can be classified into laminar, transitional and turbulent, two-phase flow can be classified according to the structure of interface into several groups called regimes. Namely: separated flow, transitional or mixed flow and dispersed flow. Separated flow considers two streams of different fluids separated by interfaces and dispersed flow means those consisting of finite particles that are distributed in a connected volume of the continuous phase, as Brennen (2005) refers.

The variety of two-phase flows depends on combinations of two phases as well on interface structures, which may be several and possess discontinuities. An example of two-phase flow is a mixture of a liquid and a gas, for instance, liquid droplets in a gas.

In order to describe a two-phase flow, three conservation equations are required for each phase: mass, momentum and energy conservation. Accordingly to Hirsch (2007), the equation for mass conservation is also called the continuity equation, the momentum conservation is also expressed by Newton's law, which defines the equation of motion of a fluid. The energy conservation law is also referred to as the expression of the first principle of Thermodynamics.

In order to simulate a two-phase flow, several other equations should be implemented to supplement the conservation laws, namely equations that specify molecular diffusions, turbulent transports, an interfacial transfer mechanism as well as a relation between the thermodynamic state variables.

2.3 Phase Change Phenomena

The melting of ice and solidification of water are, as Johnsson (2013) states, examples of phase transformation, a discontinuous change of the properties in the substance. In the transition, the different stages of aggregation are named phases, sharing the same physical properties, such as density and chemical composition. Accordingly to Alexiades and Solomon (1993) heat transfer, mass transfer, absorption or release of latent heat are just some of the different processes involved in a phase change.

Before we comprehend the process of phase change it is primarily required to comprehend the basic concepts. In a solid it occurs a vibration of the molecules around fixed equilibrium positions. In liquids, the molecules may occupy different equilibrium positions. In a macroscopic visualization, this vibrational energy is called heat or thermal energy, measured by temperature.

In order to a phase change to occur it is necessary a certain amount of energy, referred as Latent Heat, L . It represents the difference of thermal energy levels, also called enthalpy, between the two states. It is important to refer that there is no change in temperature during this period.

Heat transfer may occur in three different modes, namely conduction, convection and radiation.

Heat transfer by conduction can be defined as the transfer of kinetic energy between atoms by any number of ways such as the collision of neighboring atoms and the movement of electrons. The material does not suffer any flow or mass transfer. In a liquid, heat can also be transferred by convection, which is by flow of particles. Heat flow can be understood using statistical

mechanics that use probability theory applied to thermodynamics, as referred by Johnsson (2013).

The absorption or release of latent heat, also known as the transition from one phase to the other, occurs at the temperature at which the stability of one phase breaks down in favor of the other phase accordingly to the available energy. This phase change can be described by T_m , melting temperature and depends on pressure. In case of a fixed pressure, T_m may be a fixed value characteristic of each material. For instance, pure water under atmospheric pressure freezes at 273.15 K.

As already mentioned in Chapter 1, supercooling may occur in a freezing process, meaning that exists liquid at temperatures below T_m .

Figure 2.1 shows the curves for a) normal freezing and b) supercooling, which allows observing the possible effects of supercooling.

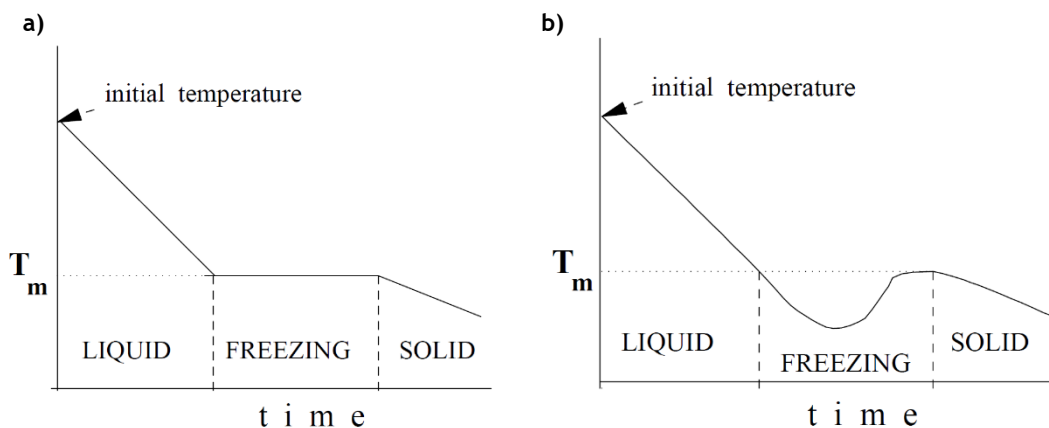


Figure 2.1 - Cooling curves for a) normal freezing and b) with supercooling, adapted from Alexiades and Solomon (1993).

These curves represent the temperature of a sample of material as a function of time as heat is extracted from the sample at a constant rate. It is noticeable that in supercooling the temperature rapidly rises back to T_m when the crystallization process takes place. This is only possible if the latent heat released upon freezing is sufficient to raise the temperature to T_m , meaning that the liquid was not cooled too much. The phase-transition region in which solid and liquid coexist is called the interface.

The most fundamental and pronounced effects are caused due to changes in material density. When freezing or melting occur, density changes are in the range of 5% to 10%, however, they can reach up to 30%. This density variation with the temperature induces flow by natural convection in the presence of gravity which causes rapidly equalizing the temperature in the

liquid, therefore affecting heat transfer. A material that undergoes a phase change is often referred to as by PCM (Phase Change Material).

2.3.1 The Stefan Problem

The Stefan problem is the simplest mathematical model of a phenomenon of phase change. Accordingly to Alexiades and Solomon (1993), this model known as The Classical Stefan Problem constitutes the foundation on which progressively more complex models can be built by incorporating some of the effects that initially are left out. Phase change problems have the particularity that in addition to the temperature field, the location of the interface is unknown.

The classical problem considers an initial boundary value problem for a differential equation. Since a portion of the domain is a free boundary, two boundary conditions have to be considered to obtain a well-posed problem. Some complexity can be added to the classical problem itself if effects that are not considered in the classical approach be taken into account.

Accordingly to the physical factors involved in phase change processes, different assumptions must be adopted in order to solve the Stefan problem. Thus, it is necessary to know exactly which phenomena are being analyzed since the assumptions only make sense in case of a correct application on the problem.

Table 2.1 presents a summary of the physical factors involved in a phase change and the simplifying assumptions that will lead to the Classical Stefan Problem.

Table 2.1 - Physical factors involved in a phase change, adapted from Alexiades and Solomon (1993).

Physical Factors Involved in Phase Change Processes	Simplifying Assumptions for the Stefan Problem	Remarks on the Assumptions
Heat and mass transfer by conduction, convection, radiation with possible gravitational, elastic, chemical and electromagnetic effects	Heat transfer isotropically by conduction only, all other effects assumed negligible	Most common cause. Very reasonable for pure materials, small container, moderate temperature gradients
Release or absorption of latent heat	Latent heat is constant; it is released or absorbed at the phase-change temperature	Very reasonable and consistent with the rest of the assumptions
Variation of phase-change temperature	Phase-change temperature is a fixed known temperature, a property of the material	Most common case, consistent with other assumptions
Nucleation difficulties, supercooling effects	Assume not present	Reasonable in many situations
Interface thickness and structure	Assume locally planar and sharp (a surface separating the phases) at the phase-change temperature	Reasonable for many pure materials (no internal heating present)
Surface tension and curvature effects at the interface	Assume insignificantly	Reasonable and consistent with other assumptions
Variation of thermos-physical properties	Assume constant in each phase, for simplicity ($c_L \neq c_S$, $k_L \neq k_S$)	An assumption of convenience only. Reasonable for most materials under moderate temperature range variations. The significant aspect is their discontinuity across the interface, which is allowed
Density changes	Assume constant ($\rho_L = \rho_S$)	Necessary assumption to avoid movement of material. Possibly the most unreasonable of the assumptions

2.4 Physical Phenomena

In order to perform a study on the cooling and freezing of water droplets, first of all, we need to comprehend how the process begins, develops and ends, as well as the relations between all the stages and how they are influenced.

The freezing process as a whole may take only tens of seconds, depending on the ambient conditions, accordingly to Hindmarsh et al. (2003). Under certain conditions, the freezing of a single droplet occurs in a parabolic shape as stated by Elliott and Smith (2017).

2.4.1 Heat Transfer

In a cold atmosphere, in order to cool airborne droplets, heat transfer can occur by three different mechanisms according to Yao and Schrock (1976), heat transfer, mass transfer and thermal radiation from the droplet, as it was already stated. In order to model the internal heat transfer of a droplet, Yao and Schrock (1976) shown two ways of doing it. The first one by solving the internal temperature profile and the other one by assuming a uniform temperature within the droplet.

Assuming a uniform temperature implies that the transient heat transfer of the droplet can be predicted by simply balancing the heat flux from the surface by heat and mass transfer with the internal energy of the droplet. The uniform temperature within a droplet is a product of internal mixing of liquid within the droplet as it was concluded by Yao and Schrock (1976). Assuming this calculation method for the rate of mass and heat transfer, a non-mixing model can be considered.

Considering a complete mixing model it is necessary to assume that the temperature profile is planar and the only place where heat and mass transfer occur is at the drop's surface. The problem can be considered steady-state. The heat flow achieved if complete mixing is used is higher than the heat flow obtained using non-mixing model.

2.4.2 Freezing Phenomena

As Hindmarsh et al. (2003) stated, droplets generally nucleate at the surface forming a frozen shell which propagates inwardly. An accepted definition of the freezing time is the point from the onset of cooling until the center temperature reaches 263.15 K.

The temperature transition of the droplet is solved by balancing the internal energy with the energy removed by heat transfer, q_h , mass transfer, q_m and thermal radiation, q_r .

In Figure 2.2 it is possible to observe the schematic of a freezing droplet. The droplet freezes inwardly from an initial frozen shell.

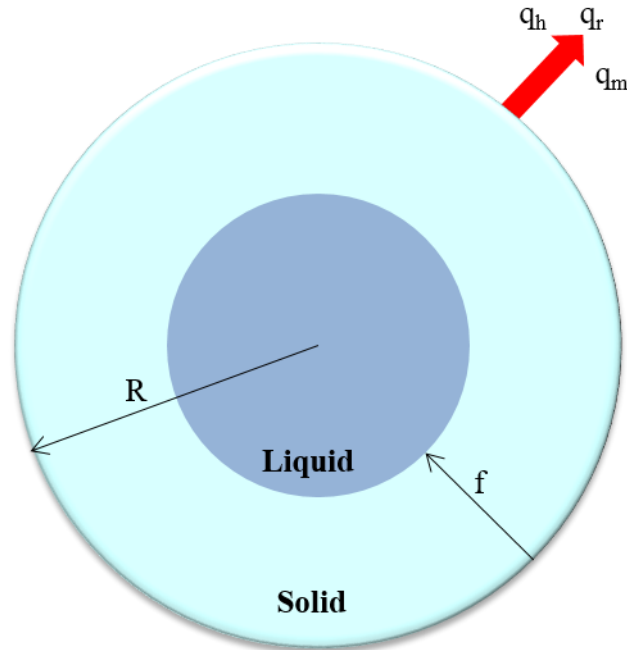


Figure 2.2 - Schematic of a freezing droplet, adapted from Hindmarsh et al. (2003).

Experimentally, Jin et al. (2015) observed that during a freezing process of a water droplet firstly the droplet stays transparent. After a certain period of time, become opaque, in which this transformation happens in a fraction of a second, referencing the three possible explanations given to this phenomenon:

1. Droplet becomes opaque due to the release of air bubbles since air is less soluble in ice than in water;
2. Light scattering due to the partially solidified water;
3. A solid ice shell forms at the droplet surface while the droplet center is still liquid.

This change in optical transparency is used to indicate the beginning of the freezing process by many authors.

Tanner (2010) presents two different models describing freezing. A model composed of four stages and another one composed of three different stages.

The cooling stages and the freezing stage can be modeled by assuming a uniform temperature or by solving the internal heat conduction of the droplet.

Regarding the internal heat conduction, assuming the droplet shape to be constant and spherical it can be described by a one-dimensional model.

The temperature formulation of the transient one-dimensional heat conduction in a spherical droplet is described by:

$$c\rho \frac{\partial T}{\partial t} = \frac{\partial}{\partial r} \left(k \frac{\partial T}{\partial r} \right) + \frac{2k}{r} \frac{\partial T}{\partial r} \quad (2.1)$$

At the droplet surface, where $r = R$, the boundary condition is the sum of the heat fluxes, q_h , q_m and q_r .

$$-k \frac{\partial T}{\partial r} = q_h + q_m + q_r \quad (2.2)$$

2.5 Freezing models

2.5.1 Four Stage Freezing Model

The four stage freezing model, according to Hindmarsh et al. (2003), is presented in Figure 2.3 where it is possible to observe the different transformations that the droplet suffers from the liquid stage till the freezing one.

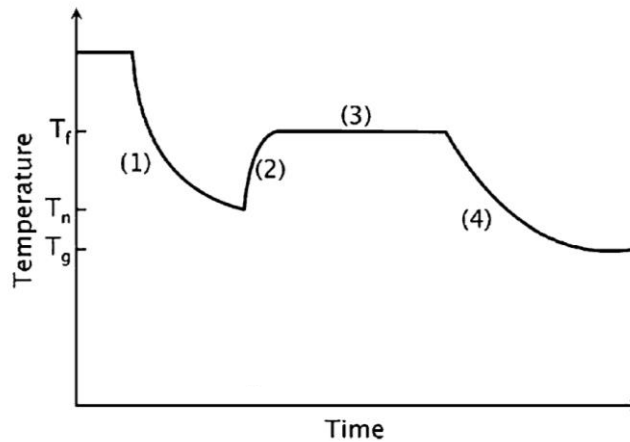


Figure 2.3 - Temperature transition of the four stages of freezing of a droplet: 1-pre-cooling or supercooling; 2-recalcescence; 3-freezing; 4-cooling or tempering, adapted from Tanner (2010).

The first stage of a droplet is referred to as the pre-cooling or supercooling stage. During this stage, the liquid droplet is cooled from its initial temperature to the nucleation temperature, T_n , which lies below the equilibrium freezing temperature, T_f .

Secondly, the recalcescence phase takes place. During this stage supercooling drives rapid kinetic crystal growth from the crystal nuclei, releasing latent heat, resulting in an increase of the temperature. When the supercooling is exhausted and the droplet has reached its equilibrium freezing temperature, T_f , this stage is completed.

The third stage, the freezing one, also called by solidification stage, occurs when crystal growth is governed by the heat transfer rate from the droplet to the point where the liquid is entirely solidified. This growth takes place at the constant equilibrium freezing temperature, T_f , until the droplet is completely solidified.

The fourth and final stage, the cooling or tempering stage, takes place when the solid droplet temperature is reduced to approximately the ambient air temperature, T_g .

Accordingly to Dragomirescu et al. (2016), in models that describe the recalescence stage, icing starts from the inside of the droplet and models describing the subsequent freezing stage typically assume ice starting from the outside.

Experimentally Talhat et al. (2015), while freezing cocoa butter droplets verified that the freezing occurred in an inward manner.

In the two stages where cooling occurs, this phenomenon is determined by the energy exchange of the particles with the environment. Assuming that the particles have a uniform temperature distribution, the rate of temperature change can be evaluated by the following expression:

$$\rho_d Vol_d C_{pd} \frac{dT_d}{dt} = -S_d (q_h + q_m + q_r) \quad (2.3)$$

Where C_{pd} is considered the heat capacity, ρ_d the density, T_d the temperature, Vol_d the volume, S_d the surface, q_h the heat flux per unit area caused by convective heat transfer, q_m the heat flux per unit area caused by the convective mass transfer and q_r the heat flux per unit area caused by the thermal radiation.

From the particle surface to the ambient gas the convective heat flux is given by:

$$q_h = h_0 (T_d - T_g) \quad (2.4)$$

Where T_g is the temperature of the ambient gas and h_0 is the convective heat transfer coefficient.

The heat flux due to the convective mass transfer is calculated by:

$$q_m = Lh_m (\rho_v - \rho_g) \quad (2.5)$$

Where L is the latent heat of phase change, ρ_v the vapor density and h_m the convective mass transfer coefficient.

The heat flux due to thermal radiation is given by:

$$q_r = \varepsilon\sigma(T_d^4 - T_g^4) \quad (2.6)$$

Where ε is the emissivity for thermal radiation and σ is the Stefan-Boltzmann constant of radiation.

The convective heat transfer coefficient, h_0 , is determined from the Ranz-Marshall correlation via the Nusselt number:

$$\text{Nu} = \frac{h_0 D}{k_g} = 2 + 0.6\text{Re}_d^{1/2}\text{Pr}_d^{1/3} \quad (2.7)$$

Where D represents the drop diameter, k_g the thermal conductivity of the ambient gas, Re_d the droplet Reynolds number and Pr_d the droplet Prandtl number, the last two calculated by, respectively:

$$\text{Re}_d = \frac{\rho_g \|U_r\| D}{\mu_g} \quad (2.8)$$

$$\text{Pr}_d = \frac{C_{pg}\mu_g}{k_g} \quad (2.9)$$

In this equations, U_r represents the relative droplet-gas velocity, which is calculated by the norm, ρ_g the density of the surrounding gas, μ_g the viscosity of the surrounding gas and C_{pg} the gas heat capacity at constant pressure.

The convective mass transfer coefficient, h_m , is obtained from the Frössling correlation, presented by Frössling (1938) via the Sherwood number:

$$\text{Sh} = \frac{h_m D}{D_{vg}} = 2 + 0.6\text{Re}_d^{1/2}\text{Sc}_d^{1/3} \quad (2.10)$$

Where D_{vg} is the vapor-gas diffusivity and Sc_d the Schmidt number, calculated by:

$$\text{Sc}_d = \frac{\mu_g}{\rho_g D_{vg}} \quad (2.11)$$

The droplet Reynolds, Prandtl and Schmidt numbers (dimensionless quantities) depend on the material properties. The μ_g , k_g and D_{vg} depend of the surrounding gas, which depends on the gas temperature near the surface of the particle.

Since the gas temperature on the particle surface is in general different from its far-field value, this difference is accounted for by using the two-third temperature average, \bar{T} , in the calculation of these material coefficients, given by:

$$\bar{T} = \frac{T_g + 2T_d}{3} \quad (2.12)$$

Being T_g the temperature of the surrounding gas and T_d the temperature of the droplet.

Incorporating functions to estimate the changing properties adds complexity to the models whilst in some cases it does not significantly increase the accuracy of the model.

In the case of supercooling, after the start of the nucleation, a water droplet experience a rapid temperature increase until it reaches the equilibrium freezing temperature, T_f . Further, the droplet is assumed to change its temperature instantly, neglecting the recalescence time as a consequence.

During this stage, the portion of the droplet volume that is solidified, V_f , can be estimated from the heat balance equation.

$$V_f = Vol_d \frac{\rho_d c_{pd}(T_f - T_n)}{\rho_s L_f} \quad (2.13)$$

Where T_f is the equilibrium freezing temperature, T_n the nucleation temperature, L_f the latent heat due to crystallization and ρ_s the solid particle density.

Compared to the other three stages, the duration of the recalescence stage is extremely short.

After the production of the partially frozen volume fraction, V_f , derived by the nucleation, the freezing of the remaining liquid is controlled by the heat transfer from the droplet to the surrounding gas at the constant equilibrium freezing temperature, T_f . In case of the nucleation being uniformly spread throughout the droplet, the latent heat due to crystallization, L_f , is removed by the external heat fluxes.

Thus, applying this assumption to equation 2.3, the droplet temperature can be deduced by the following equation:

$$\rho_d \text{Vol}_d C_{pd} \frac{dT_d}{dt} = -S_d(q_h + q_m + q_r) + L_f \rho_s \frac{dV_f}{dt} \quad (2.14)$$

Assuming a constant temperature during this stage, $dT_d/dt = 0$, it is possible to calculate the rate at which the volume of solid is produced by using the expression that follows from equation 2.14:

$$L_f \rho_s \frac{dV_f}{dt} = S_d(q_h + q_m + q_r) \quad (2.15)$$

Where V_f is obtained from equation 2.13. In the case of the outer surface of the droplet is assumed to remain liquid during this phase, it is allowed mass transfer via evaporation. In the case of being assumed to be solid, then the mass transfer is due to sublimation. Solving equation 2.15 for each time step, the droplet size has to be updated to compensate for the liquid loss by mass transfer.

The assumption of a uniform droplet temperature is only justified if the Biot number is small, typically with values of $\text{Bi} \leq 0.1$, being determined by:

$$\text{Bi} = \frac{h_0 D}{2k_d} \quad (2.16)$$

Being k_d the heat conduction coefficient inside the droplet.

This stage ends when the water droplet is completely frozen. Dragomirescu et al (2016) confirmed that the temperature in the ice phase of the total freezing process has a quasi-steady behavior.

2.5.2 Three Stage Freezing Model

The three stage model described by Tanner (2010) differentiates from the four stages model in the way that in this model of solidification does not possess the effect of supercooling, consequently, the material does not present recalescence when it starts to solidify.

As soon as the freezing temperature, T_f , is reached, the nucleation, and as a consequence, the crystallization starts. The release of latent heat occurs slowly enough that it does not lead to a temperature increase but to a significant decrease in the droplet cooling rate.

A model that considers only three stages and no significant recalescence can be divided into:

1. Initial cooling stage of the liquid;
2. Crystallization or solidification stage;
3. Cooling stage of the solid particle.

The radiation heat flux, q_r , and the mass heat flux, q_m , can be neglected since radiation is usually not an issue in a freezing spray nor the mass flux due to the fact that droplets are small and freeze rapidly.

The first and third stages are described by a convective heat transfer process with $q_m = q_r = 0$. Applying this assumption in equation 2.3, these stages are described by:

$$\rho_d Vol_d C_{pd} \frac{dT_d}{dt} = -S_d q_h \quad (2.17)$$

Once the droplet reaches the freezing temperature, T_f , the crystallization process begins. It is assumed that the droplet starts solidifying from the outer surface toward the center.

This process can be identified by a drastic decrease in the droplet freezing rate, which leads to a flatter freezing curve, which is a consequence of the release of the latent heat due to the crystallization process.

In the case that the temperature does not remain constant during this stage and assuming $q_m = q_r = 0$, this process is described by:

$$\rho_d Vol_d C_{p\gamma} \frac{dT_d}{dt} = -S_d h_0 (T_d - T_g) + L_f \rho_d \frac{dV_f}{dt} \quad (2.18)$$

Where $C_{p\gamma}$ is the heat capacity of the semisolid droplet which is assumed to vary linearly from the liquid value, C_{pl} , down to its solid value of C_{ps} .

The heat capacity of the semisolid droplet can be determined by:

$$C_{p\gamma} = (1 - \gamma)C_{pl} + \gamma C_{ps} \quad (2.19)$$

With γ being the progress variable that varies linearly from 0 to 1 and is determined by:

$$\gamma = \frac{T_f - T_d}{T_f - T_s} \quad (2.20)$$

T_s being the solidification temperature, meaning that is the temperature at which the particle is completely solidified.

In order to solve equation 2.18, it is necessary to express dV_f/dt . This can be achieved by linearly interpolating the diameter of the liquid portion of the droplet, D_l , by:

$$D_l = (1 - \gamma)D \quad (2.21)$$

Since the droplet solidifies from the surface towards the center, the frozen volume, V_f , can be expressed by the following expression:

$$V_f = \frac{\pi d^3}{6} [1 - (1 - \gamma)^3] \quad (2.22)$$

Its derivative with respect to time is given by:

$$\frac{dV_f}{dt} = -\frac{\pi d^3}{2} \frac{(1 - \gamma)^2}{T_f - T_s} \frac{dT_d}{dt} \quad (2.23)$$

The substitution of equation 2.23 in equation 2.18 gives an expression for the crystallization phase that depends only on the droplet temperature, namely:

$$\rho_g D \left[C_{p\gamma} + 3L_f \frac{(1 - \gamma)^2}{T_f - T_s} \right] \frac{dT_d}{dt} = -6h_0(T_d - T_g) \quad (2.24)$$

This equation can now be solved for the droplet temperature, T_d , keeping in mind that γ and $C_{p\gamma}$ depend on T_d as well.

2.5.3 Moving boundary models

Hindmarsh et al. (2003) stated that assuming that the solid/liquid boundary is a clearly defined interface located at radius f , which propagates at a velocity $U = df/dt$ from or towards the center of the droplet the moving boundary models have to be deployed.

For outward freezing the initial position of the solid/liquid interface is:

$$f_i = R \sqrt[3]{V_f} \quad (2.25)$$

For the inward freezing case:

$$f_i = R^3 \sqrt{1 - V_f} \quad (2.26)$$

The droplet is fully frozen once the interface f had propagated the radius of the droplet. The interface velocity V was driven by the temperature gradient at the phase front and is defined by the additional boundary condition at the solid/liquid interface ($r = l$):

$$\rho_s L_f \frac{df}{dt} = k_s \frac{\partial T_s}{\partial r} - k_l \frac{\partial T_l}{\partial r} \quad (2.27)$$

For inward freezing, the solidification takes place at the equilibrium freezing temperature, T_f . The interface velocity is then directly determined by the energy balance, equation 2.27, and depends on the temperature gradient at the phase front.

For outward solidification the heat transfer was through an undercooled melt therefore, the interface velocity was dependent on the kinetic growth rate of ice. The latter depends on molecular mechanisms.

For crystal growth from a pure melt, the interface velocity can be modeled by:

$$U = U_0 \exp \left[-\frac{E_v}{RT_f} \frac{T_f - T_i}{T_i} \right] \left[1 - \exp \left(-\frac{L_f}{R_c T_f} \frac{T_f - T_i}{T_i} \right) \right] \quad (2.28)$$

With U_0 being the molecular attachment velocity in ms^{-1} , E_v the activation energy, expressed in Jkg^{-1} and R_c the universal gas constant.

For a small undercooling, equation 2.28 is simplified to:

$$U = k_m (T_f - T_i) \quad (2.29)$$

In which k_m is the kinetic coefficient, expressed in $\text{ms}^{-1}\text{K}^{-1}$ and can be estimated from experimental measurements of the growth velocity of ice from bulk undercooled water.

Chapter III

Mathematical Models

3. Mathematical Models

In this chapter, a Two-Way Coupling model is described based on the model provided by Silva (2007) and Rodrigues (2016). The One-Way Coupling model simulated by Magalhães (2016) which the present work predictions are compared to, is also briefly explained. A description of the gaseous phase of the model is presented followed by the characterization of the particle phase and the interaction between both phases. The chapter continues with the computational domain configuration. Afterward, the cooling method adopted is presented followed by the initial conditions for the simulations. Finally, the grid independence study is presented in the last section of the chapter.

3.1 One-Way Coupling Model

Magalhães (2016) used a One-Way Coupling Model in order to make predictions on the cooling of free falling water droplets. In Chapter IV, the predictions of the present work will be also compared to the numerical predictions of Magalhães (2016).

The One-Way Coupling model implemented considered a column composed of cold air and water. A differential control volume was established to divide the water column into smaller portions in which the calculation procedure was repeated until the bottom of the column was reached.

In order to the calculation procedures initiates, the initial conditions were set. Therefore, values for the initial air and water temperature, humidity ratio, drop diameter, air column height, flow ratio and air velocity were set.

The change of energy in the water within the control volume is due to heat and mass convection from the drops and can be expressed by the following expression:

$$-m_w dh_f = h_0 A_v dVol (T_w - T_g) + \rho_g h_m A_v dVol (W_s - W) h_{fg} \quad (3.1)$$

The left-hand side represents the energy change in the water and the right-hand side represents heat transfer due to convection and evaporation.

As a representative model, a column shaped like a cylinder can be considered, as presented in Figure 3.1.

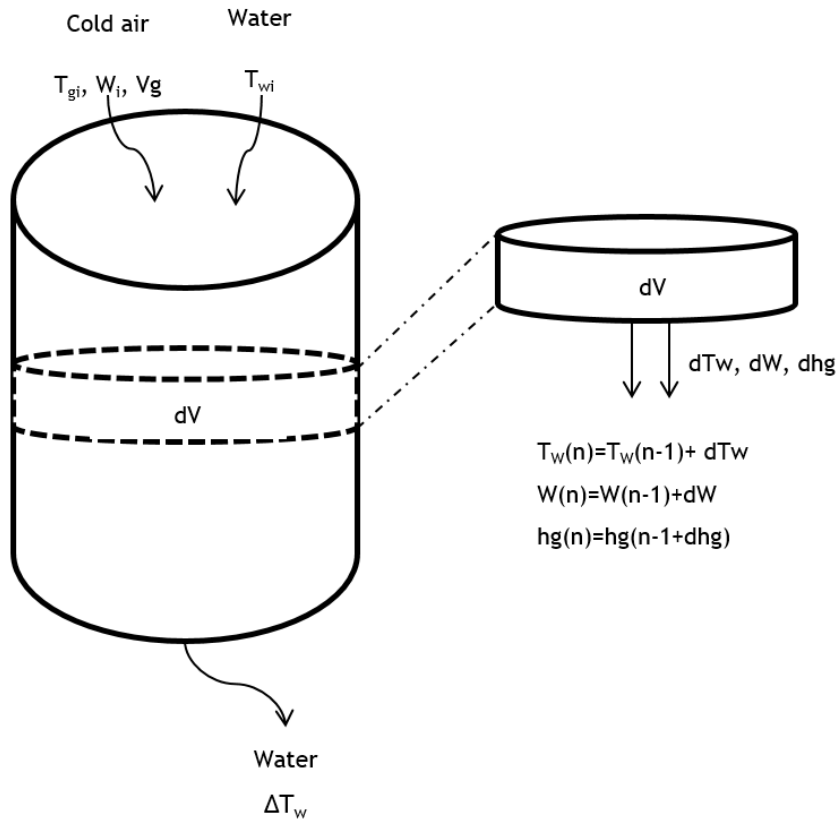


Figure 3.1 - Heat and mass balance of a column of air in a differential element, adapted from Magalhães (2016).

The enthalpy variation as the drop goes through the air column makes possible for the calculation of the temperature variation of the drop, as expressed by the following equation:

$$\Delta T_w = -\frac{m_g}{m_w C_p} (\Delta h - h_f \Delta W) \quad (3.2)$$

Figure 3.2 represents the flowchart for the calculation of rate of cooling of a system of drops in free fall used in the One-Way Coupling Model.

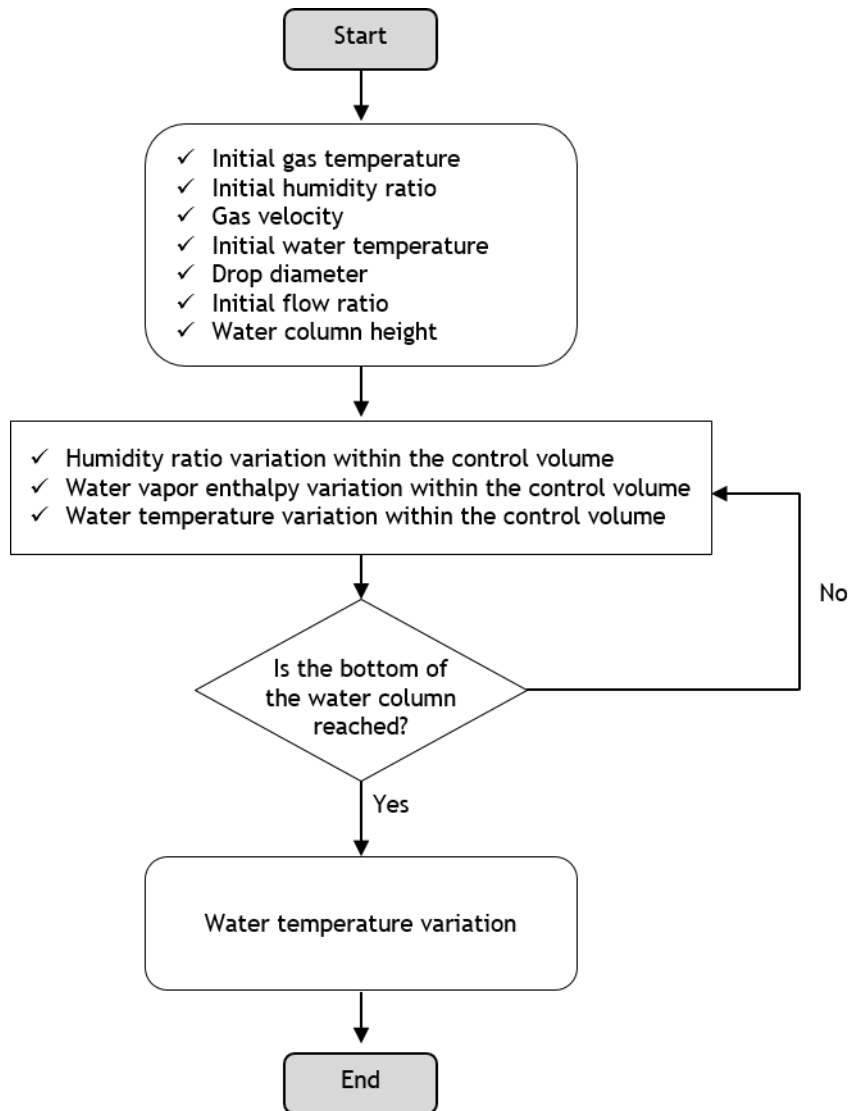


Figure 3.2 - Flowchart for the calculation of the rate of cooling of a system of drops in free fall, adapted from Magalhães (2016).

3.2 Two-Way Coupling Model

A Two-Way Coupling model allows evaluating the influence of the interactions drop-gas and gas-drop since the fluid in which the particles are traveling is affected by their presence. It is considered variable thermos-physical properties, a uniform temperature across the droplet radius and a uniform pressure around the droplet.

The model can be divided into a continuous phase in which the fluid represented is air and a dispersed phase composed by water droplets.

A two-phase flow, as it was already stated in Chapter II can be described by three conservation equations.

The mass conservation equation, in the differential form, can be expressed by the following expression:

$$\frac{d\rho}{dt} + \rho \vec{\nabla} \cdot \vec{v} = 0 \quad (3.3)$$

The momentum conservation equation, in the differential form, can be expressed by:

$$\frac{\partial d\vec{v}}{\partial t} + \vec{\nabla} \cdot (\rho \vec{v} \otimes \vec{v} + p\vec{I} - \vec{\tau}) = \rho \vec{f}_e \quad (3.4)$$

Finally, the energy conservation, also in the differential form can be expressed by the following expression:

$$\frac{\partial \rho E}{\partial t} + \vec{\nabla} \cdot (\rho \vec{v} E) = \vec{\nabla} \cdot (k \vec{\nabla} T) + \vec{\nabla} \cdot (\vec{\sigma} \cdot \vec{v}) + W_f + q_H \quad (3.5)$$

3.2.1 Continuous phase

Since the flow will be analyzed at a macroscopic length scale, the fluid will be considered as a continuum. Properties in a macroscopic scale such as density, pressure, temperature and velocity are considered to be well-defined at infinitely small points and are assumed to vary continuously from one point to another.

These equations can be applied to a single phase fluid. When any particles in a different phase are present in the fluid, their interactions are accounted through source terms. The governing equations for the gas phase state that the mass of fluid is conserved and the rate of change of momentum equals the sum of the forces on a fluid particle. For a steady, incompressible, viscous and Newtonian fluid, the resulting time-averaged partial differential equations are the continuity and momentum equations and can be expressed as follow:

$$\rho \frac{\partial \bar{U}_i}{\partial x_i} = S_m \quad (3.6)$$

and

$$\rho \bar{U}_j \frac{\partial \bar{U}_i}{\partial x_j} = -\frac{\partial \bar{P}}{\partial x_i} + \frac{\partial}{\partial x_j} \left(\mu \frac{\partial \bar{U}_i}{\partial x_j} - \rho \overline{u'_i u'_j} \right) + S_{U_i} \quad (3.7)$$

in which the over-bars represent time-averaged quantities and $\overline{u'_i u'_j}$ are additional turbulent stresses called the Reynolds stresses. The equations above are called the Reynolds-averaged Navier-Stokes equations. The source terms, i.e., S_m and S_{U_i} , are used to account for the influence of the gas phase over the particles in the dispersed phase. When introducing a general variable property per unit mass, ϕ , that may represent any of the scalar variables, velocity components, turbulent kinetic energy or dissipation properties, the partial differential equations that result for a steady incompressible flow can be reduced to a single convective-diffusive conservation equation. This equation is the transport equation for property ϕ . It addresses the various transport processes: the convective term is on the left side of the equation, whereas the diffusive and source terms are on the right side, as represented by the equation below.

$$\frac{\partial(\rho\phi U_i)}{\partial x_i} = \frac{\partial}{\partial x_i} \left[\Gamma_\phi \frac{\partial \phi}{\partial x_i} \right] + S_\phi \quad (3.8)$$

The term Γ represents the effective diffusion coefficient for quantity ϕ and S_ϕ the general source term. The latter can be divided into two parts. $S_{\phi,g}$ specifies the source term of the gas and $S_{\phi,d}$ the source term of the particle.

$$S_\phi = S_{\phi,g} + S_{\phi,d} \quad (3.9)$$

Through the “k- ϵ ” turbulence model of Launder and Spalding (1974), the turbulence is modeled. This two-equation model is one of the most used and validated approach for a wide range of applications. This model makes use of the Boussineq hypothesis, from Launder and Spalding (1974), to compute the Reynolds stresses by relating it to the mean rates of deformation as follows:

$$\rho \overline{u'_i u'_j} = -\mu_t \left(\frac{\partial \bar{U}_i}{\partial x_j} + \frac{\partial \bar{U}_j}{\partial x_i} \right) + \frac{2}{3} \rho k \delta_{ij} \quad (3.10)$$

The turbulent kinetic energy per unit mass, k , can be expressed by:

$$k = \frac{1}{2} (\overline{u'^2} + \overline{v'^2} + \overline{w'^2}) \quad (3.11)$$

The turbulent dynamic viscosity, μ_t , can be expressed by:

$$\mu_t = C_\mu \rho \frac{k^2}{\epsilon} \quad (3.12)$$

If the property ϕ is replaced by the corresponding variable and by selecting appropriate values for Γ and the source terms, it should be possible to obtain the special forms of the partial differential equations for the continuity, momentum, enthalpy, vapor mass fraction, turbulent kinetic energy or dissipation. This approach is expressed in Table 3.1, in which G is the usual turbulence energy production term and can be defined as follows:

$$G = \mu_t \left[\frac{\partial \bar{U}_i}{\partial x_j} + \frac{\partial \bar{U}_j}{\partial x_i} \right] \frac{\partial \bar{U}_i}{\partial x_j} \quad (3.13)$$

Table 3.1 - Terms in the general form of the differential equation.

ϕ	$S_{\phi,g}$	$S_{\phi,d}$	Γ_ϕ
1	–	$\overline{S_{m,d}}$	–
U_i	$-\frac{\partial}{\partial x_i} \left(P + \frac{2}{3}k \right) - \frac{\partial}{\partial x_j} \frac{2}{3} \mu_t \frac{\partial \bar{U}_j}{\partial x_i} + \rho g_i$	$\overline{S_{U_i,d}}$	$\mu + \mu_t$
T	0	$\overline{S_{T,d}}$	$\frac{\mu}{Pr} + \frac{\mu_t}{Pr_t}$
Y	0	$\overline{S_{Y,d}}$	$\frac{\mu}{Sc} + \frac{\mu_t}{Sc_t}$
k	$G - \rho \varepsilon$	$\overline{S_{k,d}}$	$\mu + \frac{\mu_t}{\sigma_k}$
ε	$C_{\varepsilon 1} \frac{\varepsilon}{k} G - C_{\varepsilon 2} \rho \frac{\varepsilon^2}{k}$	$\overline{S_{\varepsilon,d}}$	$\mu + \frac{\mu_t}{\sigma_\varepsilon}$

The coefficients of the “k- ε ” turbulence model given by Launder and Spalding (1974) are presented in Table 3.2.

Table 3.2 - Coefficients of the “k- ε ” turbulence model, adapted from Launder and Spalding (1974).

$C_{\varepsilon 1}$	$C_{\varepsilon 2}$	σ_k	σ_ε	$C_{\varepsilon 3}$	Pr_t	Sc_t	Pr	Sc
1.44	1.92	1.0	1.3	1.1	0.6	0.85	$\frac{\mu C_p}{K_g}$	$\frac{\mu}{\rho C_d}$

In order to solve the differential equations for a turbulent flow, it is required a finite-difference method to obtain a system of algebraic equations that can be solved numerically. Those equations can be converted from the transport equation using a control-volume based technique. Therefore, the quadratic upstream interpolation for convective kinetics (QUICK) scheme of Leonard (1974) has been adopted.

The solution procedure for the continuous phase is based on the semi-implicit method for the pressure-linked equations (SIMPLE) algorithm, described by Patankar and Spalding (1972). In this algorithm, the convective fluxes per unit area, through cell faces are evaluated from guessed velocity components. When convergence is reached, the tridiagonal matrix algorithm (TDMA), described by Thomas (1949), is then applied line-by-line to solve the set of equations.

3.2.2 Dispersed phase

In order to model the dispersion phase, it was adopted a Lagrangian approach to the problem. In this type of modeling, the individual particles are tracked as they move through the computational domain. Thus, the reference frame move with the droplet and the instantaneous position of the particle can be considered as a function of the location from where it originated and the time elapsed.

The droplet trajectory can be calculated through its equation of motion, deduced from Newton's Second Law of Motion if all the forces acting on a droplet immersed in a turbulent flow are mathematically quantified.

For dilute two-phase flows, it is possible to make three assumptions regarding the trajectory of a particle in a fluid flow, due to the difficult task to trace its trajectory. Shirolkar et al (1996) considered:

1. The particle is assumed to be spherical;
2. Particle-particle collision is neglected;
3. The particle density is assumed to be much larger than the surrounding fluid density.

The forces acting on a moving droplet that is immersed in a flowing fluid can be separated into four categories:

1. Forces that act on a droplet due to the motion of the droplet;
2. Forces that act on a droplet due to the motion of the surrounding fluid;
3. Forces that act on a droplet irrespective of the fact that the droplet is in motion or immersed in a flowing fluid (body forces);
4. Forces that act on an object immersed in fluid irrespective of either droplet or fluid motion (buoyancy forces, for instance).

The mathematical expression for the equation of motion of a spherical droplet that accounts for all four types of forces is the following:

$$\begin{aligned}
 m_d \frac{du_{d,i}}{dt} = & 3\pi\mu_f d_d f(u_{f,i} - u_{d,i}) + K_B d_d^2 \sqrt{\pi\rho_f\mu_f} \int_0^t \frac{d}{dt'} (u_{f,i} - u_{d,i}) \frac{dt'}{\sqrt{t-t'}} + K_m \rho_d \frac{\pi}{6} d_d^3 \frac{d}{dt} (u_{f,i} - u_{d,i}) \\
 & + \frac{\pi}{8} \rho_f D_d^3 \bar{\omega}_d \varepsilon_{ijk} n_{1,j} (u_{f,i} - u_{d,i}) + m_d g_i - \rho_f \frac{\pi}{6} D_d^3 g_i
 \end{aligned}
 \tag{3.14}$$

Since the ratio between the particle density and the gas density is greater than 200, $\rho_d/\rho_g > 200$, as Barata (2005) states, the drop momentum equation can be simplified to the following:

$$\frac{\partial U_i}{\partial t} = \frac{1}{\tau_d} (U_{gi} - U_i) + g_i \quad (3.15)$$

in which g_i represents the external forces, such as gravity, centrifugal and Coriolis forces and τ_d , the droplet relaxation time. It is defined as the rate of response of droplet acceleration to the relative velocity between the droplet and the carrier fluid. If the droplet is dense $\rho_d > \rho_g$, the inertial force at the fluid-droplet interface will decrease the fluctuations in its velocity compared to the fluctuations observed. This reduction is known as inertia effect and can be characterized by τ_d and expressed as follows:

$$\tau_d = \frac{24\rho D^2}{18\mu C_D \text{Re}_p} \quad (3.16)$$

in which, Re_d corresponds to the particle Reynolds number, which is expressed by:

$$\text{Re}_d = \frac{\rho |U - U_g| D}{\mu} \quad (3.17)$$

with C_D being the drag coefficient, that may be expressed, accordingly to Crowe et al (2012), as:

$$C_D = \begin{cases} \left(\frac{24}{\text{Re}_d} \right) (1 + 0.15 \text{Re}_d^{0.687}) & \text{Re}_d < 1000 \\ 0.44 & \text{Re}_d \geq 1000 \end{cases} \quad (3.18)$$

Substituting equations 3.17 and 3.18 into equation 3.16, the droplet relaxation time assumes the following expression:

$$\tau_d = \frac{m}{3\pi\mu D} \frac{1}{1 + 0.15 \text{Re}_d^{0.687}} \quad (3.19)$$

Equations 3.15 and 3.19 are the most commonly used expressions in Lagrangian models in order to generate the particle trajectories.

3.2.3 Interaction between the continuous phase and the dispersed phase

Interactions between the continuous phase and the dispersed phase are very complex physical processes, in which due to exchanges of mass, momentum and energy between the two phases, both the gas flow and the droplets behavior are modified. The interaction between the two phases is introduced by treating particles as sources of mass, momentum and energy in the gaseous phase. Thus, the source terms due to the particles are calculated for each Eulerian cell of the continuous phase by following equation 3.20:

$$S_{\phi,d} = S_{\phi,i} + S_{\phi,m} \quad (3.20)$$

In which $S_{\phi,i}$ denotes the source term due to inter-phase transport and $S_{\phi,m}$ the transfer caused by cooling.

The source terms are summarized in Table 3.3.

Table 3.3 - Source terms of the dispersed phase, adapted from Sommerfeld (1998).

$S_{\phi,d}$	$S_{\phi,i}$	$S_{\phi,m}$
$\overline{S_{\rho,d}}$	0	$\sum_k \frac{\dot{m}_k N_k}{U_{i,j}}$
$\overline{S_{U,d}}$	$-\sum_k \frac{\dot{m}_k N_k}{U_{i,j}} [(U_k^{t+\Delta t} - U_k^t) g_i \Delta t]$	$\sum_k \frac{\dot{m}_k N_k U_{ia}}{U_{i,j}}$
$\overline{S_{T,d}}$	$-\sum_k \frac{N_k}{U_{i,j}} (L\dot{m}_k + Q_L)$	$\sum_k \frac{\dot{m}_k N_k}{U_{i,j}} C_{vap}(T_k) T_k$
$\overline{S_{Y_{air},d}}$	0	0
$\overline{S_{Y_{water},d}}$	0	$\sum_k \frac{\dot{m}_k N_k}{U_{i,j}}$
$\overline{S_{k,d}}$	$\overline{U_j S_{U,j,i}} - \overline{U_j} \overline{S_{U,j,i}}$	$\overline{U_j S_{U,j,m}} - \overline{U_j} \overline{S_{U,j,i}} + \frac{1}{26} \overline{U_j} \overline{U_j} \overline{S_m} - \frac{1}{2} \overline{U_j} \overline{U_j} \overline{S_m}$
$\overline{S_{\varepsilon,d}}$	$C_{\varepsilon^3} \frac{\varepsilon}{k} \overline{S_{k,i}}$	$C_{\varepsilon^3} \frac{\varepsilon}{k} \overline{S_{k,m}}$

3.2.4 Solution procedure

In order to solve the problem, the initial conditions can be established by defining the grid and the characteristics of the initial drops. Afterward, it is performed a calculation of the gas flow field without the contribution of the source terms of the dispersed phase. The particles are then traced through the flow field in the dispersed phase and the values of the source terms are calculated. The gas is then recomputed with the contribution of the source terms of the dispersed phase. The process is then repeated until convergence is achieved. Finally, the post-processing of the data occurs.

The flowchart presented in Figure 3.3 illustrates the iterative process of the model as it is exemplified by Rodrigues (2016).

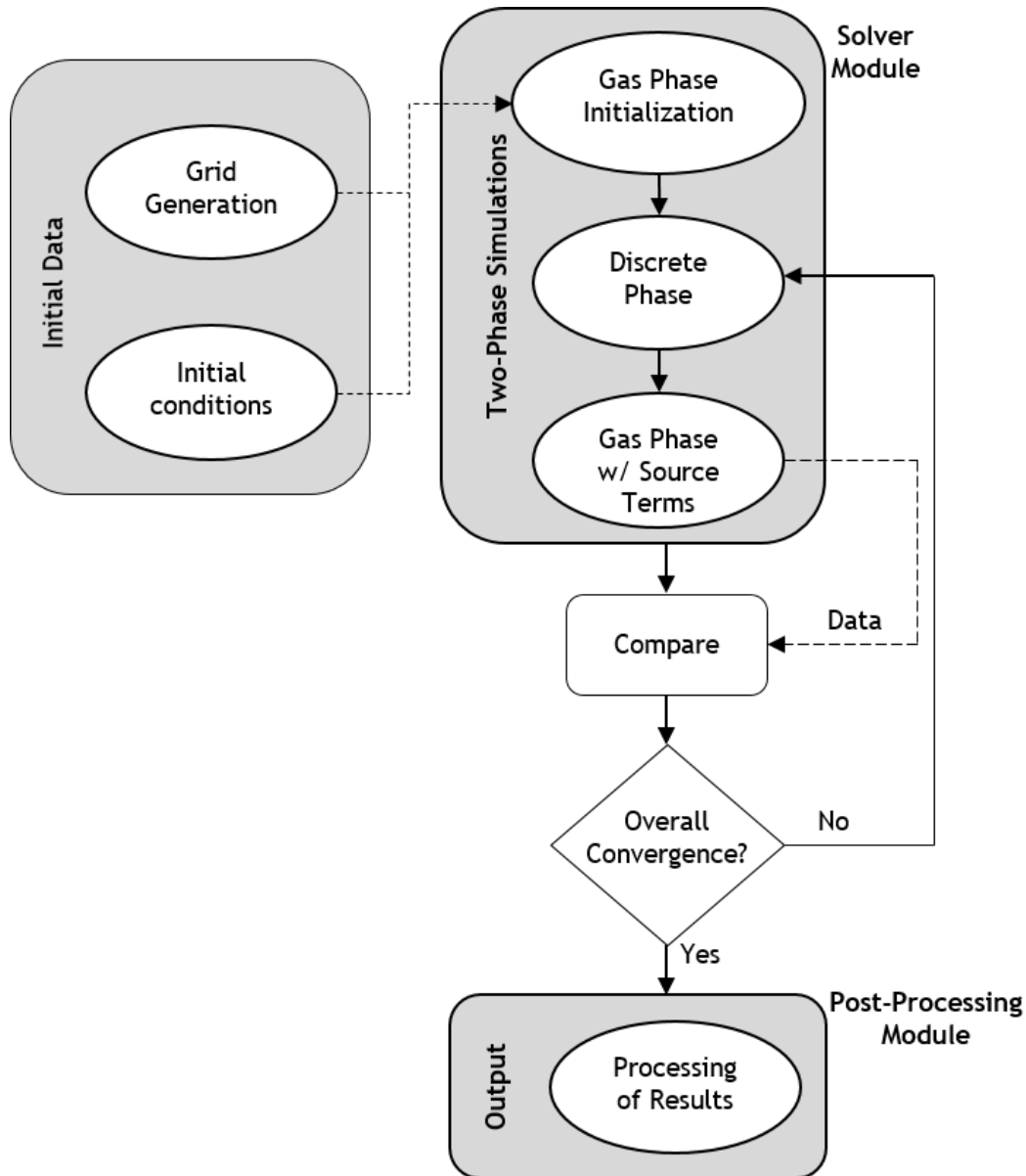


Figure 3.3 - Flowchart of the iterative process, adapted from Rodrigues (2016).

3.3 Computational domain configuration

In this section, a description of the numerical simulations performed will be presented as well as the configuration of the computational domain. The objective of the present work is to perform a simulation of droplets cooling in free fall and compare it with the data retrieved from Yao and Schrock (1976) and Magalhães (2016). Drops are injected into a tunnel on the center cross-section, as presented in Figure 3.4. As seen on the figure, the tunnel has a section of 170x170 mm with a height of 3000 mm. Air is injected at a velocity of 3 cm/s.

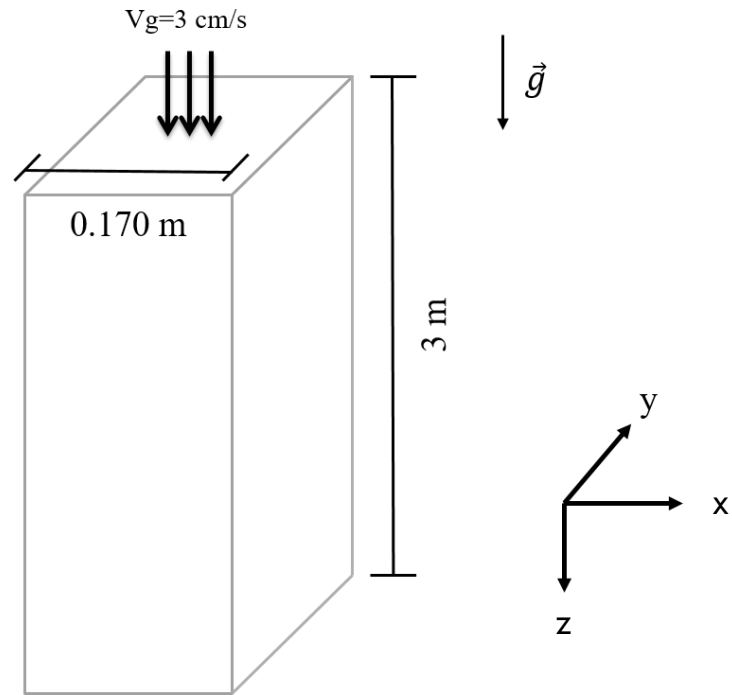


Figure 3.4 - Computational Domain.

Figure 3.5 represents a schematic of the representation of the simulations in a 2D view.

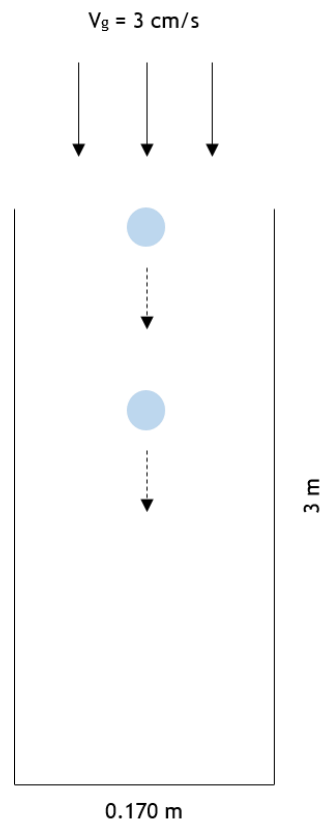


Figure 3.5 - Computational Domain in a 2D schematic.

3.3.1 Boundary Conditions

The solution domain is composed of six boundaries:

1. An inlet plane;
2. An outlet plane;
3. A symmetry plane;
4. Three solid walls at the sides of the tunnel.

3.4 Cooling Model

In this section, the description of the Cooling Model adapted is presented. The main assumptions of this model are:

1. Spherical symmetry
2. Quasi-steady gas film around the droplet
3. Uniform physical properties of the surrounding fluid
4. Uniform pressure around the droplet
5. Liquid/vapor thermal equilibrium on the droplet surface

The effect of the convective transport caused by the motion of the droplet relative to the gas is accounted for by the introduction of the Ranz-Marshall relations, namely the Nusselt number and Sherwood number, which can be used in order to calculate the heat transfer coefficient and mass transfer coefficient, which has been explained in the previous chapter. The heat transfer coefficient and the mass transfer coefficient are presented in equations 3.21 and 3.22, respectively.

$$h_0 = (2 + 0.6\text{Re}_d^{1/2} \text{Pr}_d^{1/3}) \frac{k_g}{D} \quad (3.21)$$

$$h_m = (2 + 0.6\text{Re}_d^{1/2} \text{Sc}_d^{1/3}) \frac{D_{vg}}{D} \quad (3.22)$$

The differential equation for the temporal changes in drop temperature in order to solve the problem is the following:

$$\frac{dT}{dt} = \frac{6Q_L}{\pi C_p D^3} \quad (3.23)$$

In which, Q_L , the heat penetrating into the drop is calculated by the following expression:

$$Q_L = \dot{m} \left(\frac{\overline{C}_{pg}(T_g - T_{sf})}{B_M} - L(T_{sd}) \right) \quad (3.24)$$

in which the subscripts sd and g correspond to the droplet surface and to ambient conditions, respectively.

The total mass flow through the control surface around the droplet corresponds to the cooling rate, \dot{m} :

$$\dot{m} = \pi \overline{\rho}_g \overline{C}_d D (2 + 0.6 \text{Re}_d^{1/2} \text{Sc}_d^{1/3}) \ln(1 + B_M) \quad (3.25)$$

$$\dot{m} = \pi \frac{\overline{K}_G}{\overline{C}_{pg}} D (2 + 0.6 \text{Re}_d^{1/2} \text{Pr}_d^{1/3}) \ln(1 + B_T) \quad (3.26)$$

By assuming a Lewis number of unity, the quantity $\overline{\rho}_g \overline{C}_d$ can be replaced by $\overline{K}_G / \overline{C}_{pg}$.

The Spalding mass number, B_M , and the heat transfer number, B_T , are calculated by the following expressions:

$$B_M = \frac{Y_{wsd} - Y_{wg}}{1 - Y_{Fsd}} \quad (3.27)$$

$$B_T = \frac{\overline{C}_{pg}(T_g - T_{sf})}{L(T_{sd}) + \frac{Q_L}{\dot{m}}} \quad (3.28)$$

in which Y_{wsf} correspond to the water mass fraction on the droplet surface, expressed as:

$$Y_{wsd} = \left[1 + \left(\frac{P}{P_{ws}} - 1 \right) \frac{M_A}{M_w} \right] \quad (3.29)$$

The parameter M_A is the molar mass of air and M_w the molar mass of water. $L(T_{sd})$ corresponds to the latent heat at temperature T_{sd} . Accordingly to Watson (1931), $L(T_{sd})$ may be given by:

$$L(T_{sd}) = L(T_{bn}) \left(\frac{T_{cr} - T_{sd}}{T_{cr} - T_{bn}} \right)^{-0.38} \quad (3.30)$$

The vapor pressure, for any value of surface temperature, can be calculated using the Clausius-Clapeyron equation:

$$P_{w_s} = \exp\left(a - \frac{b}{T_{sd} - 43}\right) \quad (3.31)$$

The parameters a and b are constants of water.

In the boundary layer near the droplet surface of the air/vapor mixture, it should be used the one-third rule of Sparrow and Gregg (1958), since the best results are obtained using this method, in which average properties are evaluated at the following reference and composition:

$$T_{ref} = T_{sd} + \frac{T_g - T_{sd}}{3} \quad (3.32)$$

$$Y_{wref} = Y_{wsd} + \frac{Y_{wg} - Y_{wsd}}{3} \quad (3.33)$$

With these reference values, it is possible to obtain the specific heat at constant pressure with the following expression:

$$C_{pg} = Y_{Aref} C_{p_{air}}(T_{ref}) + Y_{wref} C_p(T_{ref}) \quad (3.34)$$

in which

$$Y_{Aref} = 1 - Y_{wref} \quad (3.35)$$

The temporal changes of drop temperature can be obtained by the following expression:

$$\frac{dT}{dt} = \frac{12K_g \ln(1 + B_M)}{C_{pg} \rho D C_p} (1 + 0.3 \text{Re}_d^{1/2} \text{Pr}_d^{1/3}) \left(\frac{C_{pg}(T_g - T_{sd})}{B_M} - L(T_{sd}) \right) \quad (3.36)$$

3.4.1 Convection effects correlations

The convection effects are taken into account by the introduction of correlations. It was previously stated that the Ranz-Marshall relations were used. Nevertheless, the other two correlations are also considered.

In order to take into account vibrations and deformations of the falling drops, factor that has an impact on heat and mass transfer coefficients' values, a correction factor can be implemented onto the Ranz-Marshall relations. The correction factor is presented in equation 3.37, as developed by Yao and Schrock (1976).

$$C. F. = 25 \left(\frac{Z}{D} \right)^{-0.7} \quad (3.37)$$

The heat and mass transfer coefficients are then calculated by equations 3.38 and 3.39.

$$h_0 = \left(2 + 15 \text{Re}_d^{1/2} \text{Pr}_d^{1/3} \left(\frac{Z}{D} \right)^{-0.7} \right) \frac{k_g}{D} \quad (3.38)$$

$$h_m = \left(2 + 15 \text{Re}_d^{1/2} \text{Sc}_d^{1/3} \left(\frac{Z}{D} \right)^{-0.7} \right) \frac{D_{vg}}{D} \quad (3.39)$$

The cooling rate is calculated by the following expression:

$$\dot{m} = \pi \bar{\rho}_g \bar{C}_d D \left(2 + 15 \text{Re}_d^{1/2} \text{Sc}_d^{1/3} \left(\frac{Z}{D} \right)^{-0.7} \right) \ln(1 + B_M) \quad (3.40)$$

$$\dot{m} = \pi \frac{\bar{K}_g}{C_{p_g}} D \left(2 + 15 \text{Re}_d^{1/2} \text{Pr}_d^{1/3} \left(\frac{Z}{D} \right)^{-0.7} \right) \ln(1 + B_T) \quad (3.41)$$

The temporal change of drop temperature can be calculated by equation 3.42.

$$\frac{dT}{dt} = \frac{12 K_g \ln(1 + B_M)}{C_{p_g} \rho D C_p} \left(1 + 7.5 \text{Re}_d^{1/2} \text{Pr}_d^{1/3} \left(\frac{Z}{D} \right)^{-0.7} \right) \left(\frac{C_{p_g} (T_g - T_{sd})}{B_M} - L(T_{sd}) \right) \quad (3.42)$$

Another correlation that can also be considered is based upon Ambramzon and Sirignano (1989) approach, in which the Nusselt number and the Sherwood number suffer modified correlations.

The equations for the cooling rate vary from the expressions predicted by the classical model since the non-dimensional parameters, Nu_0 and Sh_0 , are substituted by the modified Nusselt number, Nu^* , and Sherwood number, Sh^* , expressed by the following expressions, respectively:

$$\text{Nu}^* = 2 + \frac{(\text{Nu}_0 - 2)}{F_T} \quad (3.43)$$

$$\text{Sh}^* = 2 + \frac{(\text{Sh}_0 - 2)}{F_M} \quad (3.44)$$

Accordingly to the equations above, Nu^* and Sh^* tend to Nu_0 and Sh_0 as F_T and F_M tend to unity. The expressions for Nu_0 and Sh_0 can be calculated employing the Frössling correlations, described by Frössling (1938).

$$\text{Nu}_0 = 2 + 0.552\text{Re}_d^{1/2}\text{Pr}_d^{1/3} \quad (3.45)$$

$$\text{Sh}_0 = 2 + 0.552\text{Re}_d^{1/2}\text{Sc}_d^{1/3} \quad (3.46)$$

The heat and mass transfer coefficients are then calculated by equations 3.47 and 3.48.

$$h_0 = \left(2 + \frac{0.552\text{Re}_d^{1/2}\text{Pr}_d^{1/3}}{F_T}\right) \frac{k_g}{D} \quad (3.47)$$

$$h_m = \left(2 + \frac{0.552\text{Re}_d^{1/2}\text{Sc}_d^{1/3}}{F_M}\right) \frac{D_{vg}}{D} \quad (3.48)$$

For the case of an isothermal surface and constant physical properties of the fluid, the problem has a similar solution and the correction factors, F_T and F_M do not depend upon the local Reynolds number. It is known that both values are practically indifferent to the Schmidt and Prandtl numbers. Thus, these correction factors can be approximated by the following expressions:

$$F_M = F(B_M) \quad (3.49)$$

$$F_T = F(B_T) \quad (3.50)$$

The function $F(B)$ is the universal function given by:

$$F(B) = (1 + B)^{0.7 \frac{\ln(1+B)}{B}} \quad (3.51)$$

The cooling rate, \dot{m} , is given by:

$$\dot{m} = \pi \bar{\rho}_g \bar{C}_d D \left(2 + \frac{0.552\text{Re}_d^{1/2}\text{Sc}_d^{1/3}}{F_M}\right) \ln(1 + B_M) \quad (3.52)$$

$$\dot{m} = \pi \frac{\bar{K}_g}{\bar{C}_{pg}} D \left(2 + \frac{0.552\text{Re}_d^{1/2}\text{Pr}_d^{1/3}}{F_T}\right) \ln(1 + B_T) \quad (3.53)$$

The temporal changes of the droplet temperature are calculated by the following expression:

$$\frac{dT}{dt} = \frac{12K_g \ln(1 + B_M)}{C_{pg} \rho D C_p} \left(1 + \frac{0.276\text{Re}_d^{1/2}\text{Pr}_d^{1/3}}{F_M}\right) \left(\frac{C_{pg}(T_g - T_{sd})}{B_M} - L(T_{sd})\right) \quad (3.54)$$

3.5 Initial conditions

In this section, the initial conditions will be set. For the numerical simulations with the objective of cooling water droplets, the initial conditions are described in Table 3.4. Water drops with diameters of 3 mm, 4 mm, 5 mm and 6 mm are injected into the tunnel presented in Section 3.3.. The velocity of air that enters the tunnel corresponds to 3 cm/s and are considered two cases. First, a single droplet is simulated and in the second case, a flow mass ratio of water/air of $0.1 \text{ kg}_{\text{water}}/\text{kg}_{\text{air}}$ is considered. The values for the humidity ratios considered are 0.29, 0.36, 0.52 and 1.00.

Table 3.4 - Initial conditions for the simulations.

Droplet diameter [mm]	Initial droplet temperature [°C]	Initial air temperature [°C]	Humidity Ratio
3	40.70	23.29	0.29
3	40.73	22.31	0.36
3	40.69	23.33	1.00
4	40.74	22.44	0.36
4	40.64	21.33	0.52
4	40.79	23.33	1.00
5	40.68	22.88	0.29
5	40.72	22.56	0.36
5	40.74	23.61	1.00
6	40.74	22.14	0.36
6	40.66	21.33	0.52
6	40.70	23.33	1.00

3.6 Grid Independence

Figure 3.6 represents a horizontal velocity profile for different locations, used to test the grid dependency of the computations, showing the comparison between the obtained data for different grids, presented as dimensionless quantities. The horizontal component, x , is normalized by the width of the tunnel, l , in the vertical axis, and the vertical component of velocity, V , is normalized by the gas velocity, V_g , in the horizontal axis. Figure 3.6 shows that the results are already independent of numerical influences for $7 \times 12 \times 115$. Nevertheless, to increase the precision a finer grid of $8 \times 16 \times 150$ was adopted, with a total of 19200 points.

Numerical Modeling of Cooling Water Droplets using a Two-Way Coupling Approach

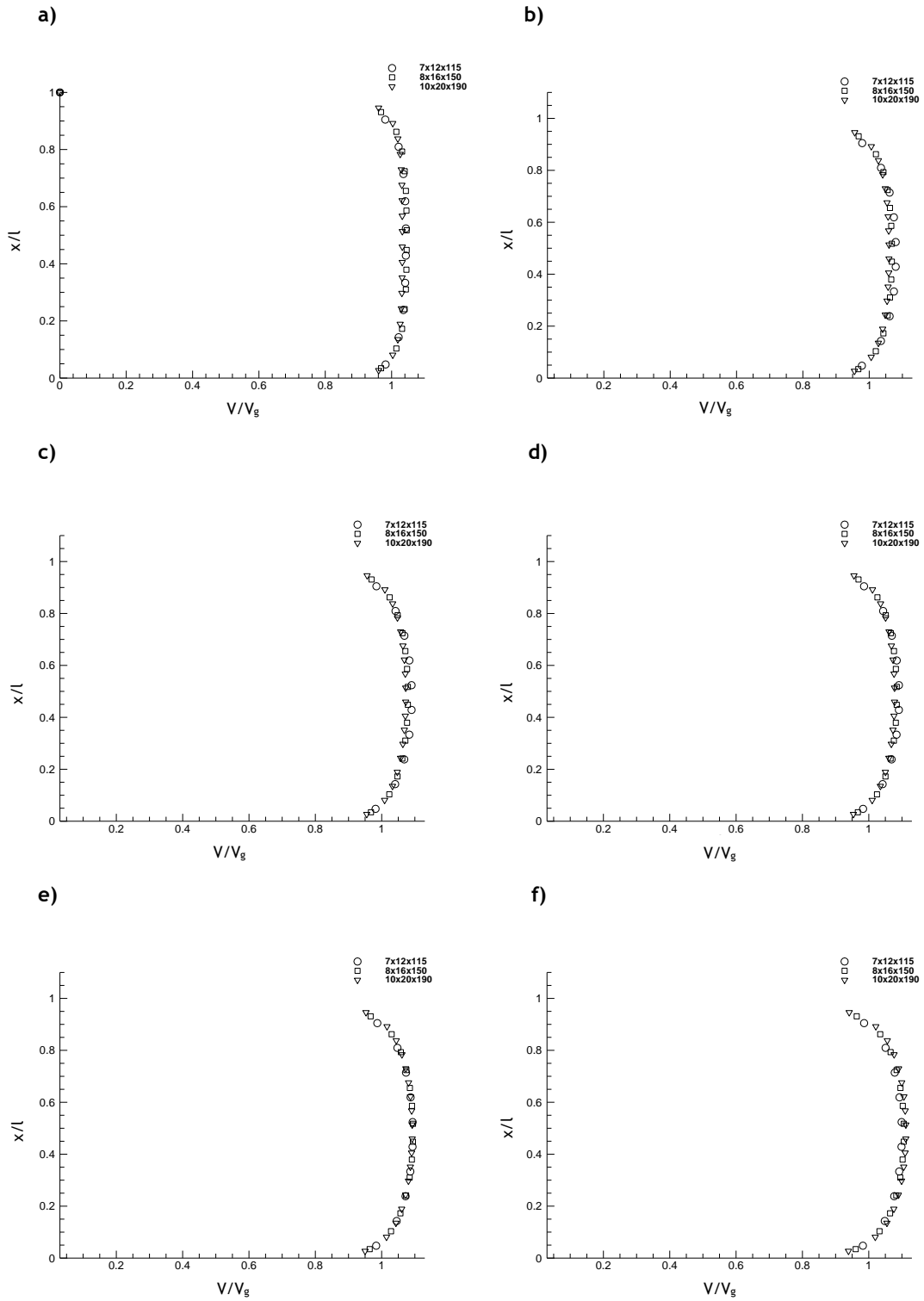


Figure 3.6 - Grid independence for positions of a) $x/l=0.25$, b) $x/l=0.50$, c) $x/l=0.75$, d) $x/l=1.00$, e) $x/l=1.50$ and f) $x/l=2.00$.

Chapter IV

Results and Discussion

4. Results and Discussion

This chapter presents the predictions obtained with the implementation of the model described in the previous chapter. Several simulations were carried out for a range of values of drop diameters and humidity ratios, accordingly to the experimental data acquired from Yao and Schrock (1976). Predictions were compared with the experimental data but also with numerical prediction obtained by Magalhães (2016), in which a One-Way Coupling model was implemented using the Ranz-Marshall classical formulation but also the Ranz-Marshall relations with the correction factor of equation 3.37. Section 4.1 considers the influence of humidity ratio and drop diameter on the cooling process of a single drop free falling. Subsection 4.1.1 contemplates the classical formulation of Ranz-Marshall, while subsection 4.1.2 considers also the Ranz-Marshall relations with a correction factor and a correlation based on Abramzon and Sirignano (1989) approach. In section 4.2 a flow mass ratio of water/air of $0.1 \text{ kg}_{\text{water}}/\text{kg}_{\text{air}}$ was simulated and compared with the numerical and experimental data, considering all of the correlations stated above. Lastly, this chapter concludes with a brief summary.

4.1 Influence of humidity ratio and drop diameter on the cooling process of a single drop free falling

4.1.1 Ranz-Marshall classical formulation

In this section a study is performed on the influence of variable droplet diameter and humidity ratio on the cooling process, considering a single drop free falling. A comparison between the data gathered by Yao and Schrock (1976) and simulated by Magalhães (2016), which model was considered One-Way Coupling, made use of the Ranz-Marshall classical formulation and simulated a flow mass ratio of water/air of $0.1 \text{ kg}_{\text{water}}/\text{kg}_{\text{air}}$, is performed with the predictions of the present work considering a single drop. The complete falling distance is established as 3 m and the velocity of the air stream is set to 3 cm/s. Drops with diameters of 3 mm, 4 mm, 5 mm and 6 mm are simulated and humidity ratios of 0.29, 0.36, 0.52 and 1.00 are considered.

The results represent the variation on drop's temperature falling through the air for different diameters and humidity ratios.

For every figure in the present section, filled circles correspond to the experimental data, by Yao and Schrock (1976), while hollow ones with the use of a dash-dot line represent predictions made by Magalhães (2016), performed using a One-Way Coupling approach, using the Ranz-Marshall relations without the addition of a correction factor. The dashed line corresponds to

the predictions made using the Two-Way Coupling approach, using the Ranz-Marshall relations. The results are presented as dimensionless quantities. The horizontal axis represents the falling distance divided by the drop’s diameter, z/D . The vertical axis corresponds to the dimensionless temperature variation, τ , expressed as follow:

$$\tau = \frac{T_d - T_{d_i}}{T_{g_i} - T_{d_i}} \quad (4.1)$$

The initial conditions for the case of humidity ratio of 0.29 and diameters of 3 mm and 5 mm are summarized in Table 4.1.

Table 4.1 - Initial conditions for the simulation of a humidity ratio of 0.29.

Droplet diameter [mm]	Initial droplet	Initial air temperature	Humidity ratio
	temperature [°C]	[°C]	
3	40.70	23.29	0.29
5	40.68	22.88	0.29

Figure 4.1 represents the variation on drop’s temperature falling through the air for a diameter of 3 mm and 5 mm for a humidity ratio of 0.29. For a diameter of 3 mm, the Two-Way Coupling model fails in approximating the experimental data, while the One-Way Coupling model provides a better approximation of the experimental data. For a diameter of 5 mm, the Two-Way Coupling model only approximates the experimental data up to 200 z/D , failing to predict for the remaining regions. The predictions of the present work are closer to the experimental data when considering the larger drops of 5 mm. These results hint the presence of a regime of steady-state conditions for the cooling for a humidity ratio of 0.29.

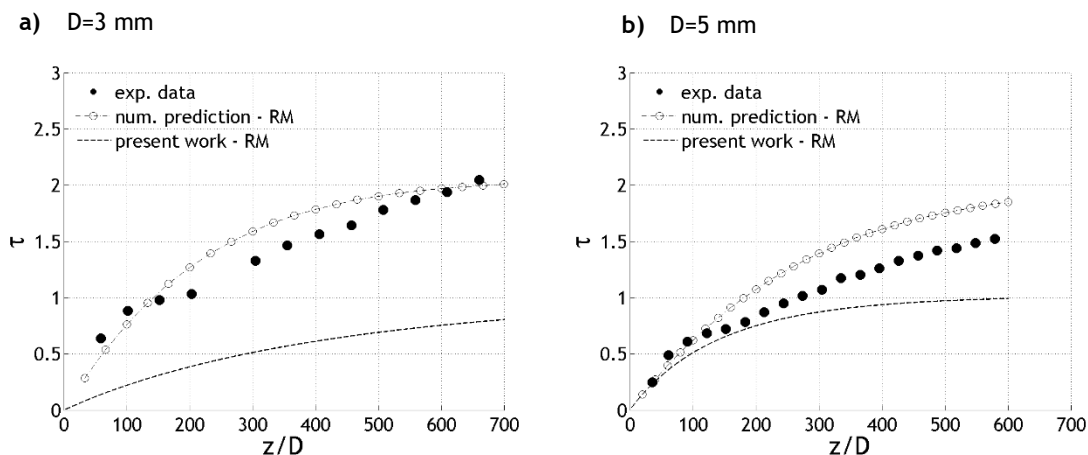


Figure 4.1 - Variation on a single drop temperature falling through the air for a humidity ratio of 0.29 and a diameter of a) 3 mm and b) 5 mm.

The initial conditions for the case of humidity ratio of 0.36 and diameters of 3 mm, 4 mm, 5 mm, and 6 mm are summarized in Table 4.2.

Table 4.2 - Initial conditions for the simulation of a humidity ratio of 0.36.

Droplet diameter [mm]	Initial droplet temperature [°C]	Initial air temperature [°C]	Humidity ratio
3	40.73	22.31	0.36
4	40.74	22.44	0.36
5	40.72	22.56	0.36
6	40.74	22.14	0.36

Figure 4.2 represents the variation on drop's temperature falling through the air for a diameter of 3 mm, 4 mm, 5 mm and 6 mm for a humidity ratio of 0.36. The One-Way Coupling model fails to approximate the experimental data for all four diameters. For the case of 5 mm, the Two-Way Coupling model is able to approximate experimental data up to 200 z/D, while it fails to do so for the remaining diameters, except for the case of 6 mm, in which up to 50 z/D and between 400 and 500 z/D it can predict with some accuracy. It is noticeable that for the diameter of 3 mm and 4 mm the predictions completely fail, whilst for the larger diameters, the model is able to predict certain regions.

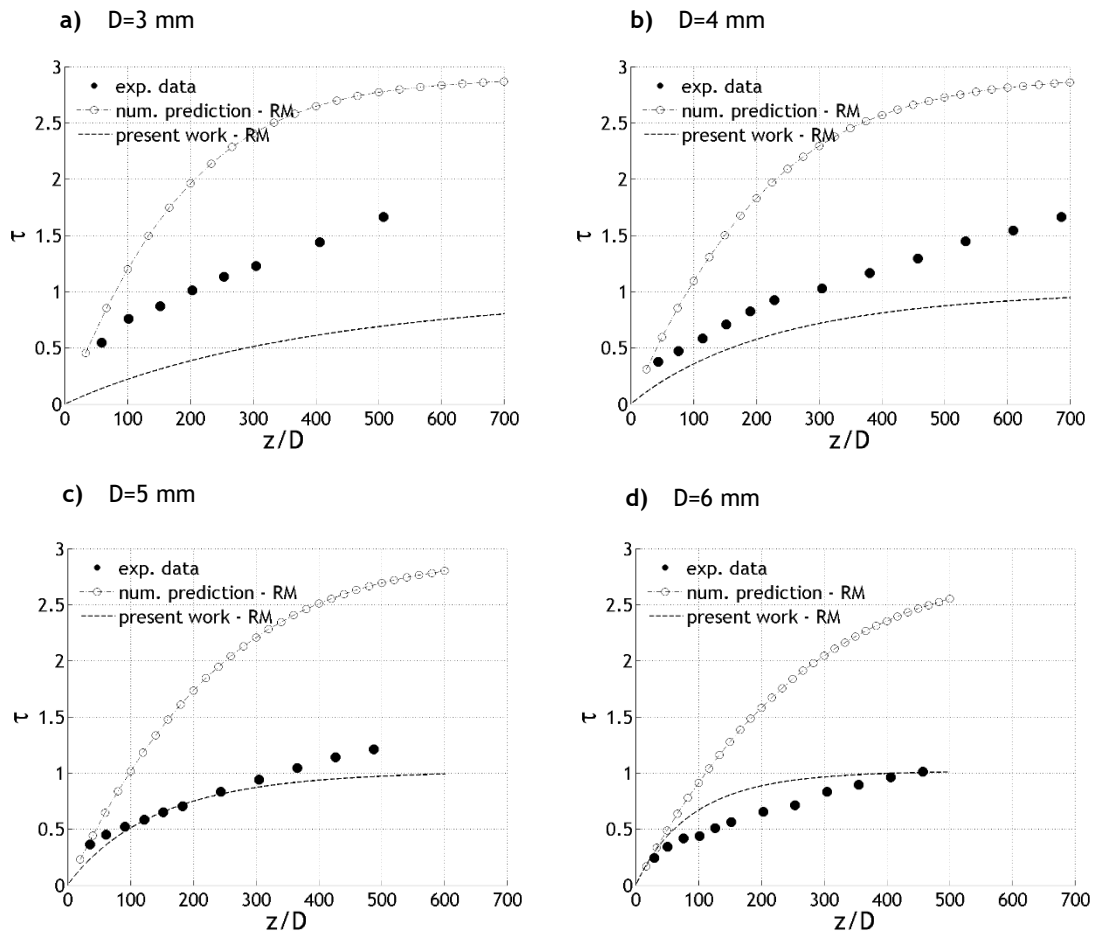


Figure 4.2 - Variation on a single drop temperature falling through the air for a humidity ratio of 0.36 and a diameter of a) 3 mm, b) 4 mm, c) 5 mm and d) 6 mm.

The initial conditions for the case of humidity ratio of 0.52 and diameters of 4 mm and 6 mm are summarized in Table 4.3.

Table 4.3 - Initial conditions for the simulation of a humidity ratio of 0.52.

Droplet diameter [mm]	Initial droplet temperature [°C]	Initial air temperature [°C]	Humidity ratio
4	40.64	21.33	0.52
6	40.66	21.33	0.52

Figure 4.3 represents the variation on drop’s temperature falling through the air for a diameter of 4 mm and 6 mm for a humidity ratio of 0.52. For both cases, the One-Way Coupling fails to approximate the experimental data while the Two-Way Coupling model is able to provide a good approximation of the experimental data. The results hint the presence of a transient regime for a humidity ratio of 0.52.

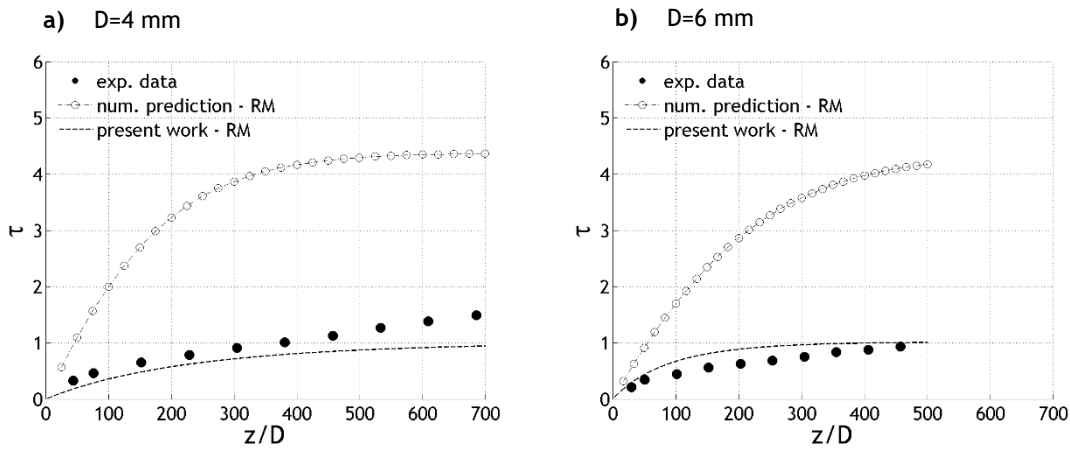


Figure 4.3 - Variation on a single drop temperature falling through the air for a humidity ratio of 0.52 and a diameter of a) 4 mm and b) 6 mm.

The initial conditions for the case of humidity ratio of 1.00 and diameters of 3 mm, 4 mm, 5 mm, and 6 mm are summarized in Table 4.4.

Table 4.4 - Initial conditions for the simulation of a humidity ratio of 1.00.

Droplet diameter [mm]	Initial droplet temperature [°C]	Initial air temperature [°C]	Humidity ratio
3	40.69	23.33	1.00
4	40.79	23.33	1.00
5	40.74	23.61	1.00
6	40.70	23.33	1.00

Figure 4.4 represents the variation on drop’s temperature falling through the air for a diameter of 3 mm, 4 mm, 5 mm and 6 mm for a humidity ratio of 1.00. The One-Way Coupling completely fails in approximating the experimental data for all four diameters. By using the Two-Way Coupling model it is possible to predict with accuracy the data by Yao and Schrock (1976). The results suggest that for a diameter of 1.00 a regime of transient conditions is present.

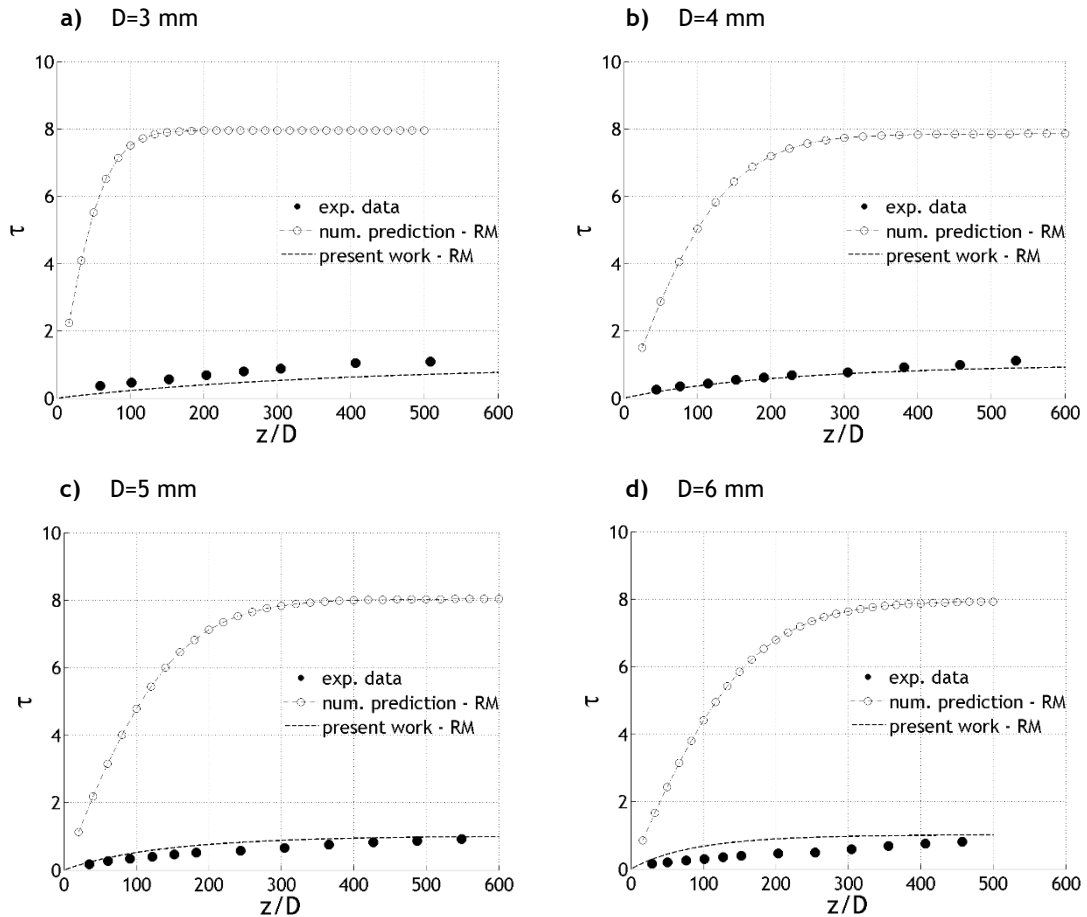


Figure 4.4 - Variation on a single drop temperature falling through the air for a humidity ratio of 1.00 and a diameter of a) 3 mm, b) 4 mm, c) 5 mm and d) 6 mm.

4.1.2 Ranz-Marshall classical formulation, Ranz-Marshall correction factor and Abramzon and Sirignano correlations

In this section a study is performed on the influence of variable droplet diameter and humidity ratio on the cooling process, considering a single drop free falling and different correlations to take into account the convection effects. The results represent the variation on drop's temperature falling through the air for different diameters and humidity ratios. The predictions are performed making use of the classical formulation of the Ranz-Marshall relations, the Ranz-Marshall relations adding the correction factor presented in equation 3.37 and the correlation based on Abramzon and Sirignano approach. The complete falling distance is established as 3 m and the velocity of the air stream is set to 3 cm/s. The initial conditions are the same as in the previous subsection.

For every figure in the present section, filled circles correspond to the experimental data, by Yao and Schrock (1976), while hollow ones with the use of a dash-dot line represent predictions made by Magalhães (2016), performed using a One-Way Coupling approach, in which the black color corresponds to the classical formulation of the Ranz-Marshall relations and the red one

corresponds to the use of the Ranz-Marshall relations with the adding factor that is presented in equation 3.37. The black dashed line corresponds to the predictions made using the Two-Way Coupling approach, using the Ranz-Marshall relations, the red dashed line corresponds to the predictions made with the use of the Ranz-Marshall relations with the addition of the correction factor and the green dashed line the predictions performed by using the correlation based on Abramzon and Sirignano (1989).

The results are presented as dimensionless quantities. The horizontal axis represents the falling distance divided by the drop's diameter, z/D . The vertical axis corresponds to the dimensionless temperature variation, τ .

Table 4.5 summarizes the correlations used to take into account the convection effects and presented in the previous chapter.

Table 4.5 - Convection effects correlations.

Author	Designation	h_0	h_m
Ranz-Marshall	RM	$(2 + 0.6\text{Re}_d^{1/2}\text{Pr}_d^{1/3})\frac{k_g}{D}$	$(2 + 0.6\text{Re}_d^{1/2}\text{Sc}_d^{1/3})\frac{D_{vg}}{D}$
Ranz-Marshall (correction factor)	RMcf	$(2 + 15\text{Re}_d^{1/2}\text{Pr}_d^{1/3}\left(\frac{z}{D}\right)^{-0.7})\frac{k_g}{D}$	$(2 + 15\text{Re}_d^{1/2}\text{Sc}_d^{1/3}\left(\frac{z}{D}\right)^{-0.7})\frac{D_{vg}}{D}$
Abramzon and Sirignano	AS	$(2 + \frac{0.552\text{Re}_d^{1/2}\text{Pr}_d^{1/3}}{F_T})\frac{k_g}{D}$	$(2 + \frac{0.552\text{Re}_d^{1/2}\text{Sc}_d^{1/3}}{F_M})\frac{D_{vg}}{D}$

The initial conditions for the case of humidity ratio of 0.29 and diameters of 3 mm and 5 mm are summarized in Table 4.1.

Figure 4.5 represents the variation on drop's temperature falling through the air for a diameter of 3 mm and 5 mm for a humidity ratio of 0.29. For a diameter of 3 mm, the predictions made with the One-Way Coupling approach and classical formulation of Ranz-Marshall relations in overall predict with higher accuracy the experimental data than all of the other simulations. For a diameter of 5 mm and up to 200 z/D , the Two-Way Coupling model predicts with accuracy using the Ranz-Marshall relations, both with and without the correction factor. The Abramzon and Sirignano approach only approximates the data for a region near 200 z/D . In overall, the One-Way Coupling model with the use of the Ranz-Marshall relations without the addition of the correction factor proves to be the better approximation to the data gathered by Yao and Schrock (1976). The results suggest the presence of a steady-state regime for a humidity ratio of 0.29. All of the three correlations considered in the Two-Way Coupling model are found to predict with proximity between them. The present work predictions are found to be closer to the experimental data when considering a diameter of 5 mm.

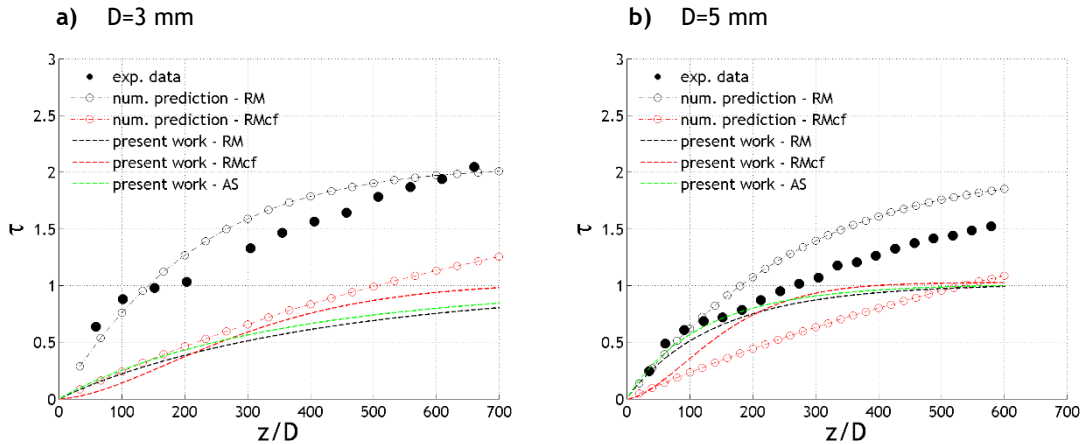


Figure 4.5 - Variation on a single drop temperature falling through the air for a humidity ratio of 0.29 and a diameter of a) 3 mm and b) 5 mm for different correlations.

The initial conditions for the case of humidity ratio of 0.36 and diameters of 3 mm, 4mm, 5 mm, and 6 mm are summarized in Table 4.2.

Figure 4.6 represents the variation on drop's temperature falling through the air for a diameter of 3 mm, 4 mm, 5 mm, and 6 mm for a humidity ratio of 0.36. The One-Way Coupling model using the correction factor in the Ranz-Marshall relations proves to be the better approximation, by predicting the data from Yao and Schrock (1976) with accuracy for all four diameters. For all four diameters, the One-Way Coupling model using the classical formulation of the Ranz-Marshall relations completely fails in approximating the experimental data. The three different correlations used in the Two-Way Coupling model produce predictions similar to each other. The higher diameters of 5 mm and 6 mm are able to provide better predictions than the smaller diameters of 3 mm and 4 mm.

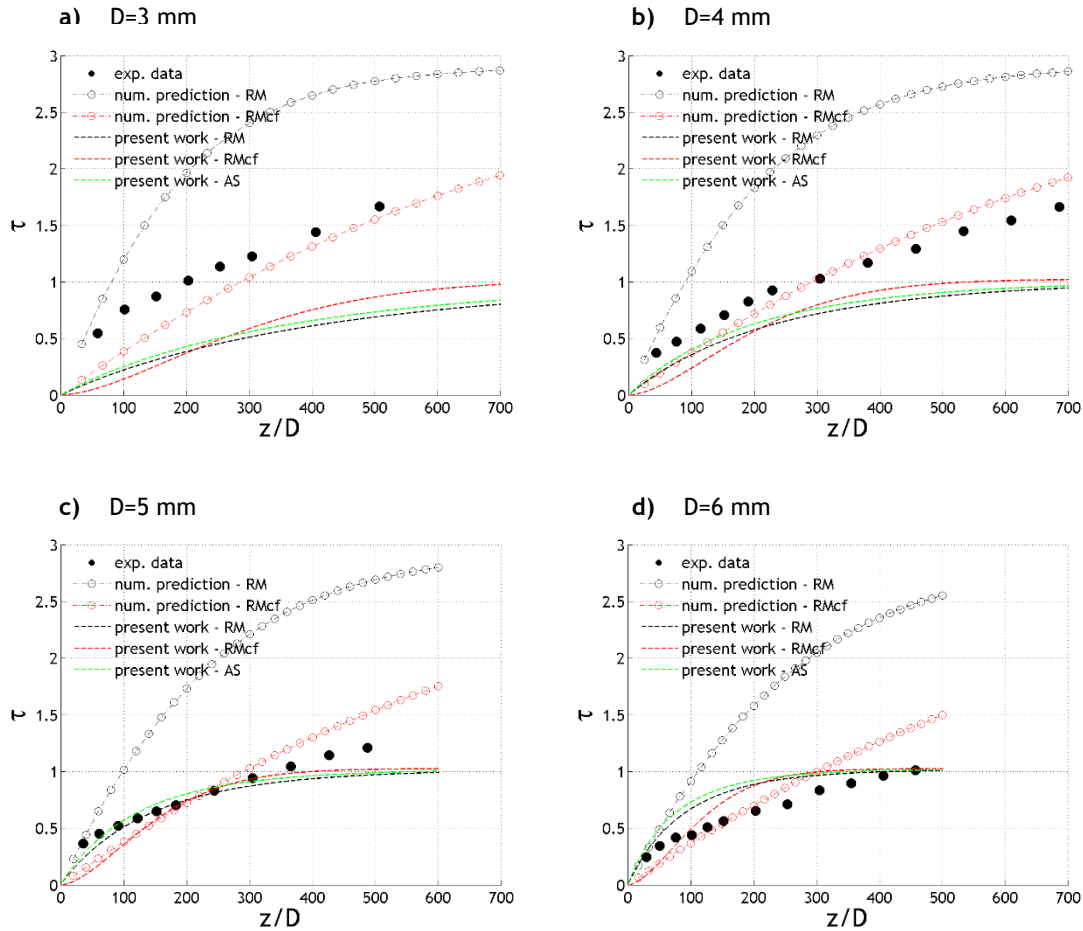


Figure 4.6 - Variation on a single drop temperature falling through the air for a humidity ratio of 0.36 and a diameter of a) 3 mm, b) 4 mm, c) 5 mm and d) 6 mm for different correlations.

The initial conditions for the case of humidity ratio of 0.52 and diameters of 4 mm and 6 mm are summarized in Table 4.3.

Figure 4.7 represents the variation on drop's temperature falling through the air for a diameter of 3 mm and 5 mm for a humidity ratio of 0.52. For both diameters, the One-Way Coupling model using the Ranz-Marshall classical formulation fails to predict the experimental data. With the correction factor added to the Ranz-Marshall relations in the One-Way Coupling model, for a diameter of 4 mm it gives a good approximation up to 75 z/D and for a diameter of 6 mm up to 100 z/D . The Two-Way Coupling model is found to produce in overall a good approximation of the experimental data. The different correlations used produced very similar results. The results hint the presence of a regime of transient conditions for the cooling of the drop. It is noticeable that the several correlations used in the Two-Way Coupling start to produce very similar predictions.

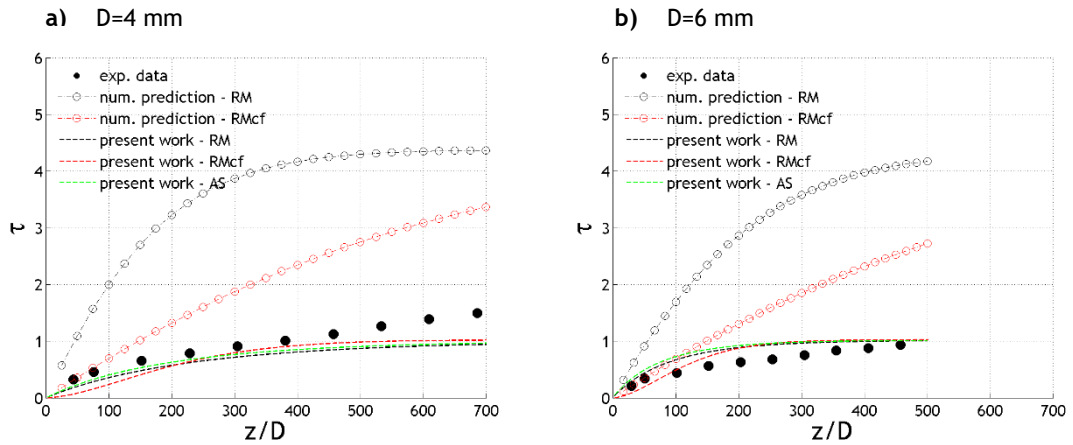


Figure 4.7 - Variation on a single drop temperature falling through the air for a humidity ratio of 0.52 and a diameter of a) 4 mm and b) 6 mm for different correlations.

The initial conditions for the case of humidity ratio of 1.00 and diameters of 3 mm, 4 mm, 5 mm, and 6 mm are summarized in Table 4.4.

Figure 4.8 represents the variation on drop's temperature falling through the air for a diameter of 3 mm, 4 mm, 5 mm and 6 mm for a humidity ratio of 1.00. The One-Way Coupling model fails to approximate the experimental data for both the case of Ranz-Marshall classical formulation and with the adding of the correction factor. The predictions obtained with the Two-Way Coupling model have found to be in close agreement with the experimental data no matter what the correlation may be. The results suggest the presence of a regime of transient conditions. The three different correlations regarding the convection effects predict with values nearly identical which may be caused by the saturation of air that occurs at a humidity ratio of 1.00.

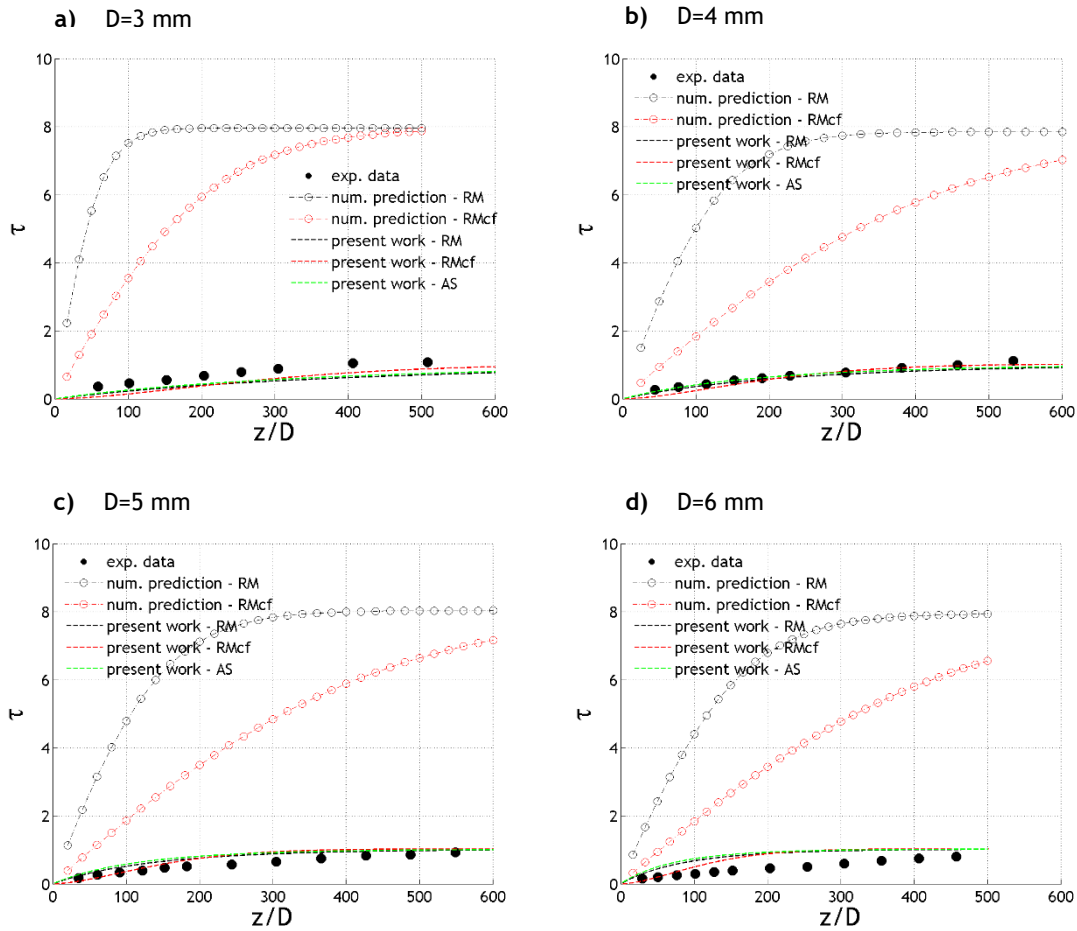


Figure 4.8 - Variation on a single drop temperature falling through the air for a humidity ratio of 1.00 and a diameter of a) 3 mm, b) 4 mm, c) 5 mm and d) 6 mm for different correlations.

4.2 Influence of humidity ratio and drop diameter on the cooling process of drop free falling considering a flow mass ratio of $0.1 \text{ kg}_{\text{water}}/\text{kg}_{\text{air}}$

4.2.1 Ranz-Marshall classical formulation, Ranz-Marshall correction factor and Abramzon and Sirignano correlations

In this section a study is performed on the influence of variable droplet diameter and humidity ratio on the cooling process, considering a flow mass ratio of water/air of $0.1 \text{ kg}_{\text{water}}/\text{kg}_{\text{air}}$. The results represent the variation on drop's temperature falling through the air for different diameters and humidity ratios. The predictions are performed making use of the Ranz-Marshall classical formulation, the Ranz-Marshall relation adding the correction factor and the Abramzon and Sirignano approach. The complete falling distance is established as 3 m, the velocity of the air stream is set to 3 cm/s and a flow mass ratio of $0.1 \text{ kg}_{\text{water}}/\text{kg}_{\text{air}}$ is considered.

For every figure in the present section, filled circles correspond to the experimental data, by Yao and Schrock (1976), while hollow ones with the use of a dash-dot line represent predictions made by Magalhães (2016), performed using a One-Way Coupling approach, in which the black color corresponds to the classical formulation of the Ranz-Marshall relations and the red one corresponds to the use of the Ranz-Marshall relations with the adding factor that is presented in equation 3.37. The black dashed line corresponds to the predictions made using the Two-Way Coupling approach, using the Ranz-Marshall relations, the red dashed line corresponds to the predictions made with the use of the Ranz-Marshall relations with the addition of the correction factor and the green dashed line the predictions performed by using the correlation based on Abramzon and Sirignano (1989).

The initial conditions for the case of humidity ratio of 0.29 and diameters of 3 mm and 5 mm are summarized in Table 4.1.

Figure 4.9 represents the variation on drop's temperature falling through the air for a diameter of 3 mm and 5 mm for a humidity ratio of 0.29. For a diameter of 3 mm, the predictions made with the One-Way Coupling approach and classical formulation of Ranz-Marshall relations in overall predict with higher accuracy the experimental data than all of the other simulations. For a diameter of 5 mm and up to 200 z/D , the Two-Way Coupling model predicts with accuracy using the Ranz-Marshall relations, both with and without the correction factor. The Abramzon and Sirignano approach only approximates the data for a region near 200 z/D . In overall, the One-Way Coupling model with the use of the Ranz-Marshall relations without the addition of the correction factor proves to be the better approximation. The results suggest the presence of a steady-state regime for a humidity ratio of 0.29. All of the three correlations considered in the Two-Way Coupling model are found to predict with proximity between them. The results are very similar to the predictions in which a single drop was simulated. As noticed in the previous subsection in this case also the higher diameter produces better predictions than the lower diameter of 3 mm.

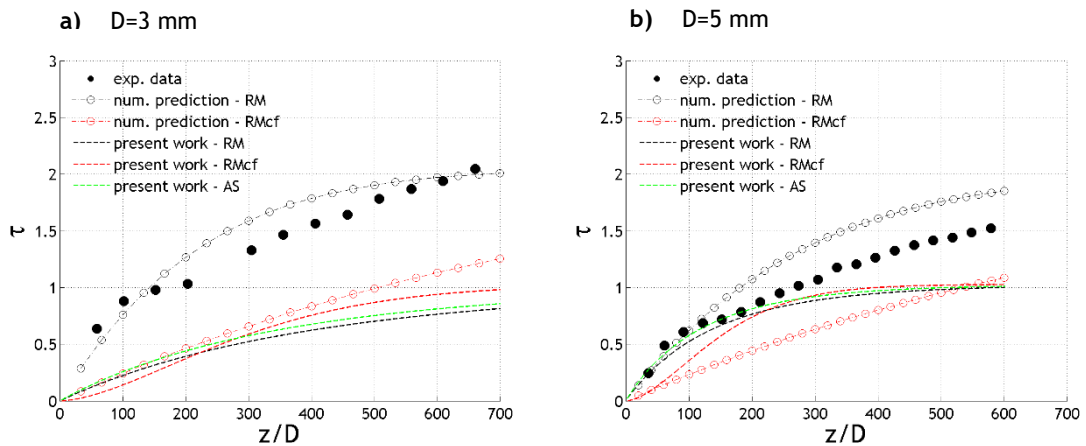


Figure 4.9 - Variation on drop temperature falling through the air for a humidity ratio of 0.29 and a diameter of a) 3 mm and b) 5 mm for a flow mass ratio of 0.1 and different correlations.

The initial conditions for the case of humidity ratio of 0.36 and diameters of 3 mm, 4 mm, 5 mm, and 6 mm are summarized in Table 4.2.

Figure 4.10 represents the variation on drop's temperature falling through the air for a diameter of 3 mm, 4 mm, 5 mm, and 6 mm for a humidity ratio of 0.36. The One-Way Coupling model using the correction factor in the Ranz-Marshall relations prove to be the better approximation when comparing it with the other predictions for all diameters. For all four diameters, the One-Way Coupling model using the classical formulation of the Ranz-Marshall relations completely fails in approximating the experimental data. The three different correlations used in the Two-Way Coupling model produce predictions similar to each other. The predictions are very similar to the results obtained for a single droplet. The smaller diameters, 3 mm and 4 mm produce worse predictions than diameters of 5 mm and 6 mm.

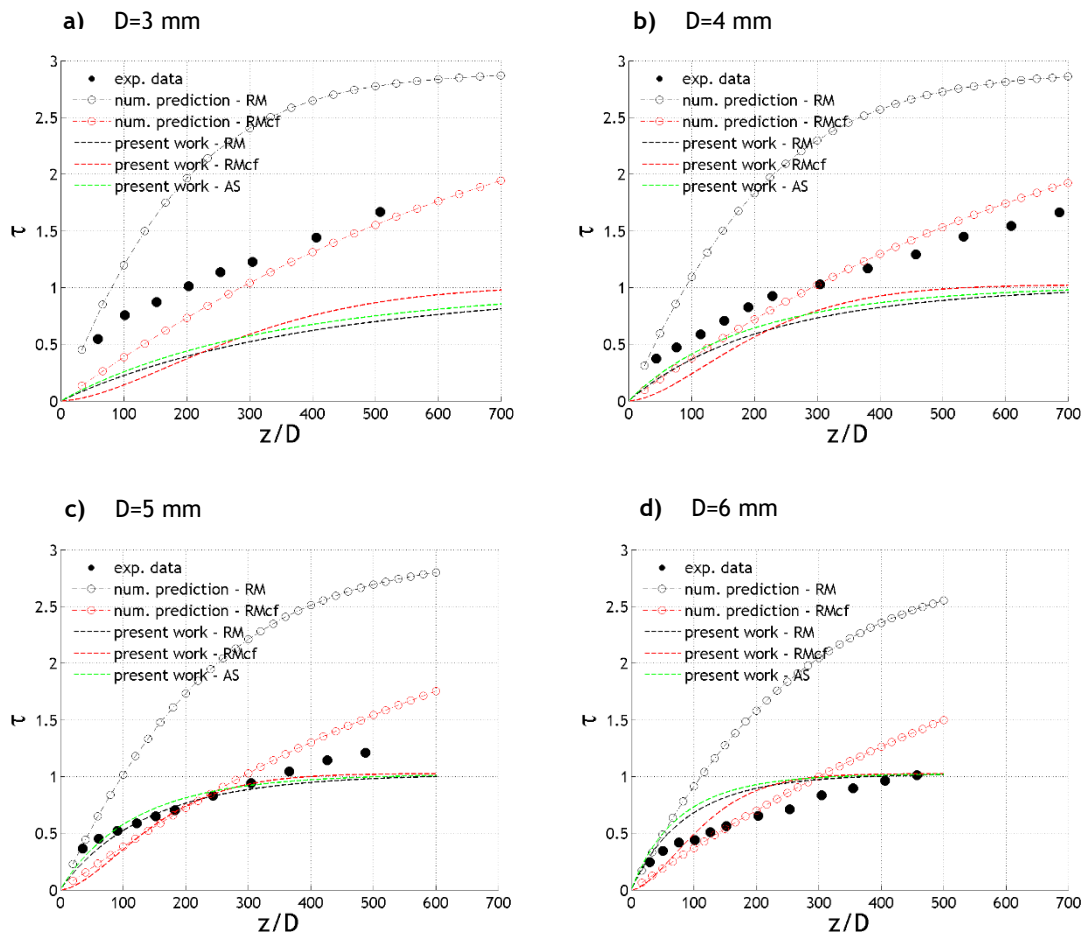


Figure 4.10 - Variation on drop temperature falling through the air for a humidity ratio of 0.36 and a diameter of a) 3 mm, b) 4 mm, c) 5 mm and d) 6 mm for a flow mass ratio of 0.1 and different correlations.

The initial conditions for the case of humidity ratio of 0.52 and diameters of 4 mm and 6 mm are summarized in Table 4.3.

Figure 4.11 represents the variation on drop's temperature falling through the air for a diameter of 3 mm and 5 mm for a humidity ratio of 0.52. For both diameters, the One-Way Coupling model using the Ranz-Marshall classical formulation fails to predict the experimental data. With the correction factor added to the Ranz-Marshall relations in the One-Way Coupling model, for a diameter of 4 mm it gives a good approximation up to 75 z/D and for a diameter of 6 mm up to 100 z/D. The Two-Way Coupling model is found to produce in overall a good approximation of the experimental data. The different correlations used produces very similar results. The results hint the presence of a regime of transient conditions for the cooling of the drop. The results obtained are very similar to the ones predicted by simulating a single drop.

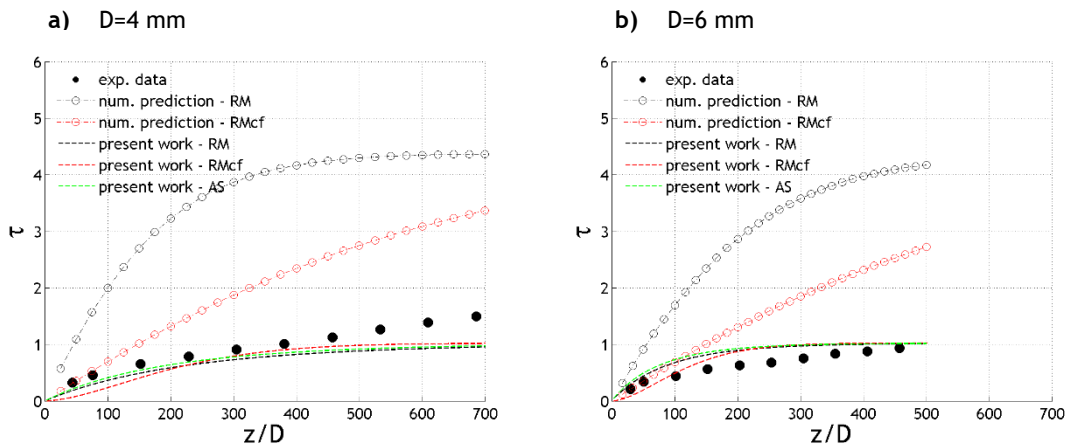


Figure 4.11 - Variation on drop temperature falling through the air for a humidity ratio of 0.52 and a diameter of a) 4 mm and b) 6 mm for a flow mass ratio of 0.1 and different correlations.

The initial conditions for the case of humidity ratio of 1.00 and diameters of 3 mm, 4 mm, 5 mm, and 6 mm are summarized in Table 4.4.

Figure 4.12 represents the variation on drop's temperature falling through the air for a diameter of 3 mm, 4 mm, 5 mm and 6 mm for a humidity ratio of 1.00. The One-Way Coupling model fails to approximate the experimental data for both the case of Ranz-Marshall classical formulation and with the adding of the correction factor. The predictions obtained with the Two-Way Coupling model have found to be in close agreement with the experimental data no matter what the correlation may be. The results suggest the presence of a regime of transient conditions. The three different correlations regarding the convection effects predict with values nearly identical which may be caused by the saturation that occurs at a humidity ratio of 1.00. The results obtained are very similar to the ones predicted by simulating a single drop.

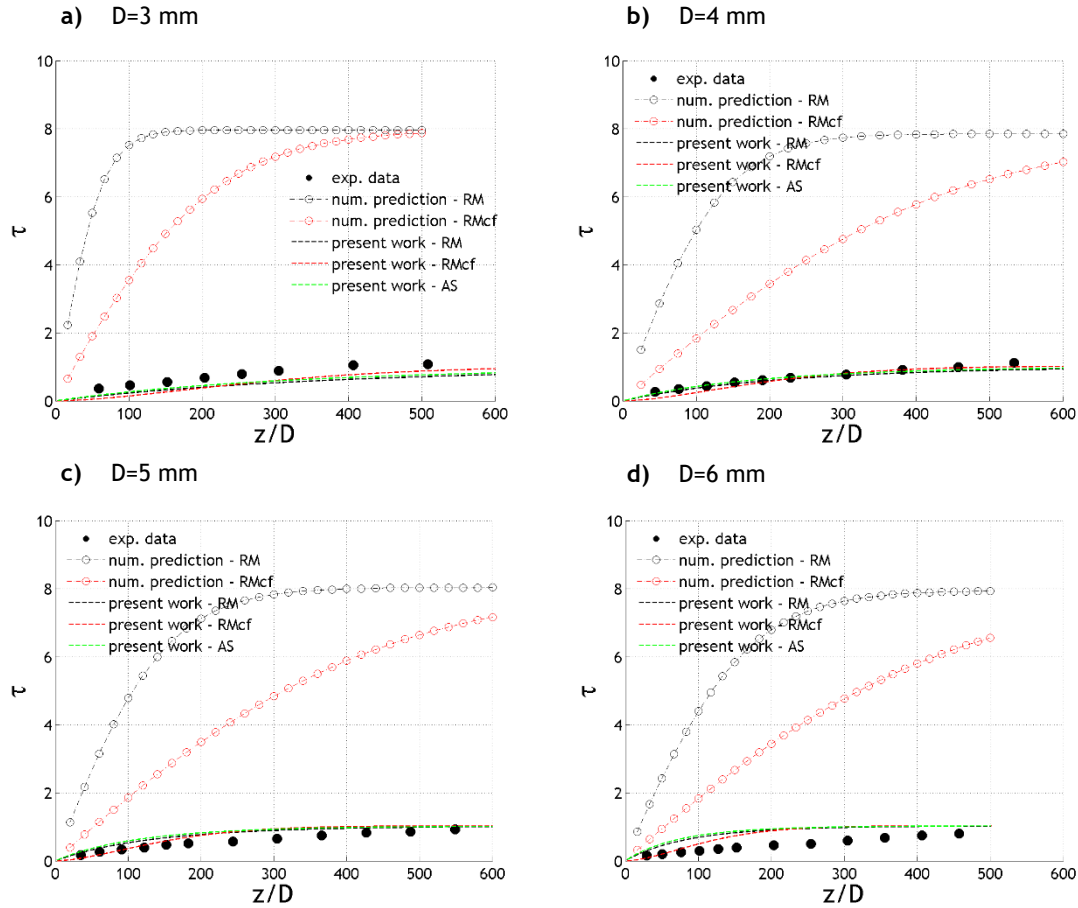


Figure 4.12 - Variation on drop temperature falling through the air for a humidity ratio of 1.00 and a diameter of a) 3 mm, b) 4 mm, c) 5 mm and d) 6 mm for a flow mass ratio of 0.1 and different correlations.

4.3 Summary

In this chapter, predictions were presented regarding the study of free falling water droplets for different diameters and humidity ratios. The predictions were compared with experimental data and numerical predictions of a One-Way Coupling model. It was analyzed the influence of diameter, humidity ratio and different correlations regarding the convection effects.

For the lower humidity ratio (0.29), the present work does not present a close agreement with the experimental data, which suggest a regime of steady-state conditions for the cooling. The predictions of Magalhães (2016) using the One-Way Coupling formulation with the Ranz-Marshall relations are found to be in a closer agreement, in which a complete mixing model was used, which also supports the indication of a regime of steady-state conditions.

For a humidity ratio of 0.36, the data suggests a transition between the steady state and the transient regime.

Increasing the humidity ratio, for a ratio of 0.52 and 1.00, the obtained data suggest the presence of a transient regime.

For a humidity ratio of 0.29 and 0.36 the higher diameters produce better predictions than the smaller diameters.

The different correlations are found to have great proximity between them. Increasing the humidity ratio, the predictions become further similar, possibly due to the reach to saturation of the air.

The results showed very small differences between the simulations of a single drop and for a flow mass ratio of $0.1 \text{ kg}_{\text{water}}/\text{kg}_{\text{air}}$.

Chapter V

Conclusions and Future Work

5. Conclusions and Future Work

Numerical simulations were carried out for the cooling of free falling water droplets under several humidity conditions and drops' diameters, using a Two-Way Coupling model. The predictions were compared to experimental data and numerical predictions, in which a One-Way Coupling method was used. In order to take into account convection effects the Ranz-Marshall relations with and without the addition of a correction factor and the Abramzon and Sirignano approach were used. Both a single droplet and a flow mass ratio of $0.1 \text{ kg}_{\text{water}}/\text{kg}_{\text{air}}$ were simulated.

Predictions were found to be in close proximity to the experimental data when considering high humidity ratios and failed to approximate the data obtained experimentally for lower humidity ratios.

For the lower humidity ratio (0.29), the present work suggests a regime of steady-state conditions for the cooling. Increasing the humidity ratio, for a ratio of 0.52 and 1.00, the obtained data suggest the presence of a transient regime.

For a humidity ratio of 0.29 and 0.36 the higher diameters produced better predictions than the smaller diameters.

The different correlations are found to have great proximity between them. Increasing the humidity ratio, the predictions become further similar, possibly due to the reach to saturation of the air.

The results showed very small differences between the simulations of a single drop and for a flow ratio of $0.1 \text{ kg}_{\text{water}}/\text{kg}_{\text{air}}$.

In future studies, the complete freezing process should be implemented, and the steady-state regime also considered in the Two-Way Coupling model. This topic of study should incorporate impingement models to recreate real-life situations, such as ice accretion upon impact.

Chapter VI

Bibliographic References

6. Bibliographic References

Abramzon, B., Sirignano, W.A., Droplet Vaporization Model for Spray Combustion Calculations, *International Journal of Heat and Mass Transfer* 32 (1989) 1605-1618.

Alexiades, V., Solomon, A.D., *Mathematical Modeling of Melting and Freezing Processes*, first ed., Taylor & Francis, Washington DC, USA, 1993.

Barata, J., Modelowanie Ruchu Kropel Paliwa, Rozpylenia i Parowania Podczas Przepływu Burzliwego, *Silniki Spalinowe* 44 (2005) 42-55.

Benson, C.S., Ice Fog: Low Temperature Air Pollution defined with Fairbanks, Alaska as Type Locality, *CRREL Research Report* (1970) AD708544.

Brennen, C.E., *Fundamentals of Multiphase Flows*, first ed., Cambridge University Press, Pasadena, California, 2005.

Caliskan, F., Hajiyev, C., A Review of in-Flight Detection and Identification of Aircraft Icing and Reconfigurable Control, *Progress in Aerospace Sciences* 60 (2013) 12-34.

Cao, Y., Huang, J., Xu, Z., Yin, J., Insight into Rime Ice Accretion on an Aircraft Wing and Corresponding Effects on Aerodynamic Performance, *The Aeronautical Journal* 120 (2016) 1101-1122.

Cao, Y., Tan, W., Wu, Z., Aircraft Icing: An Ongoing Threat to Aviation Safety, *Aerospace Science and Technology* 75 (2018) 353-385.

Cao, Y., Wu, Z., Su, Y., Xu, Z., Aircraft Flight Characteristics in Icing Conditions, *Progress in Aerospace Sciences* 74 (2015) 62-80.

Chao, B.T., Transient Heat and Mass Transfer to a Translating Droplet, *Journal of Heat Transfer* 91 (1969) 273-280.

Chen, K.H., Trezek, G.J., The Effect of Heat Transfer Coefficient, Local Wet Bulb Temperature and Droplet Size Distribution Function on Thermal Performance of Sprays, *Journal of Heat Transfer* 99 (1977) 381-385.

Chen, Y., Lu, P., Shen, C., Zhang, Q., Experimental Study on Frost Formation on a Cold Surface in Low Atmospheric Pressure, *Applied Thermal Engineering* 90 (2015) 86-93.

Crowe, C.T., Schwarzkopf, J.D., Sommerfeld, M., Tsuji, Y., *Multiphase Flows with Droplets and Particles*, second ed., CRC Press Taylor & Francis, New York, 2012.

Dickinson, D.R., Marshall, W.R., The Rates of Evaporating of Sprays, *Journal of the American Institute of Chemical Engineers* 14 (1968) 541-552.

Dragomirescu, F.I., Eisenschmidt, K., Rohde, C., Weigand, B., Perturbation Solutions for the Finite Radially Symmetric Stefan Problem, *International Journal of Thermal Sciences* 104 (2016) 386-395.

Elliott, J.W., Smith, F.T., Ice Formation on a Smooth or Rough Cold Surface due to the Impact of a Supercooled Water Droplet, *Journal of Engineering Mathematics* 102 (2017) 35-64.

Frössling, N., The evaporation of falling drops (in German), *Gerlands Beiträge zur Geophysik* 52 (1938) 170-216.

Hindmarsh, J.P., Russell, A.B., Chen, X.D., Experimental and Numerical Analysis of the Temperature Transition of a Suspended Freezing Water Droplet, *International Journal of Heat and Mass Transfer* 46 (2003) 1199-1213.

Hirsch, C., *Numerical Computation of Internal and External Flows: Fundamentals of Computational Fluid Dynamics*, second ed., Elsevier, Oxford, 2007.

Hughes, R.R., Gilliland, E.R., The Mechanisms of Drops, *Chemical Engineering Progress* 48 (1952) 497-504.

Ishii, M., Hibiki, T., *Thermo-Fluid Dynamics of Two-Phase Flow*, first ed., Springer, New York, 2006.

Jin, Z., Sui, D., Yang, Z. The Impact, Freezing, and Melting Processes of a Water Droplet on an Inclined Cold Surface, *International Journal of Heat and Mass Transfer* 90 (2015) 439-453.

Jin, Z., Wang, Y., Yang, Z., An Experimental Investigation into the Effect of Synthetic Jet on the Icing Process of a Water Droplet on a Cold Surface, *International Journal of Heat and Mass Transfer* 72 (2014) 553-58.

Jones, S.M., Reveley, M.S., Evans, J.K., Barrientos, F.A., *Subsonic Aircraft Safety Icing Study*, NASA TM-215107, 2008.

Jonsson, T., *On the One-Dimensional Stefan Problem with Some Numerical Analysis*, Bachelor Thesis, UMEÅ Universitet, Sverige, Sweden, 2013.

Kollár, L.E., Farzaneh, M., Karev, A.R., Modeling Droplet Collision and Coalescence in an Icing Wind Tunnel and the Influence of These Processes on Droplet Size Distribution, *International Journal of Multiphase Flow* 31 (2005) 69-92.

Kong, W., Liu, H., An Ice Accretion Model for Aircraft Icing Based on Supercooled Icing: Theory and Application, in: 50th AIAA Aerospace Science Meeting including the New Horizons Forum and Aerospace Exposition, 9-12 January 2012, Nashville, Tennessee.

Langham, E.J., Mason, B.J., The Heterogeneous and Homogeneous Nucleation of Supercooled Water, *Proceedings of the Royal Society A* 247 (1958) 493-504.

Lapple, E.J., Sheperd, C.B., Calculation of Particle Trajectories, *Industrial & Engineering Chemistry* 32 (1940) 605-617.

Lauder, B.E., Spalding, D.B., The Numerical Computation of Turbulent Flows, *Computer Methods in Applied Mechanics and Engineering* 3 (1974) 269-289.

Leonard, B.P., A Stable and Accurate Convective Modeling Procedure Based on Quadratic Upstream Interpolation, *Computer Methods in Applied Mechanics and Engineering* 19 (1979) 59-98.

Magalhães, L.B., Numerical Study of Freezing Droplets, Master Thesis, University of Beira Interior, Covilhã, Portugal, 2016.

Magalhães, L.B., Barata, J., Silva, A.R.R., Numerical Study of Freezing Droplets, in: CEM 2016-Mechanical Engineering Conference, 1-3 June 2016, Porto, Portugal, 31-37.

Messinger, B.L., Equilibrium temperature of an unheated icing surface as a function of air speed, *Journal of the Aeronautical Science* 20 (1953) 29-42.

Myers, T.G., Charpin, J.P.F., Thompson, C.P., Slowly Accreting Ice due to Supercooled Water Impacting on a Cold Surface, *Physics of Fluids* 14 (2002) 240-256.

Nauenberg, M., Theory and Experiments on the Ice - Water Front Propagation in Droplets Freezing on a Subzero Surface, *European Journal of Physics* 37 (2016) 1-11.

Patankar, S.V., Spalding, D.B., A Calculation Procedure for Heat, Mass and Momentum Transfer in Three-Dimensional Parabolic Flows, *International Journal of Heat and Mass Transfer* 15 (1972) 1787-1806.

Ranz, W.R., Marshall, W.R., Evaporation from Drops, *Chemical Engineering Progress* 48 (1952) 141-46, 173-80.

Rodrigues, C.M.G., Modelling of Spray-Wall Impingement, PhD Thesis, University of Beira Interior, Covilhã, Portugal, 2016.

Ruberto, S., Reutzsch, J., Weigand, B., Experimental Investigation of the Evaporation Rate of Supercooled Water Droplets at Constant Temperature and Varying Relative Humidity, *International Communications in Heat and Mass Transfer* 77 (2016) 190-194.

Shirokar, J.S., Coimbra, C.F.M., Mcquay, M.Q., Fundamental Aspects of Modeling Turbulent Particle Dispersion in Dilute Flows, *Progress in Energy and Combustion Science* 22 (1996) 363-399.

Silva, A.R.R., Experimental and Numerical Study of Physical Aspects of Fuel Processes, PhD Thesis, University of Beira Interior, Covilhã, Portugal, 2007.

Sommerfeld, M., Analysis of Isothermal and Evaporating Turbulent Sprays by Phase-Doppler Anemometry and Numerical Calculations, *International Journal of Heat and Fluid Flow* 19 (1998)173-186.

Sparrow, E.M., Gregg, J.L., The Variable Fluid-Property Problem in Free Convection, *Transactions of the American Society of Mechanical Engineers* 80 (1958) 879-886.

Talhat, A.M., Lister, V.Y., Moggridge, G.D., Rasburn, J.R., Wilson, D.I., Development of a Single Droplet Freezing Apparatus for Studying Crystallisation in Cocoa Butter Droplets, *Journal of Food Engineering* 156 (2015) 67-83.

Tanner, F.X., Droplet Freezing and Solidification, in: Ashgriz, N. (Ed), Handbook of Atomization and Sprays, Springer, Boston, 2010, 327-338.

Thomas, L.H., Elliptic Problems in Linear Differential Equations over a Network, *Watson Science Computer Laboratory Report*, Columbia University, New York, 1949.

Wang, C., Chang, S., Leng, M., Wu, H., Yang, B., A Two-Dimensional Splashing Model for Investigating Impingement Characteristics of Supercooled Large Droplets, *International Journal of Multiphase Flow* 80 (2016) 131-49.

Watson, K.M., Prediction of Critical Temperatures and Heats of Vaporization, *Industrial & Engineering Chemistry* 23 (1931) 360-364.

Xin, L., Junqiang, B., A Spongy Icing Model for Aircraft Icing, *Chinese Journal of Aeronautics* 27 (2014) 40-51.

Yao, S.-C., Schrock, V.E., Heat and Mass Transfer from Freely Falling Drops, *Journal of Heat Transfer* 98 (1976) 120-126.

Zarling, J.P., Heat and Mass Transfer from Freely Falling Drops at Low Temperatures, *CRREL Research Report* (1980) ADA090522.

Zhou, Z.-H., Yi, X., Gui, Y.-W., Du, Y.-X., Study on the Heat Transfer Characteristics in Aircraft Icing, *Procedia Engineering* 99 (2015) 671-676.

Attachments

Attachment A. List of publications

Oral Communication:

Franco, A., Silva, A., Barata, J., Numerical Modelling of a Cooling Droplet Using a Two Phase Flow Approach, in: IV LAETA Young Researchers Meeting, 9-10 November 2017, Covilhã, Portugal.

Franco, A., Barata, J., Silva, A., Numerical Modeling of a Cooling and Freezing Water Droplet Using a Two-Phase Flow Approach, in: AIAA Science and Technology Forum and Exposition 2019, 7-11 January 2019, San Diego, California, USA. (Extended Abstract).

Franco, A., Barata, J., Silva, A., Numerical Modeling of a Cooling Water Droplet Using a Two-Phase Flow Approach, in: AIAA Science and Technology Forum and Exposition 2019, 7-11 January 2019, San Diego, California, USA.

NUMERICAL MODELLING OF A COOLING DROPLET USING A TWO PHASE FLOW APPROACH

André Franco^{a*}, André Silva^a, Jorge Barata^a

a) AeroG - LAETA, Calçada Fonte do Lameiro, 6201-001 Covilhã

*email: andreromaofranco@gmail.com

Keywords: Ice accretion, heat and mass transfer, supercooling, Ranz-Marshall relations, cooling droplets

Abstract.

The present work aims to study the freezing of droplets and the ice formation in the several surfaces of an aircraft. These processes have gain increased importance in the aeronautical field, due to the impact that ice accretion has on standard operation of an aircraft. It is known that 12% of all aircraft flight accidents, which took place in adverse weather conditions between 1999 and 2000, occurred due to the icing phenomena. There were reported 730 accidents between 1998 and 2007, related with icing. If there is not any change both in the current rate of accidents and incidents and in the continued growth in air transportation, there will be more than 4500 air travel fatalities per year due to icing related accident, by 2025. In order to prevent the solidification of water droplets and the subsequent ice accretion on an airplane surface, several methods to avoid and to remove the ice are implemented in the present days. However those measures can evaporate impinging water droplets or melt the accreted ice, there is still the potential risk of runback ice forming further downstream due to a refreezing of the ice-water mixture on unprotected areas. Supercooled large droplets tend to have greater inertia and are able to impinge on aircraft surfaces far beyond the limits of the ice protection systems. Aircraft often fly under subfreezing temperatures, in which the water droplets can still be liquid, experiencing a supercooling stage. In a cold atmosphere, in order to cool airborne droplets, heat transfer can occur by three different mechanisms, namely: convective heat transfer, convective mass transfer and thermal radiation from the droplet surface. Droplets generally nucleate at the surface forming a frozen shell which propagates inwardly. The temperature transition of the droplet is solved by balancing the internal energy with the energy removed by heat transfer, mass transfer and thermal radiation. Several models can be used with the purpose of describing the droplet freezing process. One of these models is composed by four stages, which includes supercooling. To solve it is necessary to make use of the Ranz-Marshall relations. The goal of the present work is to simulate the cooling of a water droplet using a two phase flow approach. It is intended to study the interaction between the liquid-gas phases of the droplet and air surrounding it.

Numerical Modeling of a Cooling and Freezing Water Droplet Using a Two-Phase Flow Approach

André Franco¹, Jorge Barata², and André Silva³
Universidade da Beira Interior, Covilhã, 6200-001, Portugal

Extended Abstract

The cooling and freezing of water droplets have gained increased importance in the aeronautical field, due to the impact that ice accretion in the several aircraft surfaces has on standard operation of an aircraft. The necessity of studying the cooling and freezing phenomena, which has always been somewhat neglected in favor of the heating and evaporation of droplets, arises from the several accidents and incidents that occurred due to this hazard. An accretion of ice of merely 0.4 mm on a wing upper surface may cause a loss of 25% of lift and decrease the stall angle of attack by 6° [1] and aircraft often fly under subfreezing temperatures [2]. At these temperatures the water droplets can still be liquid, experiencing a supercooling stage.

In a report with the goal of studying the Subsonic Aircraft Safety Icing, NASA gathered incident reports between January 1988 and February 2007 [3]. Table 1 presents the ASRS (Aviation Safety Reporting System) icing related incidents by flight stage, concluding that the height of the incidents occurs during cruise flight with 325 incidents, followed by descent operations.

Table 1 ASRS Icing related Incidents by Flight Stage

FLIGHT STAGE	NUMBER OF INCIDENTS REPORTED
CLIMB-OUT	98
CRUISE	325
DESCENT	193
GROUND	106
LANDING	133

Table 2 shows icing related incidents grouped by engine type, being clearer that the reciprocating and turbojet aircraft are the most likely to suffer from icing.

Table 2 ASRS Icing related Incidents by Engine Type

ENGINE TYPE	NUMBER OF INCIDENTS REPORTED
RECIPROCATING	223
TURBOJET	208
TURBOPROP	87
UNKNOWN	46

¹ Master Student, Aerospace Sciences Department, andreromaofranco@gmail.com.

² Full Professor, Aerospace Sciences Department, and Associate Fellow of AIAA, jmmbarata@gmail.com.

³ Assistant Professor, Aerospace Sciences Department, and Member of AIAA, andre@ubi.pt.

If there is not any change both in the current rate of accidents and incidents and in the continued growth in air transportation, there will be more than 4500 air travel fatalities per year due to icing related accident, by 2025, accordingly to the FAA [4].

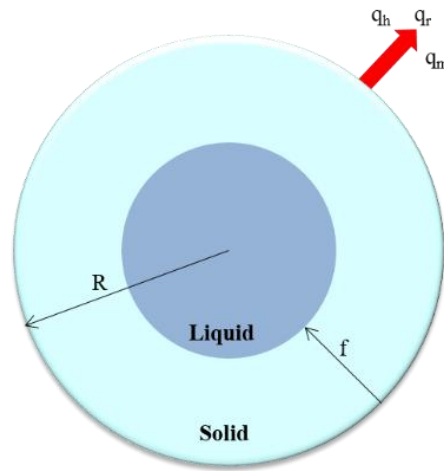


Fig. 1 Inward freezing from initial frozen shell (Adapted from [7])

To prevent the solidification of water droplets and consequently ice accretion on an aircraft surface, several methods to avoid and to remove the ice are implemented in the aircraft. Normally the critical areas of the aircraft are equipped with de-icing technology. Warm bleed air from engine compressors or forcing freezing point depressant fluid out of porous panels are methods to counter attack ice formation or accretion [5]. Although those measures can evaporate impinging water droplets or melt the accreted ice, there is still the potential risk of runback ice forming further downstream due to a refreezing of the ice-water mixture on unprotected areas. Supercooled large droplets tend to have greater inertia and can impinge on aircraft surfaces far beyond the limits of the ice protection systems [6]. It is then imperative to fully comprehend the freezing process and the ice accretion effect and develop models capable of simulate it. With those, engineers could predict with maximum efficiency freezing and avoid this phenomenon or even taking advantage of it and develop new technologies that ultimately will improve air travel.

In a cold atmosphere, in order to cool airborne droplets, heat transfer can occur by three different mechanisms, namely: convective heat transfer, convective mass transfer and thermal radiation from the droplet surface. Droplets generally nucleate at the surface forming a frozen shell which propagates inwardly [7]. The temperature transition of the droplet is solved by balancing the internal energy with the energy removed by heat transfer, mass transfer and thermal radiation. This process is presented in Fig. 1.

Several models can be used with the purpose of describing the droplet freezing process. One of these models is composed by four stages, which includes supercooling [8]. To solve it is necessary to make use of the Ranz-Marshall relations.

This paper aims to study the cooling and freezing of water droplets in free fall. In order to do so a two-way coupling model was developed based on the model presented in Ref. [9]. With this model it is possible to evaluate the influence of the interactions drop-gas and gas-drop, since the fluid in which the particles are travelling is affected by their presence. It is considered variable thermo-physical properties, a uniform temperature across the droplet radius and a uniform pressure around the droplet. The flowchart presented in Fig. 2 illustrates the iterative process of the model as it is exemplified in Ref. [10].

The model can be divided into a continuous phase in which the fluid represented is the air and a dispersed phase composed by water droplets. Regarding the continuous phase it is considered a single-phase fluid using an Eulerian approach. When any particles in a different phase are present in the fluid, their interactions are accounted through source terms. The QUICK scheme is employed to the continuous phase. Equation (1) represents a convective-diffusive conservation equation that can be applied to all the governing equations. The solution to the gas phase is based on the solution of the equations for energy, momentum and mass and the “ k - ϵ ” turbulence model is adopted. The solution procedure for the continuous phase is based on the SIMPLE algorithm and it is used a staggered grid arrangement.

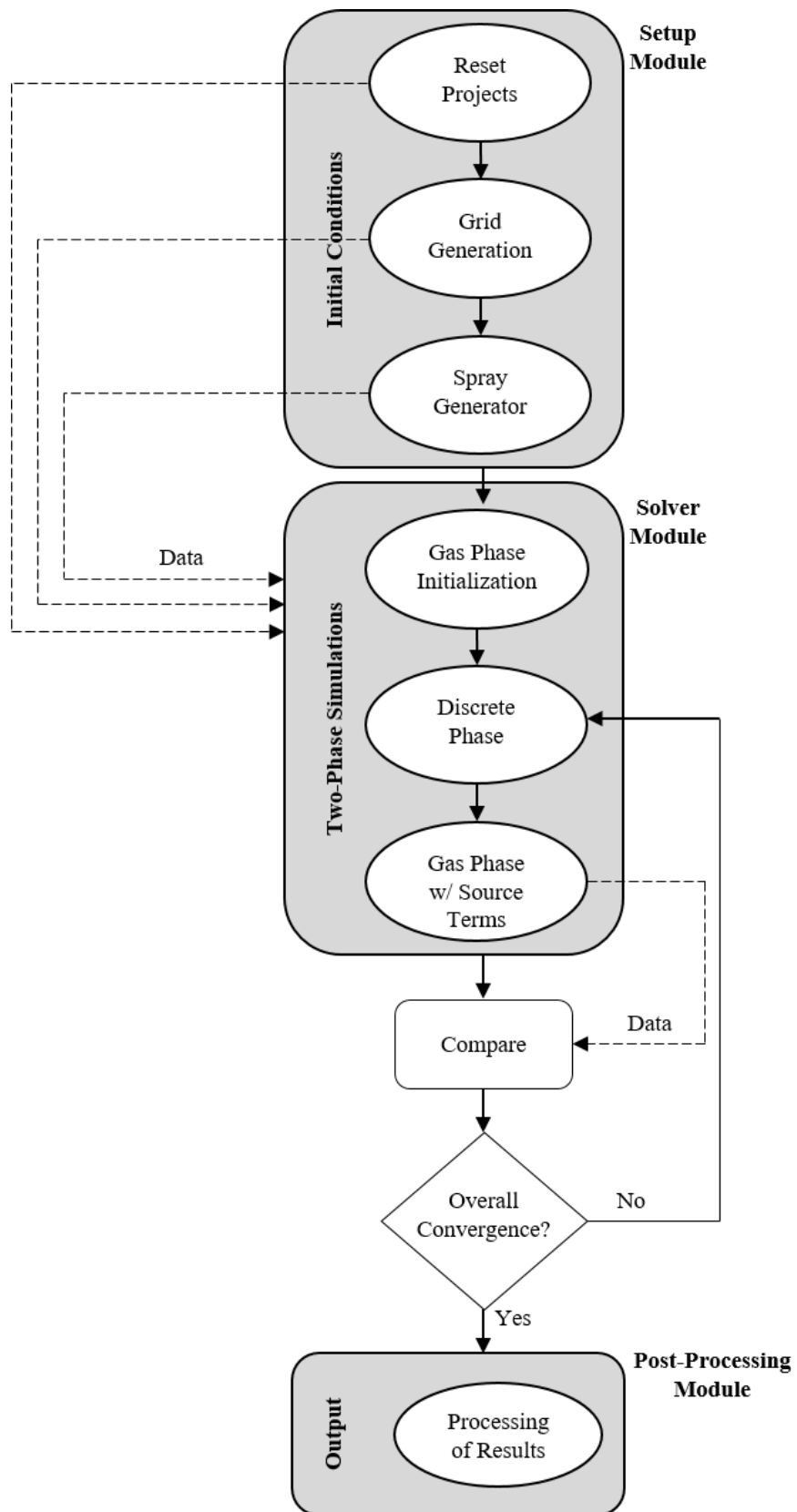


Fig. 2 Flowchart of the iterative process of the model (Adapted from [10])

$$\frac{\partial(\rho U_i \Phi)}{\partial X_i} = \frac{\partial}{\partial X_i} \left(\Gamma_\Phi \frac{\partial \Phi}{\partial X_i} \right) + S_\Phi \quad (1)$$

In order to model the dispersion phase, it was adopted a Lagrangian approach. In this type of modeling the individual particles are tracked as they move through the computational domain. Thus, the reference frame move with the droplet and the instantaneous position of the particle can be considered as a function of the location from where it originated and the time elapsed. The dispersed phase also considers anisotropy.

The simplified spherical droplet momentum equation can be written as Eq. (2). This equation takes into account the drag term and the gravity term. All the other forces are negligible, namely the Basset, virtual mass, Magnus, Saffman and buoyancy forces.

$$\frac{du_{d,i}}{dt} = \frac{1}{\tau_d} (u_{f,i} - u_{d,i}) + g_i \quad (2)$$

The temporal change of temperature of the droplet can be computed from Eq. (3).

$$\frac{dT_d}{dt} = \frac{12k_g \ln(1+B_M)}{C_{p_g} \rho_F C_{p_F} d_d^2} \left(1 + \frac{0.276 Re^{1/2} Pr^{1/3}}{F_M} \right) \left(\frac{C_{p_g} (T_\infty - T_S)}{B_M} - L(T_S) \right) \quad (3)$$

To solve the problem, the initial conditions can be established by defining the staggered grid and the characteristics of the initial drops. Afterwards it is performed a calculation of the gas flow field without the contribution of the source terms of the dispersed phase. The particles are then traced through the flow field in the dispersed phase and the values of the source terms are calculated. The gas is then recomputed with the contribution of the source terms of the dispersed phase. The process is repeated until convergence is achieved. Finally, the post-processing of the data occurs.

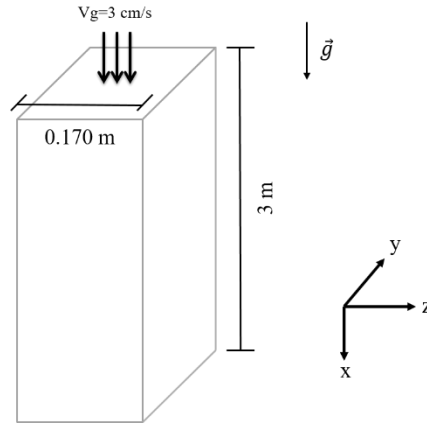


Fig. 3 Computational domain

The first stage of the present work is to perform a simulation of a droplet cooling in a free fall. Water drops with diameters of 3, 4, 5, and 6 mm are injected into a tunnel on the center cross section, as presented in Fig. 3. This simulation was designed this way to be possible to compared it to the experimental results obtained in Ref. [11] and the numerical results obtained and shown in Ref. [12] in which it was used a one-way coupling model, in which it did not existed an interaction between the dispersed phase and the continuous phase. The gas would affect the particles' properties but the particles would not affect the gas properties. A correction developed by Ranz and Marshall [13] was implemented in the simulations performed by the authors. This correction accounts for the impact that vibrations and deformations of the falling drops have on the heat and mass transfer coefficient values. This correction was also implemented in the model developed. It is expected that the two-way coupling model will prove to be a better approximation to the experimental data than the one-way coupling model.

The next stage of the present work it is going to be to freeze the droplet. The considerations needed to obtain this process are already implemented in the model. Assuming the outer surface of the droplet is solid

during the freezing process allows mass transfer via sublimation. The latent heat due to crystallization is removed by the external heat fluxes: heat transfer, mass transfer and thermal radiation.

Acknowledgments

The present work was performed under the scope of Laboratório Associado em Energia, Transportes e Aeronáutica (LAETA) – activities and it was supported by Fundação para a Ciência e Tecnologia (FCT) through the project UID/EMS/50022/2013.

References

- [1] Myers, T. G., Charpin, J. P. F., and Thompson, C. P., “Slowly Accreting Ice due to Supercooled Water Impacting on a Cold Surface,” *Physics of Fluids*, Vol. 14, No. 1, 2002, pp. 240–56.
doi: 10.1063/1.1416186
- [2] Zhou, Z.-H., Yi, X., Gui, Y.-W., and Du, Y.-X., “Study on the Heat Transfer Characteristics in Aircraft Icing,” *Procedia Engineering*, Vol. 99, September 2015, pp. 671–76.
doi: 10.1016/j.proeng.2014.12.588
- [3] Jones, S. M., Reveley, M. S., Evans, J. K., and Barrientos, F.A., “Subsonic Aircraft Safety Icing Study,” NASA TM-215107, 2008.
- [4] Caliskan, F., and Hajiyev, C., “A Review of in-Flight Detection and Identification of Aircraft Icing and Reconfigurable Control,” *Progress in Aerospace Sciences*, Vol. 60, July 2013, pp. 12–34.
doi: 10.1016/j.paerosci.2012.11.001
- [5] Elliott, J. W., and Smith, F. T., “Ice Formation on a Smooth or Rough Cold Surface due to the Impact of a Supercooled Water Droplet,” *Journal of Engineering Mathematics*, Vol. 102, No. 1, 2017 pp. 35–64.
doi: 10.1007/s10665-015-9784-z
- [6] Wang, C., Chang, S., Leng, M., Wu, H., and Yang, B., “A Two-Dimensional Splashing Model for Investigating Impingement Characteristics of Supercooled Large Droplets,” *International Journal of Multiphase Flow*, Vol. 80, April 2016, pp. 131–49.
doi: 10.1016/j.ijmultiphaseflow.2015.12.005
- [7] Hindmarsh, J. P., Russell, A. B., and Chen, X. D., “Experimental and Numerical Analysis of the Temperature Transition of a Suspended Freezing Water Droplet,” *International Journal of Heat and Mass Transfer*, Vol. 46, No. 7, 2003, pp. 1199–1213.
doi: 10.1016/S0017-9310(02)00399-X
- [8] Tanner, F. X., “Droplet Freezing and Solidification,” *Handbook of Atomization and Sprays*, edited by N. Ashgriz, Springer Science Business Media, Boston, 2010, pp. 327–38.
- [9] Silva, A. R. R., “Experimental and Numerical Study of Physical Aspects of Fuel Processes”, Ph.D. Dissertation, Aerospace Sciences Department, Universidade da Beira Interior, Covilhã, Portugal, 2007
- [10] Rodrigues, C. M. G., “Modelling of Spray-Wall Impingement”, Ph.D. Dissertation, Aerospace Sciences Department, Universidade da Beira Interior, Covilhã, Portugal, 2016.
- [11] Yao, S.-C., and Schrock, V. E., “Heat and Mass Transfer From Freely Falling Drops,” *Journal of Heat Transfer*, Vol. 98, No. 1, 1976, pp. 120–26.
doi: 10.1115/1.3450453
- [12] Magalhães, L., Barata, J., and Silva, A., “Numerical Study of Freezing Droplets,” *CEM – Mechanical Engineering Conference*, Porto, Portugal, 1-3 June 2016, pp. 31–37.
- [13] Ranz, W. R., and Marshall, W. R., “Evaporation from Drops,” *Chemical Engineering Progress*, Vol. 48, No. 3 and 4, 1952, pp. 141-146, 173-180



Numerical Modeling of a Cooling Water Droplet Using a Two-Phase Flow Approach

André Franco*, Jorge Barata†, and André Silva‡
Universidade da Beira Interior, Covilhã, 6200-001, Portugal

The study and understanding of cooling and freezing water droplets is of paramount importance due to their influence in the decrease of aerodynamic performance on lifting surfaces. It is imperative to develop models capable of simulating the freezing processes and ice accretion effects, in order to predict with maximum efficiency freezing and avoid this phenomenon or even taking advantage of it and develop new technologies that ultimately will improve air travel. As such, this paper aims to study the cooling of a water droplet in free fall. A two-way coupling is implemented to evaluate the influence of water-droplet and drop-gas interactions, numerically investigating the cooling of free falling droplets for different diameters and air humidity ratios. The predictions are compared with experimental and numerical data with the objective of providing insight into the degree of heat and mass transfer involved. Some correlations to account for the convection effects are introduced and are found to be in close agreement with the experimental data.

I. Nomenclature

B	=	transfer number
B_M	=	mass transfer number
B_T	=	thermal transfer number
$C.F.$	=	correction factor
C_p	=	specific heat at constant pressure
$C_\mu, C_{\varepsilon 1}, C_{\varepsilon 2}, C_{\varepsilon 3}$	=	coefficients in the turbulence model
D	=	droplet diameter
D_g	=	diffusion coefficient
g	=	gravitational acceleration
hr	=	humidity ratio
h_m	=	convective mass transfer coefficient
h_o	=	convective heat transfer coefficient
k	=	turbulent kinetic energy
K_g	=	thermal conductivity of the gas
L	=	Latent heat of vaporization
\dot{m}	=	rate of evaporation
$Nu = \frac{h_o D}{K_g}$	=	Nusselt number
P	=	pressure
$Pr = \frac{C_p \mu_g}{K_g}$	=	Prandtl number
Q_L	=	rate of heat transfer
$Re = \frac{\rho_g v_r D}{\mu_g}$	=	Reynolds number
S	=	source term
$Sc = \frac{\mu_g}{\rho_g D_g}$	=	Schmidt number
$Sh = \frac{h_m D}{D_g}$	=	Sherwood number
T	=	temperature

*Master Student, Aerospace Sciences Department, andreromaofranco@gmail.com.

†Full Professor, Aerospace Sciences Department, jmbarata@gmail.com, and Associate Fellow of AIAA.

‡Assistant Professor, Aerospace Sciences Department, andre@ubi.pt, and Member of AIAA.

Y	=	mass fraction
z	=	vertical coordinate
Γ	=	effective diffusion coefficient
ε	=	rate of dissipation of turbulence energy
ρ	=	density
τ	=	dimensionless temperature variation
Φ	=	dependent variable

II. Introduction

THE necessity of studying the cooling and freezing phenomena, which has always been somewhat neglected in favor of the heating and evaporation of droplets, arises from several accidents and incidents that occurred due to this hazard. An accretion of ice of merely 0.4 mm on a wing's upper surface may cause a loss of 25% of lift and decrease the stall angle of attack by 6° [1] and aircraft often fly under subfreezing temperatures [2]. Whenever an aircraft flies through clouds at an ambient temperature below freezing, water droplets suspended in the clouds can impact and accrete ice mainly on the lifting surfaces and around engine intakes [3]. Between 1986 and 1996, the passenger mortality rate reached 39% among 42 aircraft icing accidents, accordingly to the International Civil Aviation Organization (ICAO) [4]. In a report with the goal of studying the Subsonic Aircraft Safety Icing, NASA gathered incident reports between January 1988 and February 2007 [5]. Table 1 presents the ASRS (Aviation Safety Reporting System) icing related incidents by flight stage, concluding that the peak of the incidents occurs during cruise flight with 325 incidents, followed by descent operations.

Table 1 ASRS Icing Related Incidents by Flight Stage (Adapted from [5]).

Flight stage	Number of incidents reported
Climb-out	98
Cruise	325
Descent	193
Ground	106
Landing	133

Table 2 shows icing related incidents grouped by engine type, being clearer that the reciprocating and turboprop aircraft are the most likely to suffer from icing.

Table 2 ASRS Icing Related Incidents by Engine Type (Adapted from [5]).

Engine type	Number of incidents reported
Reciprocating	223
Turboprop	208
Turboprop	87
Unknown	46

If there is not any change both in the current rate of accidents and incidents and in the continued growth in air transportation, there will be more than 4500 air travel fatalities per year due to icing related accidents, by 2025, accordingly to the FAA [6]. To prevent the solidification of water droplets and consequently ice accretion on an aircraft surface, several methods to avoid and to remove the ice are implemented in the aircraft. The critical areas of the aircraft are normally equipped with de-icing technology. Although normally the methods can evaporate impinging water droplets or melt the accreted ice, there is still the potential risk of runback ice forming further downstream due to a refreezing of the ice-water mixture on unprotected areas. In a cold atmosphere, in order to cool airborne droplets, heat transfer can occur by three different mechanisms, namely: convective heat transfer, convective mass transfer and thermal radiation from the droplet surface. Droplets generally nucleate at the surface forming a frozen shell which

propagates inwardly [7]. The temperature transition of the droplet is solved by balancing the internal energy with the energy removed by heat transfer, mass transfer and thermal radiation. This process is presented in Fig. 1.

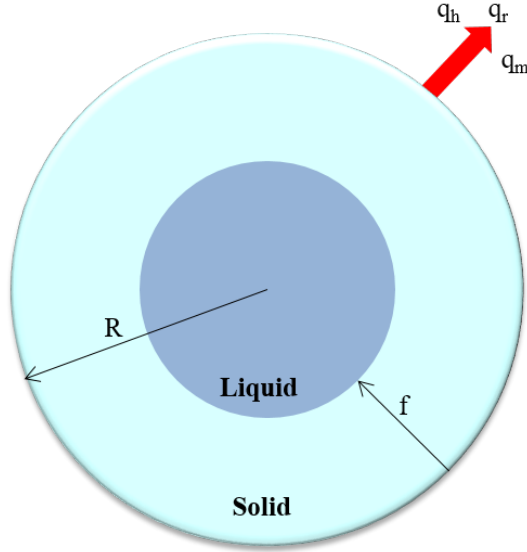


Fig. 1 Inward freezing from initial frozen shell (Adapted from [7]).

The objective is then to numerically modeling the cooling of free falling droplets for different diameters and air humidity ratios, using a two-way coupling approach. The results obtained are compared to experimental data by Yao and Schrock [8], and also numerical data from Magalhães [9], in which a one-way coupling model was used. Magalhães [9] implemented the Ranz-Marshall relations [10], with and without a correction factor. In the present work, three different correlations to take into account the convective effect are then considered.

III. Mathematical Model

In order to study the cooling of a water droplet in free fall a two-way coupling model is implemented, based on the model presented by Silva and Rodrigues [11, 12].

The particle phase is described using a Lagrangian approach while for the continuous phase an Eulerian frame is used.

The method to solve the continuous phase is based on the solution of the conservation equations for momentum and mass. Turbulence is modelled using the "k-ε" turbulence model of Launder and Spalding [13]. The QUICK scheme of Leonard [14] is used to analyze the convection terms.

All of the governing equations (continuity, momentum, turbulent kinetic energy, its dissipation, enthalpy, and vapor mass fraction) can be reduced to a single convective-diffusive conservation equation such as Eq. (1), where Φ is considered a dependent variable.

$$\frac{\partial(\rho U_i \Phi)}{\partial X_i} = \frac{\partial}{\partial X_i} \left(\Gamma_\Phi \frac{\partial \Phi}{\partial X_i} \right) + S_\Phi \quad (1)$$

The effective diffusion coefficient for quantity Φ is described by Γ_Φ . The term on the left-hand side of Eq. (1) represents the convection term while the first and second terms on the right-hand side are the diffusion and the source terms, respectively.

The source term can be divided into contributions from the gas and particle, as presented in Eq. (2).

$$S_\Phi = S_{\Phi,g} + S_{\Phi,d} \quad (2)$$

The source terms of the gas phase, $S_{\Phi,g}$ and the effective diffusion coefficient, Γ_Φ , are presented in Table 3 for different dependent variables.

Table 3 Terms in the general form of the differential equation.

ϕ	$S_{\phi,g}$	$S_{\phi,d}$	Γ_{ϕ}
1	-	$\overline{S_{m,d}}$	-
U_i	$-\frac{\partial}{\partial x_i} \left(P + \frac{2}{3}k \right) - \frac{\partial}{\partial x_j} \frac{2}{3} \mu_t \frac{\partial \overline{U_j}}{\partial x_i} + \rho g_i$	$\overline{S_{U_i,d}}$	$\mu + \mu_t$
T	0	$\overline{S_{T,d}}$	$\frac{\mu}{Pr} + \frac{\mu_t}{Pr_t}$
Y	0	$\overline{S_{Y,p}}$	$\frac{\mu}{Sc} + \frac{\mu_t}{Sc_t}$
k	$G - \rho \varepsilon$	$\overline{S_{k,d}}$	$\mu + \frac{\mu_t}{\sigma_k}$
ε	$C_{\varepsilon 1} \frac{\varepsilon}{k} G - C_{\varepsilon 2} \rho \frac{\varepsilon^2}{k}$	$\overline{S_{\varepsilon,d}}$	$\mu + \frac{\mu_t}{\sigma_{\varepsilon}}$

The solution procedure is based on the SIMPLE algorithm [15]. The tri-diagonal matrix algorithm (TDMA) [16] is then applied line-by-line to solve the set of equations.

In the dispersed phase a Lagrangian reference frame was considered, in which the particle momentum equation through the Eulerian fluid velocity field was solved to obtain the particle trajectories. The droplet momentum equation can be simplified, neglecting the effects of the Basset, virtual mass, Magnus, Saffman, and buoyancy forces, which leads to Eq. (3).

$$\frac{\partial u_{d,i}}{\partial t} = \frac{1}{\tau_d} (u_{f,i} - u_{d,i}) + g_i \quad (3)$$

To describe the cooling model, convection effects are taken into account by introducing correlations. The main assumptions are: spherical symmetry, quasi-steady gas film around the drop, uniform physical properties of the surrounding fluid, uniform pressure around the drop, and liquid/vapor thermal equilibrium on the drop surface. They are generally expressed through the Sherwood number, Sh, and Nusselt number, Nu. Three different correlations are introduced in the model in order to evaluate the convection effects. The Ranz-Marshall relations [10] and the model proposed by Ref. [17], based on the Abramzon and Sirignano [18] approach were tested. Furthermore, a third correlation, which adds a correction factor, C.F., to the Ranz-Marshall relations was also tested, accounting for vibrations and deformations of the droplet, since Ref. [8] stated that they have an impact on the heat and mass transfer coefficients.

$$\text{C.F.} = 25 \left(\frac{z}{D} \right)^{-0.7} \quad (4)$$

Table 4 summarizes the correspondent Nusselt and Sherwood numbers regarding the correlation adopted.

Table 4 Nusselt and Sherwood numbers.

Author	Case	Nu	Sh
Ranz-Marshall	1	$2 + 0.6 \text{Re}_d^{1/2} \text{Pr}_d^{1/3}$	$2 + 0.6 \text{Re}_d^{1/2} \text{Sc}_d^{1/3}$
Ranz-Marshall (correction factor)	2	$2 + 15 \text{Re}_d^{1/2} \text{Pr}_d^{1/3} \left(\frac{z}{D} \right)^{-0.7}$	$2 + 15 \text{Re}_d^{1/2} \text{Sc}_d^{1/3} \left(\frac{z}{D} \right)^{-0.7}$
Ref. [17]	3	$2 + \frac{0.552 \text{Re}_d^{1/2} \text{Pr}_d^{1/3}}{F_T}$	$2 + \frac{0.552 \text{Re}_d^{1/2} \text{Sc}_d^{1/3}}{F_M}$

To calculate the temporal change of temperature, the following differential equation has to be solved:

$$\frac{dT_d}{dt} = \frac{6Q_L}{\pi C_p D^3} \quad (5)$$

The total mass flow through this surface will be equal to the cooling rate, \dot{m} , expressed by the following expressions:

$$\dot{m} = \pi \overline{\rho_g D_g} D \text{Sh} \ln(1 + B_M) \quad (6)$$

and

$$\dot{m} = \pi \frac{\overline{K_g}}{C_{p_g}} D \text{Nu} \ln(1 + B_T) \quad (7)$$

The quantity $\overline{\rho_g D_g}$ can be replaced by $\overline{K_g}/\overline{C_{p_g}}$, assuming a Lewis number of unity. The heat released by the droplet can be expressed by the following expression:

$$Q_L = \dot{m} \left(\frac{\overline{C_{p_g}} (T_\infty - T_s)}{B_M} - L(T_s) \right) \quad (8)$$

The interaction between the two phases is introduced by treating particles as sources of mass, momentum and energy in the gaseous phase. The source terms due to the particles are calculated for each Eulerian cell of the continuous phase and are presented in Table 5.

Table 5 Dispersed phase source terms.

$S_{\Phi d}$	$S_{\Phi i}$	$S_{\Phi m}$
$\overline{S_{\rho,d}}$	0	$\Sigma_d \frac{\dot{m}_d N_d}{U_{i,j}}$
$\overline{S_{U,d}}$	$-\Sigma_d \frac{\dot{m}_d N_d}{U_{i,j}} [(U_d^{t+\Delta t} - U_d^t) g_i \Delta t]$	$\Sigma_d \frac{\dot{m}_d N_d U_{i\alpha}}{U_{i,j}}$
$\overline{S_{T,d}}$	$-\Sigma_d \frac{N_d}{U_{i,j}} (L \dot{m}_d + Q_L)$	$\Sigma_d \frac{\dot{m}_d N_d}{U_{i,j}} C_p(T_d) T_d$
$\overline{S_{Y_1,d}}$	0	0
$\overline{S_{Y_2,d}}$	0	$\Sigma_d \frac{\dot{m}_d N_d}{U_{i,j}}$
$\overline{S_{k,d}}$	$\overline{U_j S_{U_{ji}}} - \overline{U_j S_{U_{ji}}}$	$\overline{U_j S_{U_{jm}}} - \overline{U_j S_{U_{ji}}} + \frac{1}{26} \overline{U_j U_j S_m} - \frac{1}{2} \overline{U_j U_j S_m}$
$\overline{S_{\varepsilon,d}}$	$C_{\varepsilon 3} \frac{\varepsilon}{k} \overline{S_{ki}}$	$C_{\varepsilon 3} \frac{\varepsilon}{k} \overline{S_{km}}$

The source terms can be divided into the source term due to inter-phase transport, $S_{\Phi i}$, and the transfer caused by cooling, $S_{\Phi m}$, which yields the following expression:

$$S_{\Phi d} = S_{\Phi i} + S_{\Phi m} \quad (9)$$

The flowchart presented in Fig. 2 illustrates the iterative process of the model as shown by Rodrigues (2016) [12].

The study consists in the injection of drops into a tunnel on the center cross section, as presented in Fig. 3. As seen on the figure, the tunnel has a square section of 170x170 mm with a height of 3000 mm. The velocity of the air corresponds to 3 cm/s. Only half of the tunnel is simulated, with the assumption of a symmetry plane.

Figure 4 represents a horizontal velocity profile, used to test the grid dependency of the computations, showing the comparison between the obtained data for different grids, presented as dimensionless quantities. The horizontal component, x , is normalized by the width of the tunnel, l , in the vertical axis, and the vertical component of velocity, V , is normalized by the gas velocity, V_g , in the horizontal axis. Figure 4 shows that the results are already independent of numerical influences for 7x12x115. Nevertheless, to increase the precision a finer grid of 8x16x150 was adopted, with a total of 19200 points.

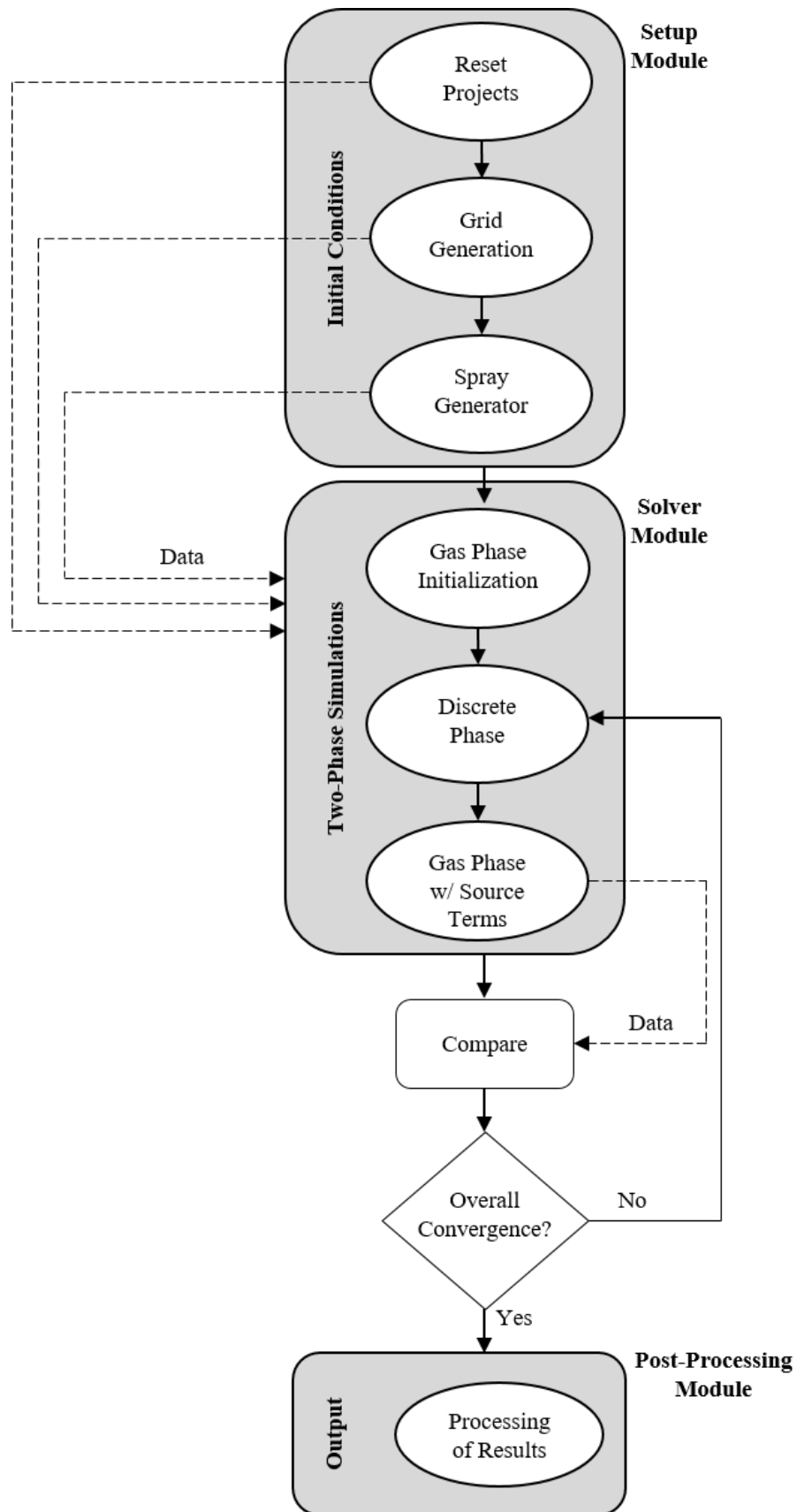


Fig. 2 Flowchart of the iterative process of the model (Adapted from [12]).

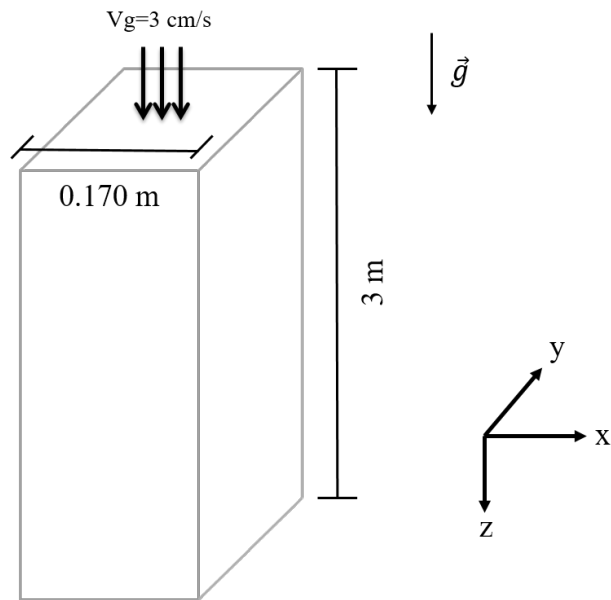


Fig. 3 Computational domain.

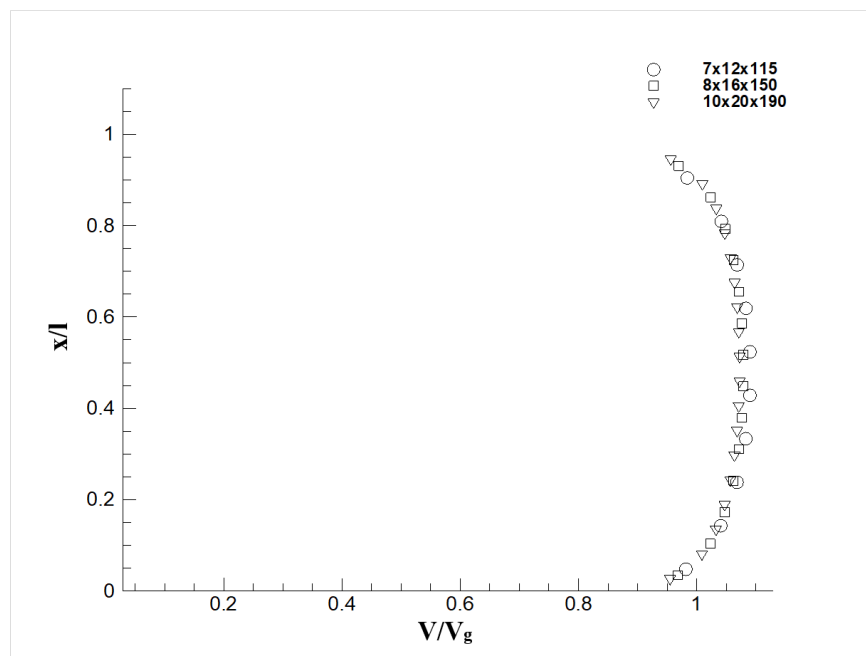


Fig. 4 Grid independence.

IV. Results and Discussion

The mathematical model described is implemented and simulations are carried out for drops with diameters of 3, 4, 5, and 6 mm, and for humidity ratios, hr , of 0.29, 0.52, and 1.00. The three correlations are applied. The predictions are compared with the experimental results of Yao and Schrock [8] and with the numerical results of Magalhães [9], which was based on a one-way coupling approach. The range of temperatures used, withdrawn from experimental data, regarding the gaseous phase was set to a minimum of 21.33 °C up to 23.61 °C and for the drop's initial temperature was set from 40.64 °C up to 40.79 °C. The velocity of the air stream was set to 3 cm/s. Table 6 summarizes the initial conditions of this study.

Table 6 Initial conditions.

Drop diameter [mm]	Drop temperature [°C]	Air temperature [°C]	Humidity ratio
3	40.70	23.29	0.29
3	40.69	23.33	1.00
4	40.64	21.33	0.52
4	40.79	23.33	1.00
5	40.68	22.88	0.29
5	40.74	23.61	1.00
6	40.66	21.33	0.52

The results presented in this section represent the variation on drop's temperature falling through the air for different humidity ratio and diameters. The horizontal axis is dimensionless, in which the falling distance is divided by the drop's diameter, z/D . The vertical axis corresponds to the dimensionless temperature variation, τ .

$$\tau = \frac{T_d - T_{d_i}}{T_{g_i} - T_{d_i}} \quad (10)$$

Eq. (10) represents the variation of the temperature of the drop by the initial temperature of the drop divided by the variation of the initial air temperature by the initial temperature of the drop. Filled symbols represent the experimental data, while hollow symbols represent numerical predictions by Ref. [9], in which the solid line represents the predictions using Ranz-Marshall classical formulation and the dash dot line using Ranz-Marshall with the addition of the correction factor. The green solid line represents Case 1, the blue solid line Case 2 and red solid line Case 3.

Figure 5 represents the variation on drop's temperature falling through the air for humidity ratios of 0.52 and 1.00 for a diameter of 4 mm. In both cases the two-way coupling model predicts with higher accuracy the experimental data, possibly due to a consideration of transient regime for the cooling of the drop. It is also possible to observe that there is not a significant difference in the predictions for Case 1, 2, and 3.

Figure 6 corresponds to the variation on drop's temperature falling through the air for a diameter of 3 mm and 5 mm for a humidity ratio of 0.29. For a diameter of 3 mm and humidity ratio 0.29, the model which predicts with higher precision corresponds to the classical formulation of Ranz-Marshall implemented by Ref. [9]. For this humidity ratio, all of the three cases of the present work failed predicting the experimental data, which hints the presence of a steady state condition for the cooling. For a diameter of 5 mm, Case 1 and Case 2 predict with accuracy the experimental data up to 200 z/D , suffering afterwards a decrease in the rate of τ . Case 2 predicts with some precision the experimental data near the region of 200 z/D . Below and after this region a closer agreement is found with the numerical predictions made by Magalhães [9] with the correction factor.

Figure 7 corresponds to the variation on drop's temperature falling through the air for a diameter of 4 mm and 6 mm for a humidity ratio of 0.52. For both cases the present work model predicts with higher accuracy the experimental data than the prediction by Magalhães [9] using the classical formulation of Ranz-Marshall. In the region below 75 z/D , for both cases, the predictions made by Magalhães [9] using Ranz-Marshall with the correction factor approximate the experimental data. Above the region of 200 z/D , Case 1, Case 2, and Case 3 predictions produce very similar results.

Figure 8 corresponds to the variation on drop's temperature falling through the air for a diameter of 3mm and 5mm for a humidity ratio of 1.00. Case 1, Case 2, and Case 3 are in close agreement with the experimental data. The predictions are also very similar between each other. The results obtained by Magalhães [9] do not predict with precision the experimental data.

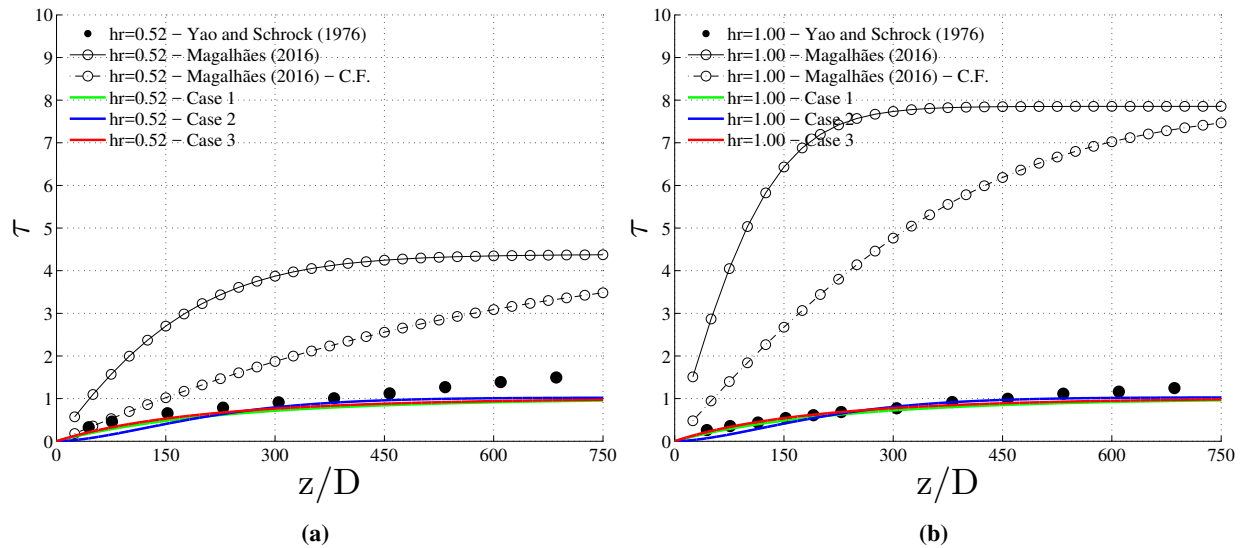


Fig. 5 Variation on drop's temperature falling through the air for a humidity ratio of 0.52 (a) and 1.00 (b) for a diameter of 4 mm.

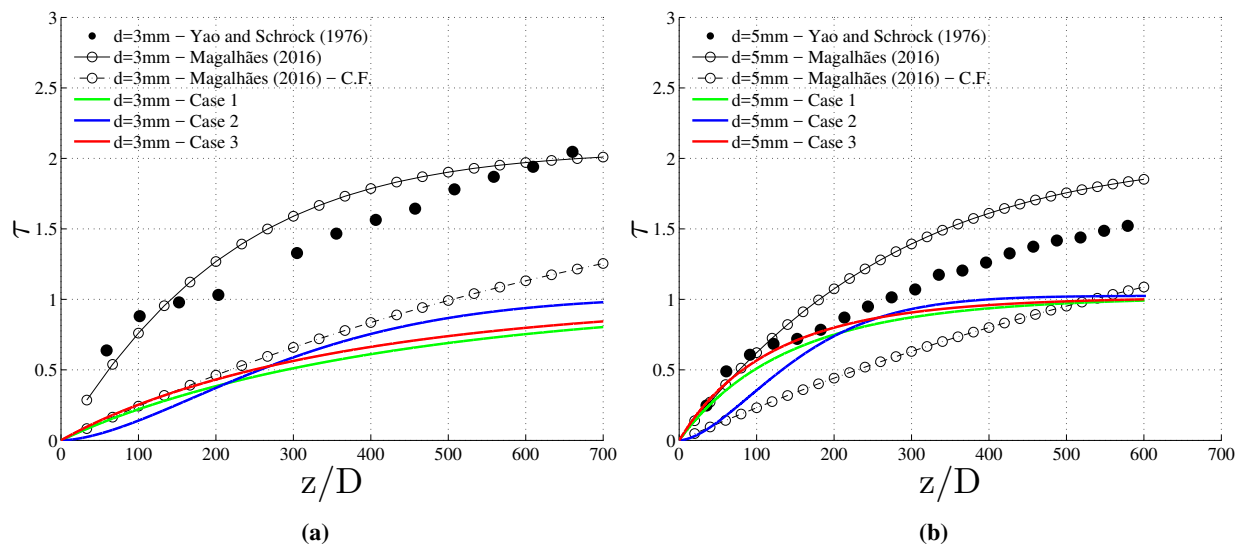


Fig. 6 Variation on drop's temperature falling through the air for a diameter of 3 mm (a) and 5 mm (b) for a humidity ratio of 0.29.

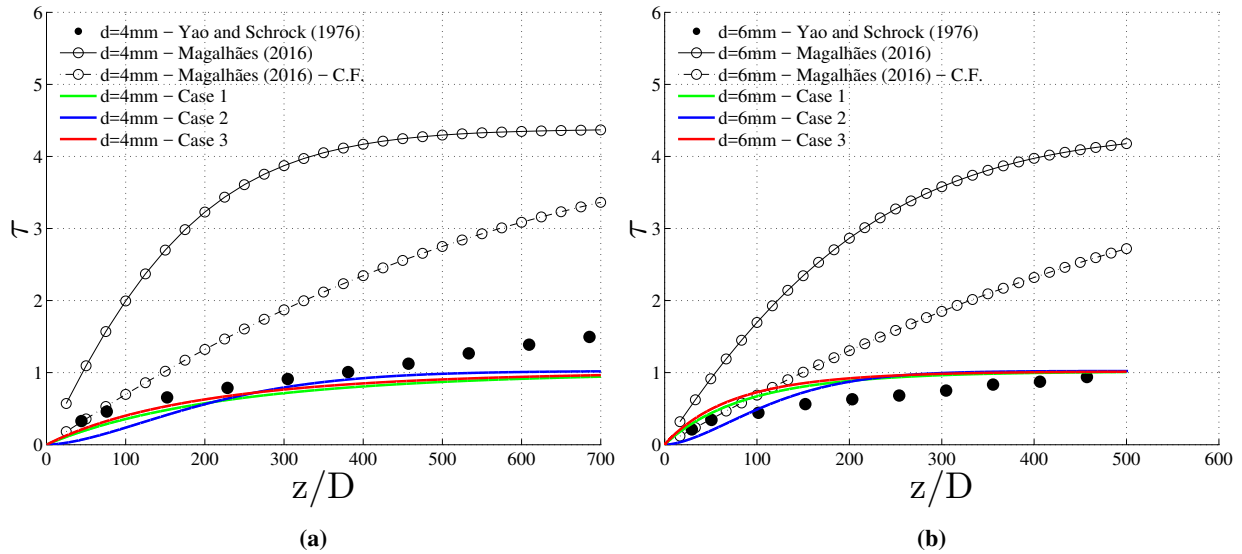


Fig. 7 Variation on drop's temperature falling through the air for a diameter of 4 mm (a) and 6 mm (b) for a humidity ratio of 0.52.

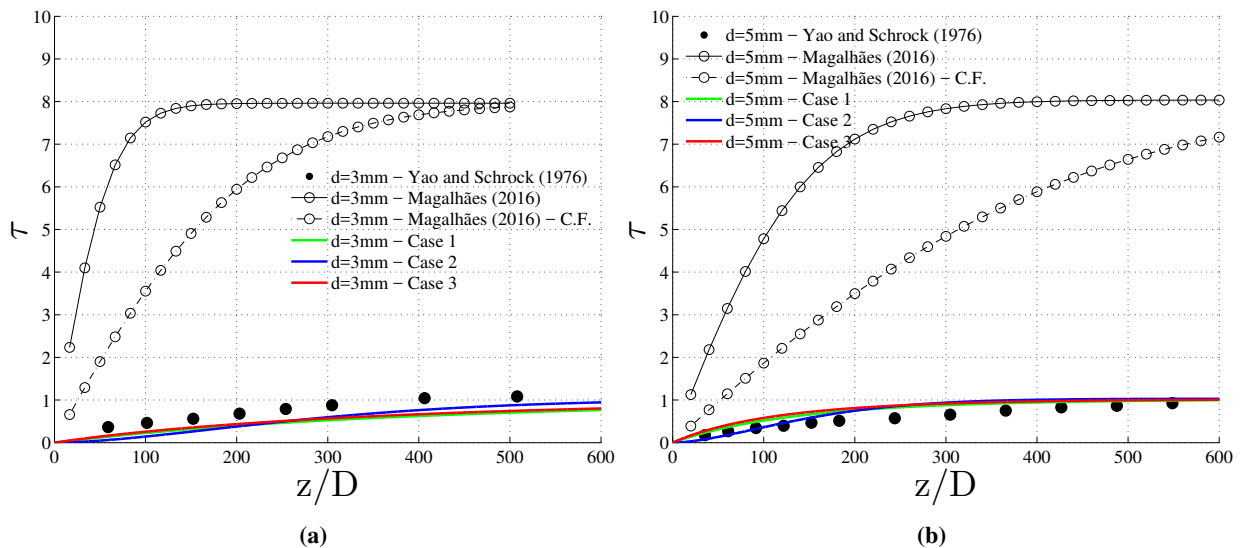


Fig. 8 Variation on drop's temperature falling through the air for a diameter of 3 mm (a) and 5 mm (b) for a humidity ratio of 1.00.

V. Conclusions

A two-way coupling model is implemented in order to evaluate the cooling of falling water drops, in which the variations in the humidity ratio and diameter of the drops are analyzed. Three different correlations are introduced in the model in order to evaluate the differences that may occur in the predictions.

For the lower humidity ratio (0.29) and diameter (3 mm), the present work model does not present a close agreement with the experimental data, which suggests a regime of steady state conditions for the cooling. The predictions of Ref. [9] using the one-way coupling formulation with the Ranz-Marshall relations are found to be in a closer agreement, in which a complete mixing model was used, which also supports the indication of a regime of steady state conditions.

Increasing the humidity ratio, the present work model proves to be a better approach to the process of cooling falling water droplets in comparison with the predictions made by Magalhães [9], meaning that for higher humidity ratios the obtained data suggests the presence of a transient regime.

The different correlations predictions are found to have great proximity between them. They are found to be in close agreement with the experimental data.

Acknowledgements

The present work was performed under the scope of Laboratório Associado em Energia, Transportes e Aeronáutica (LAETA) – activities and it was supported by Fundação para a Ciência e Tecnologia (FCT) through project UID/EMS/50022/2013, and by Fundação Luso-Americana para o Desenvolvimento (FLAD) through the project 07/2019.

References

- [1] Myers, T. G., Charpin, J. P. F., and Thompson, C. P., “Slowly Accreting Ice due to Supercooled Water Impacting on a Cold Surface,” *Physics of Fluids*, Vol. 14, No. 1, 2002, pp. 240–256. doi:10.1063/1.1416186.
- [2] Zhou, Z.-H., Yi, X., Gui, Y.-W., and Du, Y.-X., “Study on the Heat Transfer Characteristics in Aircraft Icing,” *Procedia Engineering*, Vol. 99, 2015, pp. 671–676. doi:10.1016/j.proeng.2014.12.588.
- [3] Elliott, J. W., and Smith, F. T., “Ice Formation on a Smooth or Rough Cold Surface due to the Impact of a Supercooled Water Droplet,” *Journal of Engineering Mathematics*, Vol. 102, No. 1, 2017, pp. 35–64. doi:10.1007/s10665-015-9784-z.
- [4] Cao, Y., Tan, W., and Wu, Z., “Aircraft icing: An ongoing threat to aviation safety,” *Aerospace Science and Technology*, Vol. 75, 2018, pp. 357–385. doi:10.1016/j.ast.2017.12.028.
- [5] Jones, S. M., Reveley, M. S., Evans, J. K., and Barrientos, F. (eds.), *Subsonic Aircraft Safety Icing Study*, NASA TM-215107, 2008.
- [6] Caliskan, F., and Hajiyev, C., “A Review of in-Flight Detection and Identification of Aircraft Icing and Reconfigurable Control,” *Progress in Aerospace Sciences*, Vol. 60, 2013, pp. 12–34. doi:10.1016/j.paerosci.2012.11.001.
- [7] Hindmarsh, J. P., Russell, A. B., and Chen, X. D., “Experimental and Numerical Analysis of the Temperature Transition of a Suspended Freezing Water Droplet,” *International Journal of Heat and Mass Transfer*, Vol. 46, No. 7, 2003, pp. 1199–1213. doi:10.1016/S0017-9310(02)00399-X.
- [8] Yao, S., and Schrock, V. E., “Heat and Mass Transfer From Freely Falling Drops,” *Journal of Heat Transfer*, Vol. 98, No. 1, 1976, pp. 120–126. doi:10.1115/1.3450453.
- [9] Magalhães, L. B., “Numerical Study of Freezing Droplets,” M.Sc. Dissertation, Aerospace Sciences Department, Universidade da Beira Interior, Covilhã, Portugal, 2016.
- [10] Ranz, W. R., and Marshall, W. R., “Evaporation from Drops,” *Chemical Engineering Progress*, Vol. 48, No. 3 and 4, 1952, pp. 141–146, 173–180.
- [11] Silva, A. R. R., “Experimental and Numerical Study of Physical Aspects of Fuel Processes,” Ph.D. Dissertation, Aerospace Sciences Department, Universidade da Beira Interior, Covilhã, Portugal, 2007.
- [12] Rodrigues, C. M. G., “Modelling of Spray-Wall Impingement,” Ph.D. Dissertation, Aerospace Sciences Department, Universidade da Beira Interior, Covilhã, Portugal, 2016.
- [13] Launder, B. E., and Spalding, D. B., “The Numerical Computation of Turbulent Flows,” *Computer Methods in Applied Mechanics and Engineering*, Vol. 3, No. 2, 1974, pp. 269–289.

- [14] Leonard, B. P., "A Stable and Accurate Convective Modeling Procedure Based on Quadratic Upstream Interpolation," *Computer Methods in Applied Mechanics and Engineering*, Vol. 19, No. 1, 1979, pp. 59–98.
- [15] Patankar, S. V., and Spalding, D. B., "A Calculation Procedure for Heat, Mass and Momentum Transfer in Three-Dimensional Parabolic Flows," *International Journal of Heat and Mass Transfer*, Vol. 15, No. 10, 1972, pp. 1787–1806.
- [16] Thomas, L. H. (ed.), *Elliptic Problems in Linear Differential Equations over a Network*, Watson Science Computer Laboratory Report, 1949.
- [17] Barata, J., "On the modeling of droplet transport, dispersion and evaporation in turbulent flows," *Silniki Spalinowe*, Vol. 122, No. 3, 2005, pp. 42–55.
- [18] Abmrazon, B., and Sirignano, W. A., "Droplet Vaporization Model for Spray Combustion Calculations," *International Journal of Heat and Mass Transfer*, Vol. 32, No. 9, 1989, pp. 1605–1618.